ARL 64-81
MAY 1964

Aerospace Research Laboratories

AN INVESTIGATION OF CONSTANT AREA SUPERSONIC FLOW DIFFUSION

ANDREW A. FEJER
GEORGE L. HEATH
RICHARD T. DRIFTMYER
RESEARCH FOUNDATION OF
THE UNIVERSITY OF TOLEDO
TOLEDO, OHIO

OFFICE OF AEROSPACE RESEARCH
United States Air Force

NOTICES

When Government drawings, specifications, or other data are used for any purpose other than in connection with a definitely related Government procurement operation, the United States Government thereby incurs no responsibility nor any obligation whatsoever; and the fact that the Government may have formulated, furnished, or in any way supplied the said drawings, specifications, or other data, is not to be regarded by implication or otherwise as in any manner licensing the holder or any other person or corporation, or conveying any rights or permission to manufacture, use, or sell any patented invention that may in any way be related thereto.

- - - - - - - - - -

Qualified requesters may obtain copies of this report from the Defense Documentation Center, (DDC), Cameron Station, Alexandria, Virginia.

- - - - - - - - - -

This report has been released to the Office of Technical Services, U. S. Department of Commerce, Washington 25, D. C. for sale to the general public.

- - - - - - - - - -

Copies of ARL Technical Documentary Reports should not be returned to Aerospace Research Laboratories unless return is required by security considerations, contractual obligations or notices on a specified document.

500 - July 1964 - 162-45-924

ARL 64-81

AN INVESTIGATION OF CONSTANT AREA SUPERSONIC FLOW DIFFUSION

ANDREW A. FEJER
GEORGE L. HEATH
RICHARD T. DRIFTMYER

RESEARCH FOUNDATION OF
THE UNIVERSITY OF TOLEDO
TOLEDO, OHIO

MAY 1964

Contract AF 33(616)-8271
Project 7116
Task 7116-01

AEROSPACE RESEARCH LABORATORIES
OFFICE OF AEROSPACE RESEARCH
UNITED STATES AIR FORCE
WRIGHT-PATTERSON AIR FORCE BASE, OHIO

FOREWORD

This interim technical documentary report was prepared by the Research Foundation of the University of Toledo, Toledo, Ohio on contract AF 33(616)-8271 for the Aerospace Research Laboratories, Office of Aerospace Research, United States Air Force. The research reported herein was accomplished on Task 7116-01, "Internal Flow Research" of Project 7116, "Energy Conversion Research" under the technical cognizance of Mr. Kenneth Cramer of the Thermomechanics Research Laboratory of ARL. The study was carried out under the direction of Dr. Andrew A. Fejer with the collaboration of Professors George L. Heath and Richard T. Driftmyer of the Department of Mechanical Engineering. Mr. Stanley Meyer also assisted in the work.

ABSTRACT

Experiments were conducted to determine the nature of the deceleration of supersonic airstreams in straight passages of constant cross sectional area. The magnitude of the losses associated with the recovery of kinetic energ, was established, Schlieren observations were made of the field of flow in the passage and the influence of passage length, Mach Number and effective Reynolds Number on maximum obtainable pressure rise were investigated. ( )

TABLE OF CONTENTS

LIST OF ILLUSTRATIONS

*With Boundary Layer Trip

LIST OF ILLUSTRATIONS (CONT'D)

LIST OF ILLUSTRATIONS (CONT'D)

SCHLIEREN PHOTOGRAPHS

LIST OF ILLUSTRATIONS (CONT'D)

SECTION I

INTRODUCTION

The conversion of the kinetic energy of a fluid moving through a passage with high velocity poses many problems of interest to designers of wind tunnels, combustors, jet propulsion engines, turbomachinery and other devices. When the flow entering the passage is supersonic the diffusion process is particularly difficult to analyze due to the presence of shock waves and their interaction with the boundary layers on the passage walls. While deceleration of a supersonic stream to subsonic Mach numbers requires, ideally, convergent-divergent passage geometrys, it is known that the flow has a tendency to separate from the passage walls in the divergent region. Consequently, diffusion to subsonic Mach numbers cannot be realized in this case and in addition excessive losses result due to eddies in the separated region (Ref. 1). However, if the walls of the passage are parallel, i.e., the cross sectional area is constant along the passage, pressure recoveries similar to those across normal shock waves are obtainable (Ref. 2) with the pressure rise being attributable in this case to a complex system of shocks which may extend over an axial distance representing a multiple of the channel width.

In the present study, shock configurations in constant area passages were studied experimentally. The distribution of static pressure along the passage was measured, the maximum obtainable ratio of discharge pressure to inlet pressure was determined, Schlieren photographs of the shock systems were taken and the losses in the passage were established on the basis of discharge total pressure surveys.

SECTION II

EXPERIMENTAL SET-UP AND TEST PROCEDURE

The test passage shown in Figures 1 and 2 consisted of straight metal surfaces on the top and bottom, glass side plates and a plenum chamber type discharge region fitted with a throttling mechanism which effectively separated the passage from the tunnel proper. The throttling mechanism consisted of two vertical, slotted plates, one fixed and one sliding. By changing the position of the latter by remote control the pressure in the chamber could be changed permitting, thereby, variations of the passage pressure ratio.

Note: Manuscript released January 1964 by the authors for publication as an ARL Technical Documentary Report.

The instrumentation consisted of static pressure taps located at one-half inch intervals along the centerline of the top and bottom of the passage, static pressure taps in the plenum chamber and a total pressure rake. This rake was positioned on the center line of the passage at the entrance to the plenum chamber and carried eight total pressure tubes spaced at one-eighth inch intervals with the tips of the tubes aligned with the discharge cross section of the passage. The vertical position of the rake was externally adjustable to allow total pressure surveys across the channel to be taken during a test run. The passage walls were removable and permitted, thereby, the investigation of passages of various lengths. Four passage lengths (4, 6, 8 and 10 inches) were selected; the passage height was one inch. For changes in inlet Mach numbers three sets of wind tunnel nozzles were available, designed for test section Mach numbers of 1.6, 2.0 and 2.5 respectively.

For each combination of passage length and inlet Mach number, tests were run at various throttle settings starting with the wide open throttle position. As the throttle opening was reduced gradually the shock system, located originally at the discharge end of the passage, moved toward the passage entrance until it finally moved into the stream ahead of the passage entrance. The difference between the static pressure at the exit and the static pressure at the inlet just prior to this occurance is referred to in the following as the maximum obtainable pressure rise for the particular combination of passage geometry and inlet Mach number. At each throttle position all pressures were recorded photographically along with Schlieren photographs of the shock system. During a number of runs discharge total pressure surveys were also made.

In order to determine whether the observed phenomena were sensitive to changes in the character of the boundary layer, boundary layer trips were also used. They consisted of strips of 0.02 inch thickness and 0.045 inch width that extended across the entire passage, installed both on the top and bottom plates one-half inch downstream of the passage entrance.

SECTION III

TEST PROGRAM AND EXPERIMENTAL RESULTS

A summary of the configurations that were investigated is presented in Table I. Static pressure distributions along the passage in the configurations presented in Table I are shown in Figures 3 thru 23. Averages of the pressures on the top and bottom walls are shown in terms of the inlet static pressure measured at the entrance to the test section on the wind tunnel wall.

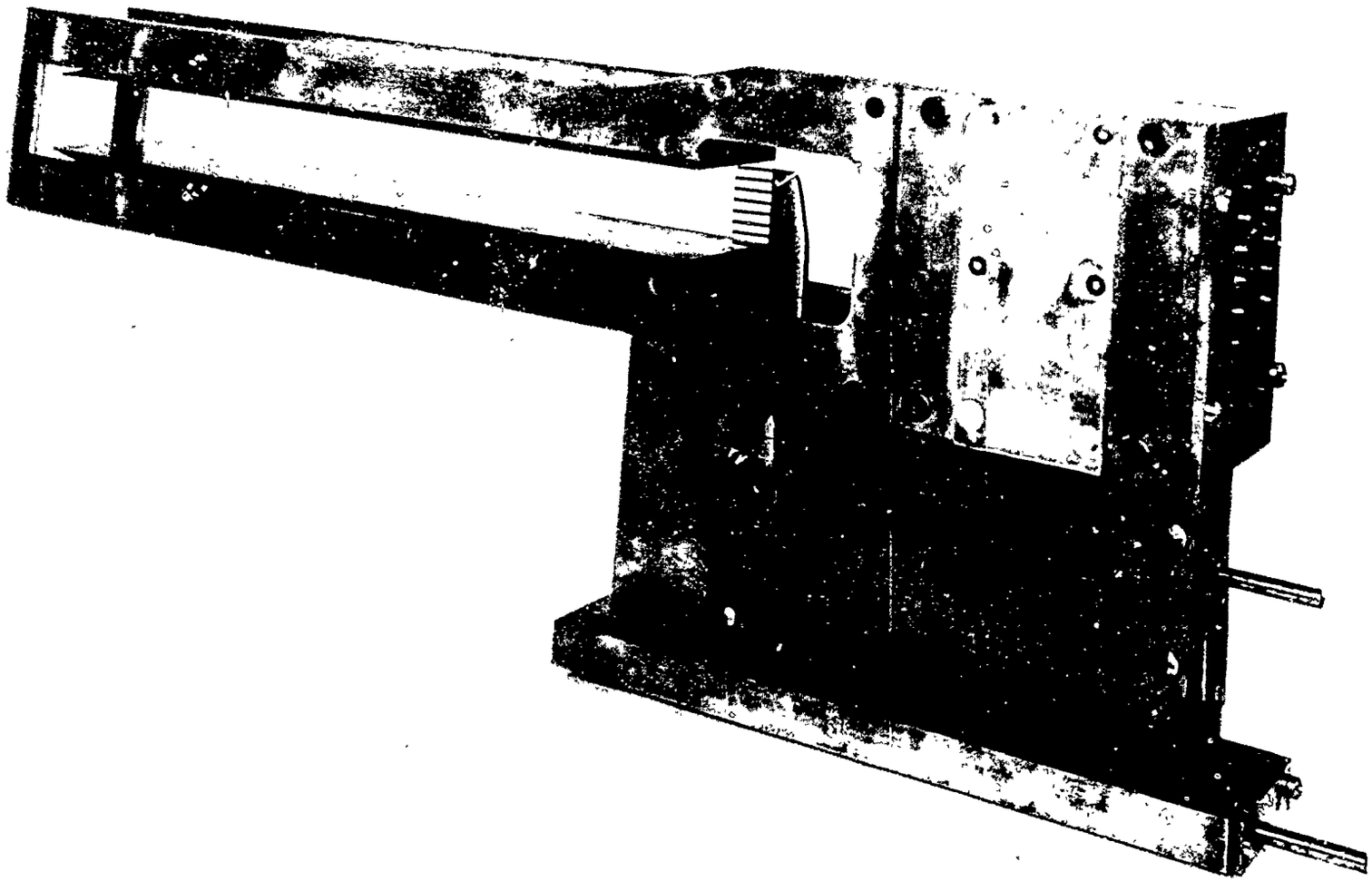

FIGURE 1 PHOTOGRAPH OF TEST PASSAGE

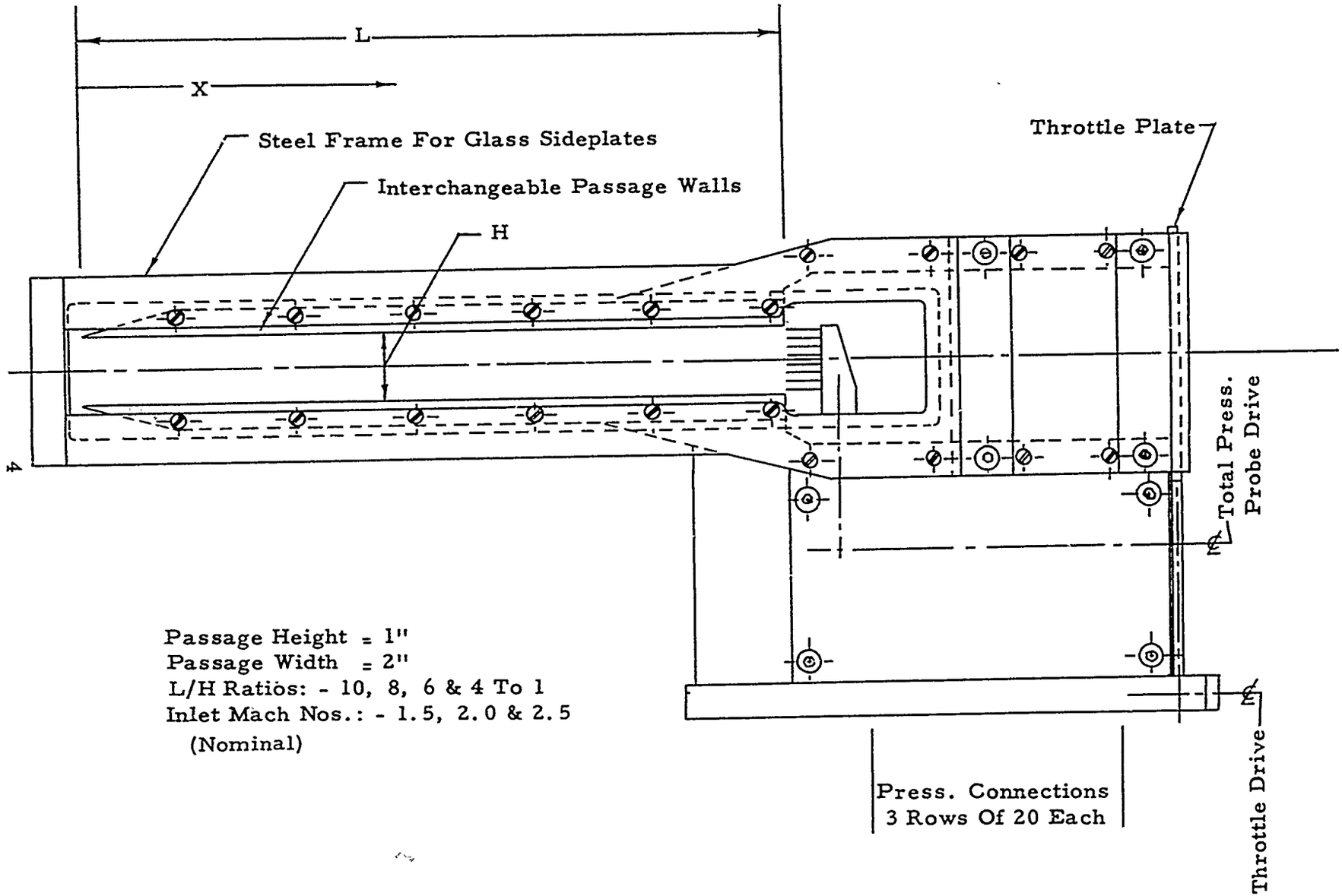

FIGURE 2 TEST PASSAGE FOR PRESSURE RECOVERY STUDIES

From the curves shown in Figures 3 thru 23 it is apparent that with wide open throttle, i.e., at minimum back pressure, the static pressure rises gradually along the passage. As the back pressure is gradually increased a small shock region appears first near the passage discharge and with increasing back pressure and corresponding increase of the shock intensity the shock region moves toward the passage entrance. At low inlet Mach numbers the shock system, manifesting itself as a region of rapidly rising pressure, was found to be quite short and downstream of it the pressure was observed to vary relatively little along the passage (Figures 3 and 4). With increasing inlet Mach numbers the axial length of the shock system grew significantly and the pressure distribution did not flatten out except at the maximum pressure ratio when the shock system was close to the passage entrance (Figures 5 and 6). And at the highest Mach numbers the passage was too short, i.e., the pressure was found to increase significantly from the front of the shock system to the passage discharge at all pressure ratios (Figures 7 and 8).

TABLE I

Passage Length/Height	Inlet Mach Number	Maximum Static Pressure Ratio	
10:1	1.60	2.45	(2.30)*
	1.95	4.08	(4.20)
	2.46	5.36	(6.33)
8:1	1.60	2.68	(2.62)
	1.975	4.15	(3.96)
	2.50	4.73	(5.64)
6:1	1.67	2.94	(2.97)
	2.00	3.88	(4.23)
	2.50	3.88	(4.48)
4:1	1.67	2.66	(2.76)
	1.96	3.61	(3.94)
	2.50	3.34	(3.90)

*The pressure ratios shown in parenthesis were obtained with boundary layer trips.

Results are presented for configurations with and without boundary layer trips. As the leading edge of the shock system moved toward the passage entrance, due to increasing pressure ratios, its position became increasingly unstable. The boundary layer trips were found to have a stabilizing effect on the fluctuations in the position of the system and thus, in the configurations employing boundary layer trips, the maximum stable forward position of the front of the shock system was closer to the passage entrance than in the absence of the trips.

Maximum obtainable discharge to inlet static pressure ratios represent flow conditions corresponding to minimum throttle valve opening for unchoked flow. They are summarized in Table I for the configurations tested and also as a function of the dimensionless passage length in Figure 24.

Whenever the distance of the shock front from the passage entrance had a significant effect on the maximum pressure ratio, i.e., the passage was too short, as in the case of all passages at M=2.5 and the four inch passage at M=2.0, the presence of the boundary layer trips resulted in an increase in maximum pressure ratio; otherwise they had no effect.

Typical total pressure surveys taken along the vertical center line of the discharge area are shown in Figures 26 thru 49. They represent uncorrected manometer readings and include, therefore, the total pressure losses due to detached shocks at the probes.

Selected Schlieren photographs showing typical shock configurations for various passage configurations and operating conditions are shown in Figures 49 thru 72. Table II, refers these photographs to the graphical results presented previously.

SECTION IV

DISCUSSION OF RESULTS

It is apparent from the experimental results described in the preceding section that constant area passages can be utilized as supersonic diffusers over a wide range of inlet Mach numbers and pressure ratios.

The pressure rise occuring in the passage is of course determined by the pressure levels existing at the inlet and discharge from the passage. The smallest pressure rise that can be realized occurs without shocks and is due to the decrease in effective passage area. When the pressure rise is small the passage flow is either free of shocks or contains a system of oblique shocks of small intensity. In either case the pressure rise is due primarily to a decrease in the effective passage area caused by the thickening of the boundary layer.

The maximum pressure ratio obtainable in a passage may approach within a few percent the value of the pressure ratio across a normal shock occuring at the passage inlet Mach number. However, in this case the passage must be of a certain optimum length ("design length"). If the passage is shorter the rise in pressure will fall short of that value by a considerable amount; if, on the other hand, the length of the passage exceeds the optimum length, the maximum pressure rise will be reached somewhere within the passage and the pressure will then drop due to friction from that point to a lower value at the discharge.

When the passage operates at the maximum pressure ratio that it is capable of maintaining, the upstream face of the shock system is located near the entrance to the passage. If the pressure in the back of the passage is raised to exceed this maximum the shock system will be ejected from the passage and, being transformed into a normal shock, will position itself on the outside near the passage entrance; the passage is then said to be choked. If, on the other hand, the back pressure is reduced the shock system will be weakened and will move further into the passage.

This behavior of supersonic flow in constant area passages, readily apparent from the pressure distributions presented earlier (Figures 3 thru 23) is summarized in Figures 24 and 25. Figure 24 shows the magnitude of the maximum obtainable pressure ratio for passages of various length to height ratios at Mach numbers of 1.6, 2.0 and 2.5. In Figure 25 these pressure ratios are compared to the normal shock pressure ratios. It can be seen from these figures that at M=1.6 the "design length" to height ratio is in the vicinity of 6:1 and that at M=2.5 even the longest of the passages tested (L/H = 10) falls short of the "design length" corresponding to that Mach number.

The foregoing is based on the data and Schlieren observations presented in this report. It is believed that a critical analysis of these data will yield further information regarding such characteristics of shock systems in constant area ducts as the relationship between minimum passage length and inlet Mach number and the efficiency of pressure recovery for various Mach numbers and passage lengths. This analysis is now in progress and its results will be included in the final report on this study.

TABLE II

Inlet Mach	Aspect Ratio	Boundary Layer Trip	Static Pressure Distribution	Total Pressure Distribution	Schlieren Photograph
1.60	10	Yes	Figure 3	Figure 26	Figure 50
1.60	10	No	4	27	51
1.95	10	Yes	5	28	52
1.95	10	No	6	29	53
2.46	10	Yes	7	30	54
2.46	10	No	8	31	55
1.60	8	Yes	Figure 9	Figure 32	Figure 56
1.60	8	No	10	33	57
1.975	8	Yes	11	34	58
1.975	8	No	12	35	59
2.50	8	Yes	13	36	60
2.50	8	No	14	37	61
1.67	6	Yes	Figure 15	Figure 38	Figure 62
1.67	6	No	16	39	63
2.00	6	Yes	17	40	64
2.00	6	No	18	41	65
2.50	6	Yes	19	42	66
2.50	6	No	20	43	67
1.67	4	Yes	Figure 21	Figure 44	Figure 68
1.67	4	No	21	45	69
1.96	4	Yes	22	46	70
1.96	4	No	22	47	71
2.50	4	Yes	23	48	72
2.50	4	No	23	49	73

LIST OF REFERENCES

1 Fejer, A. A., Supersonic Cascade Studies, WADC TR 55-396, June 1955.

2 Fejer, A. A. and Heath, G. L., Supersonic Cascade Studies, Pt. 1 Passage Studies, ARL Part 1, December 1961.

3 Liepmann, H. W. and Rosko, A., Reflection of Shock Waves from Boundary Layers, NACA TR #1100.

4 Neumann, E. P. and Lustwerk, F., "Supersonic Diffusers for Wind Tunnels", Journal of Applied Mechanics, Vol. 16 #2, June 1949.

5 Shapiro, Ascher H., The Dynamics and Thermodynamics of Compressible Fluid Flow, Volume II, Article 28.5, The Ronald Press Co., 1954 LC 53-8869.

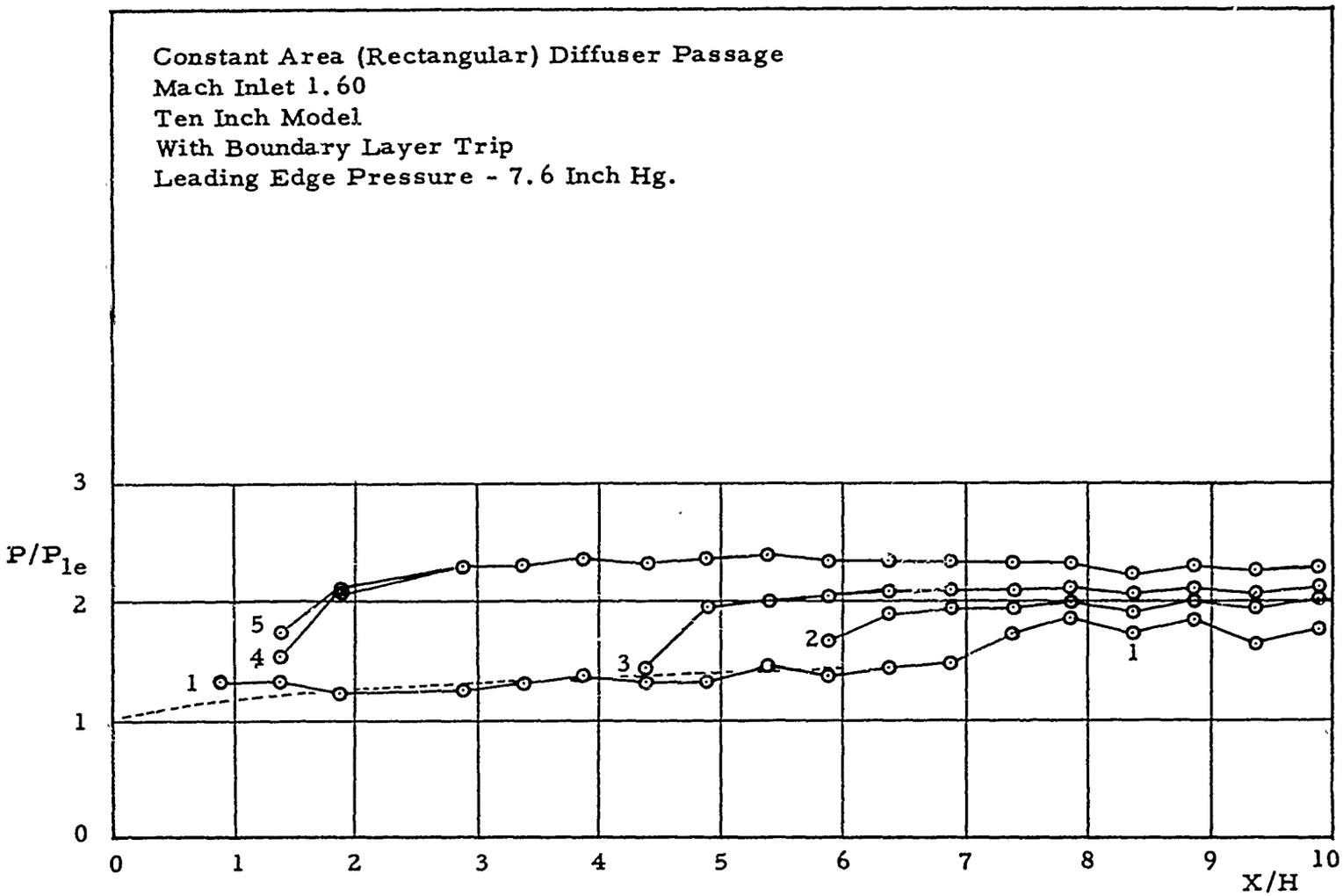

FIGURE 3 STATIC PRESSURE RATIO VERSUS LENGTH TO HEIGHT RATIO

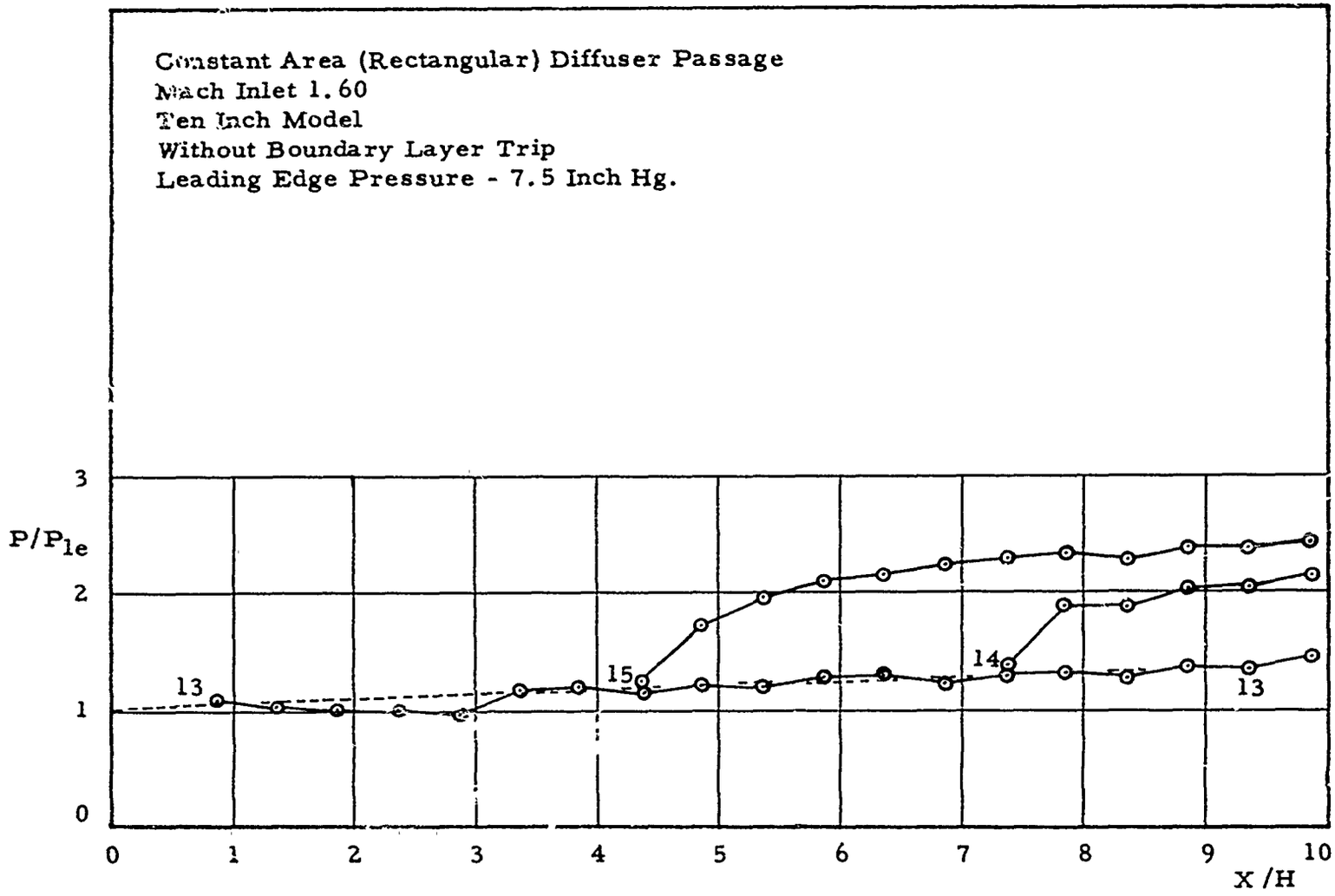

FIGURE 4 STATIC PRESSURE RATIO VERSUS LENGTH TO HEIGHT RATIO

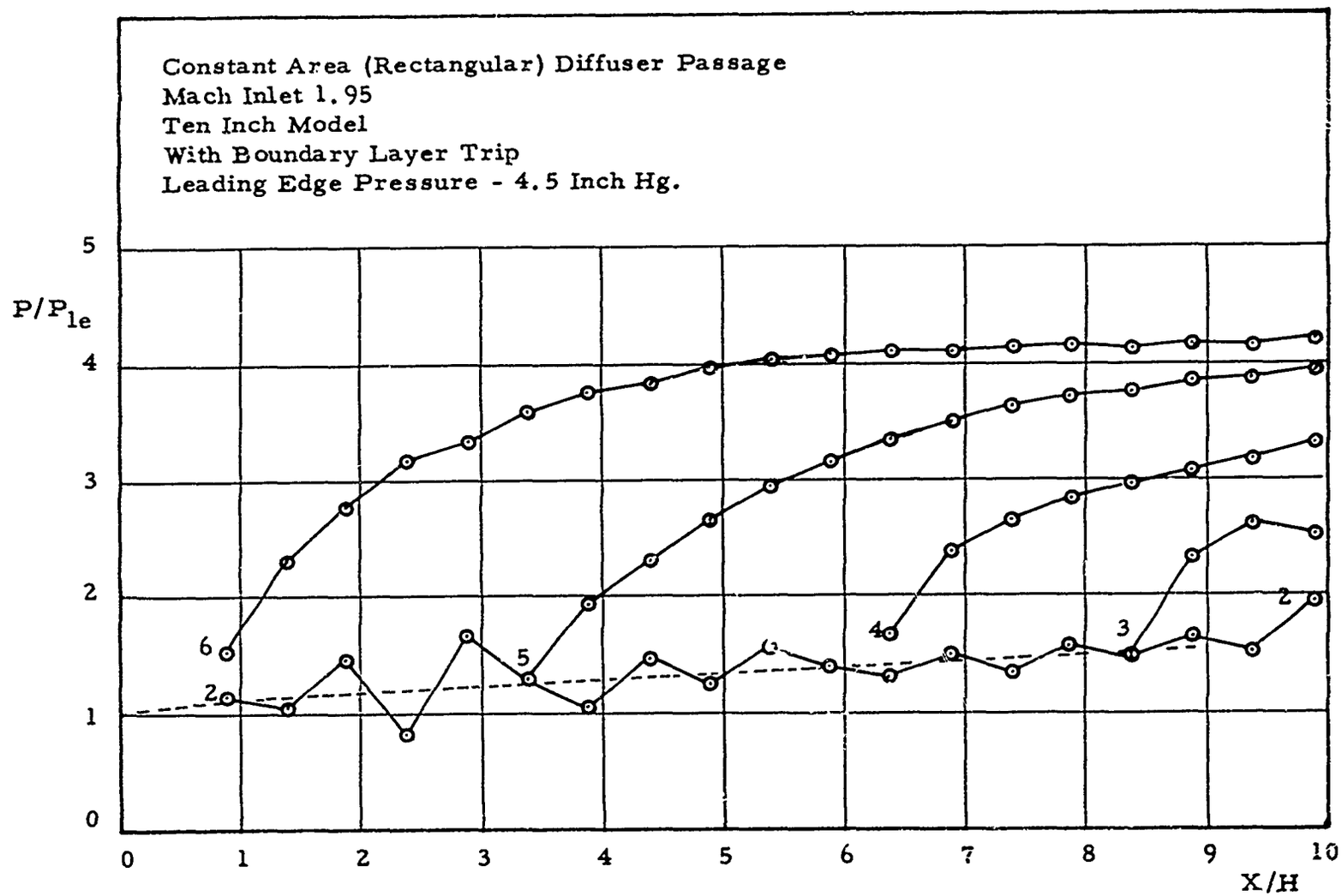

FIGURE 5 STATIC PRESSURE RATIO VERSUS LENGTH TO HEIGHT RATIO

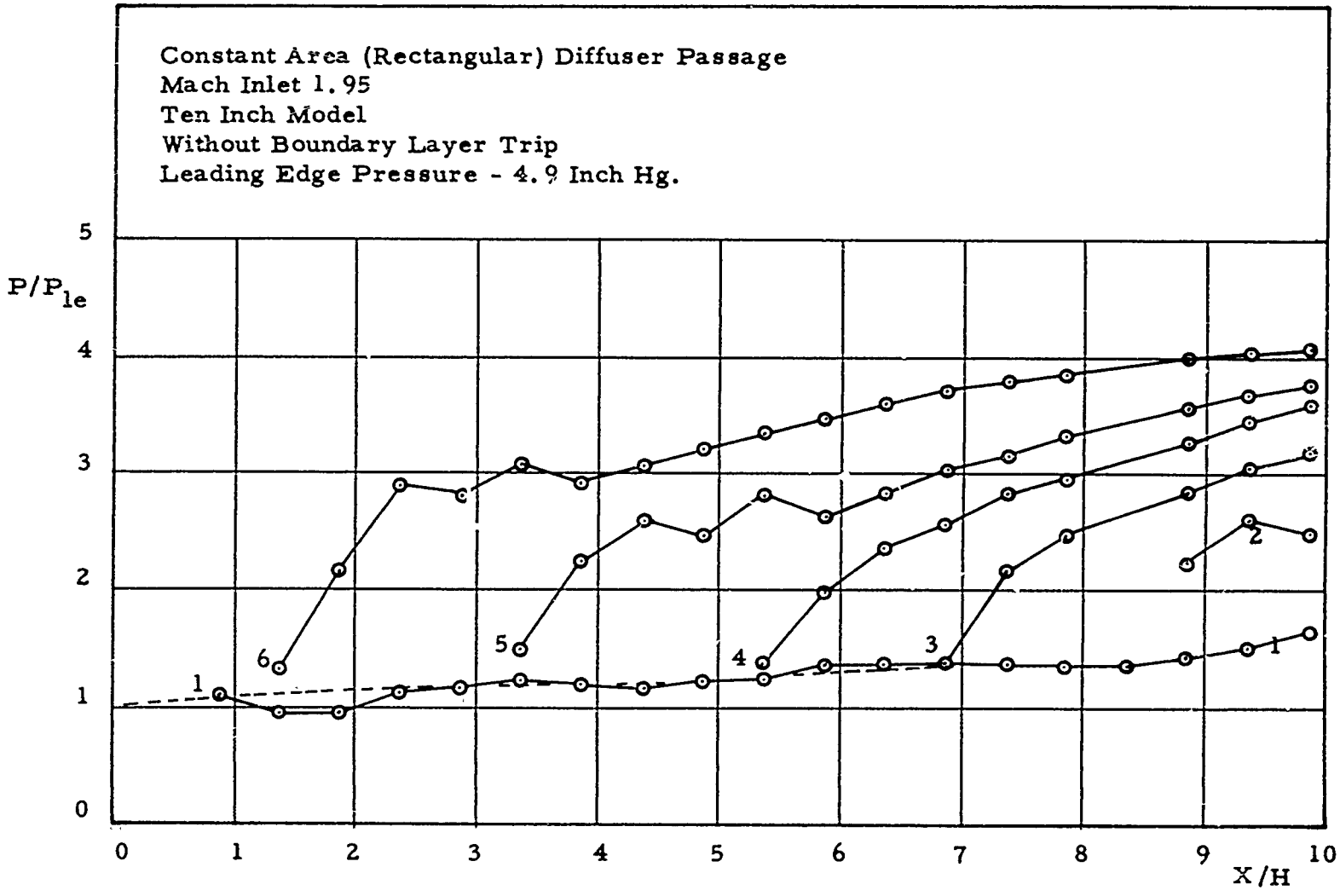

FIGURE 6 STATIC PRESSURE RATIO VERSUS LENGTH TO HEIGHT RATIO

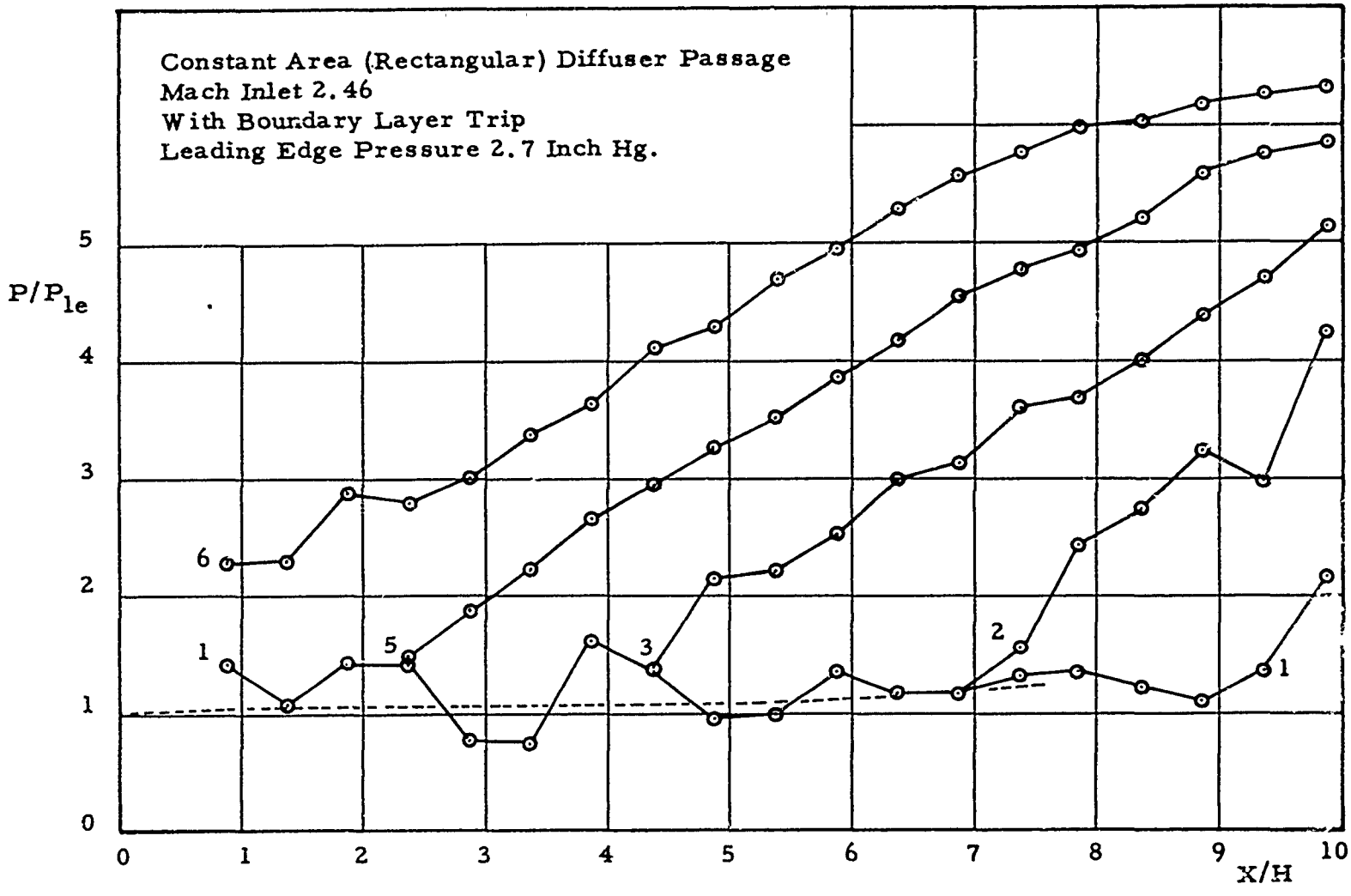

FIGURE 7 STATIC PRESSURE RATIO VERSUS LENGTH TO HEIGHT RATIO

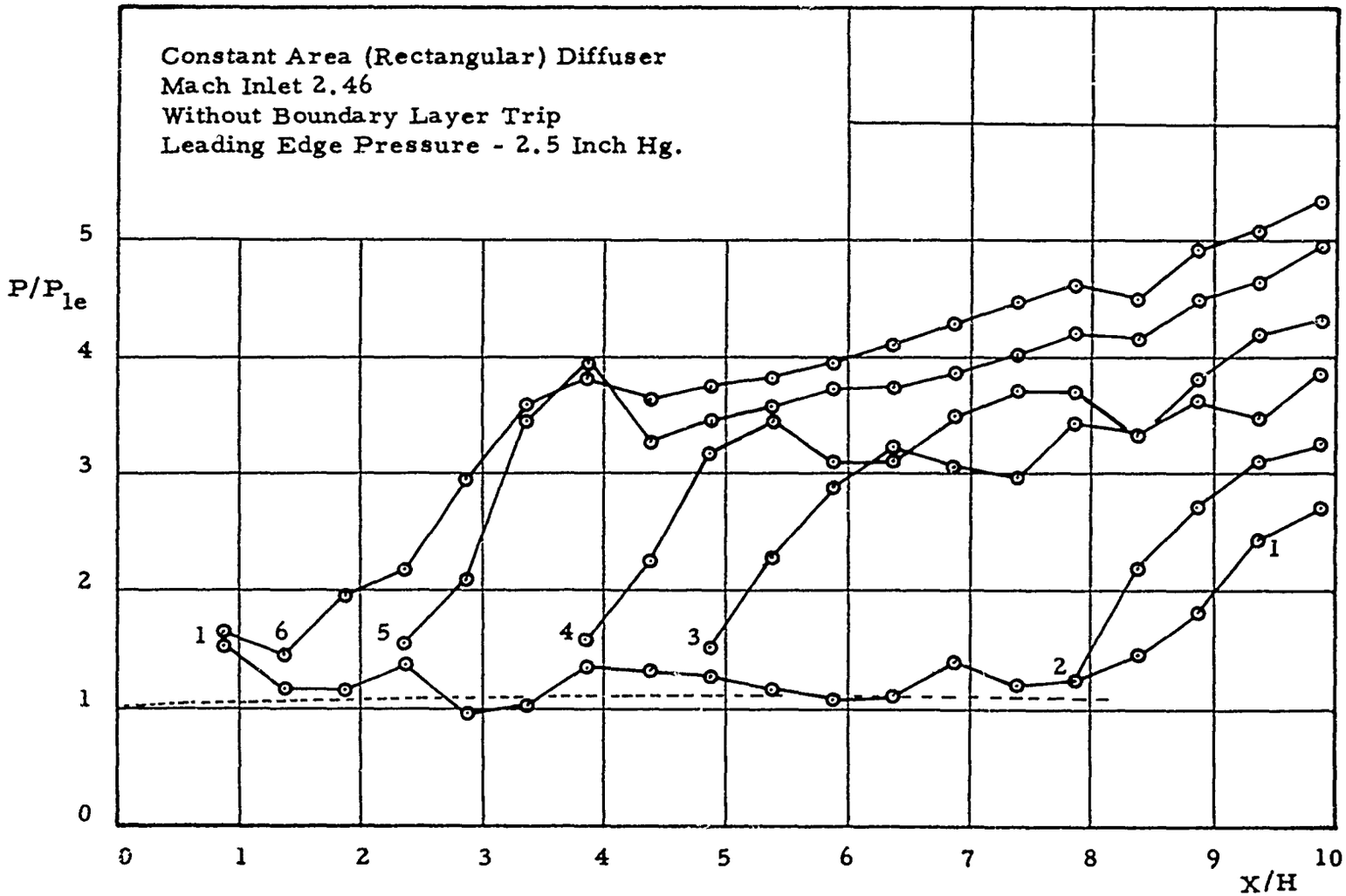

FIGURE 8 STATIC PRESSURE RATIO VERSUS LENGTH TO HEIGHT RATIO

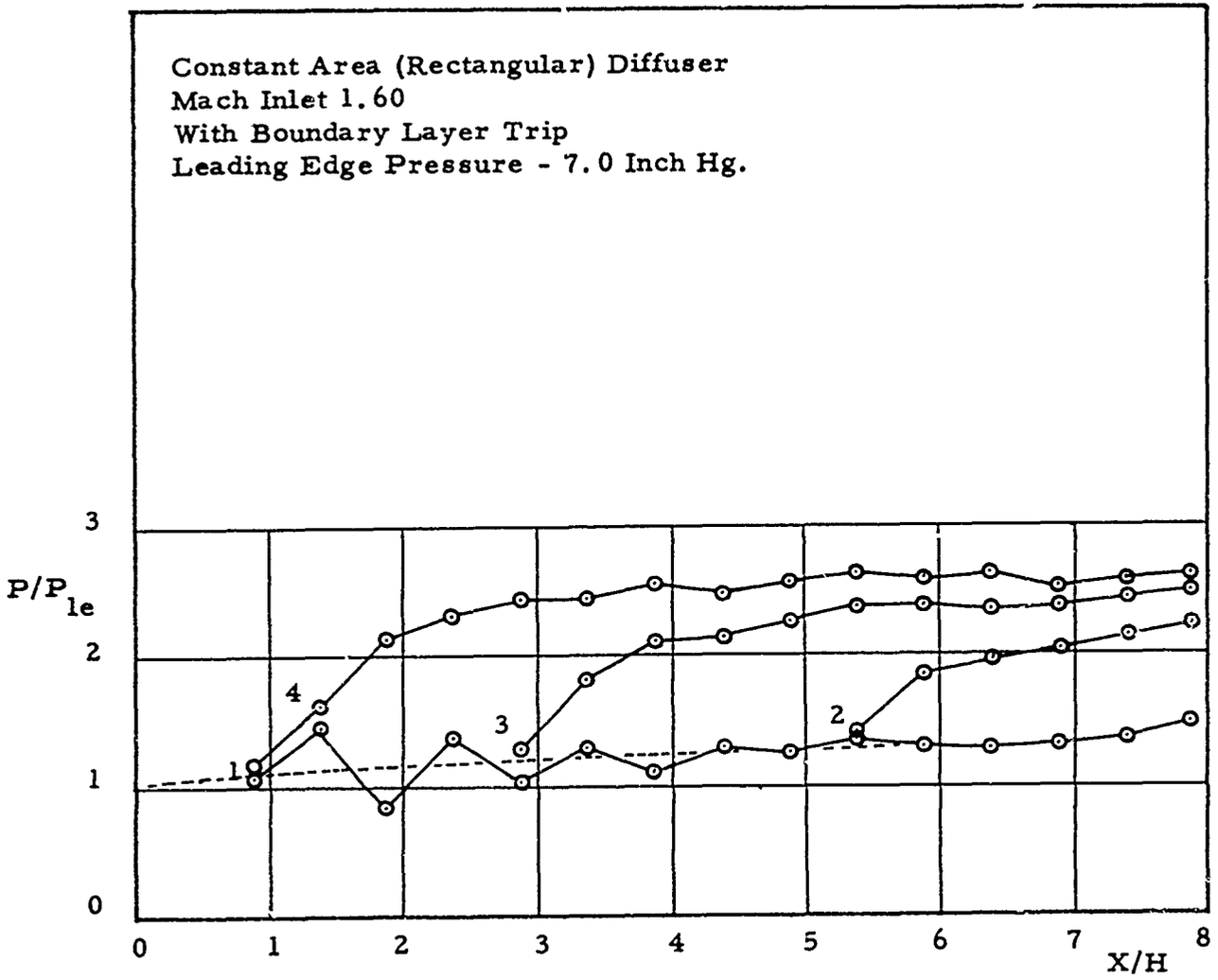

FIGURE 9 STATIC PRESSURE RATIO VERSUS LENGTH TO HEIGHT RATIO

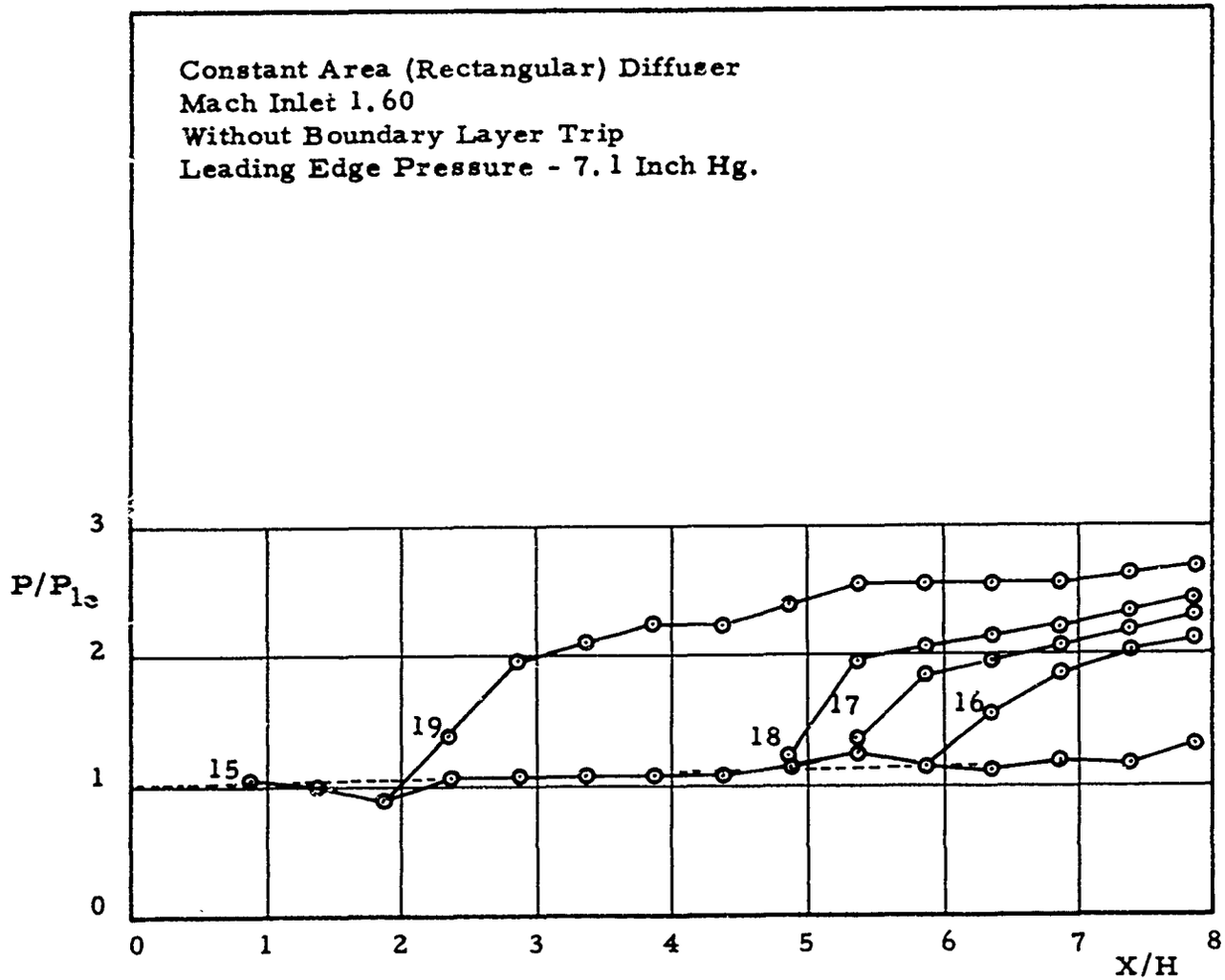

FIGURE 10 STATIC PRESSURE RATIO VERSUS LENGTH TO HEIGHT RATIO

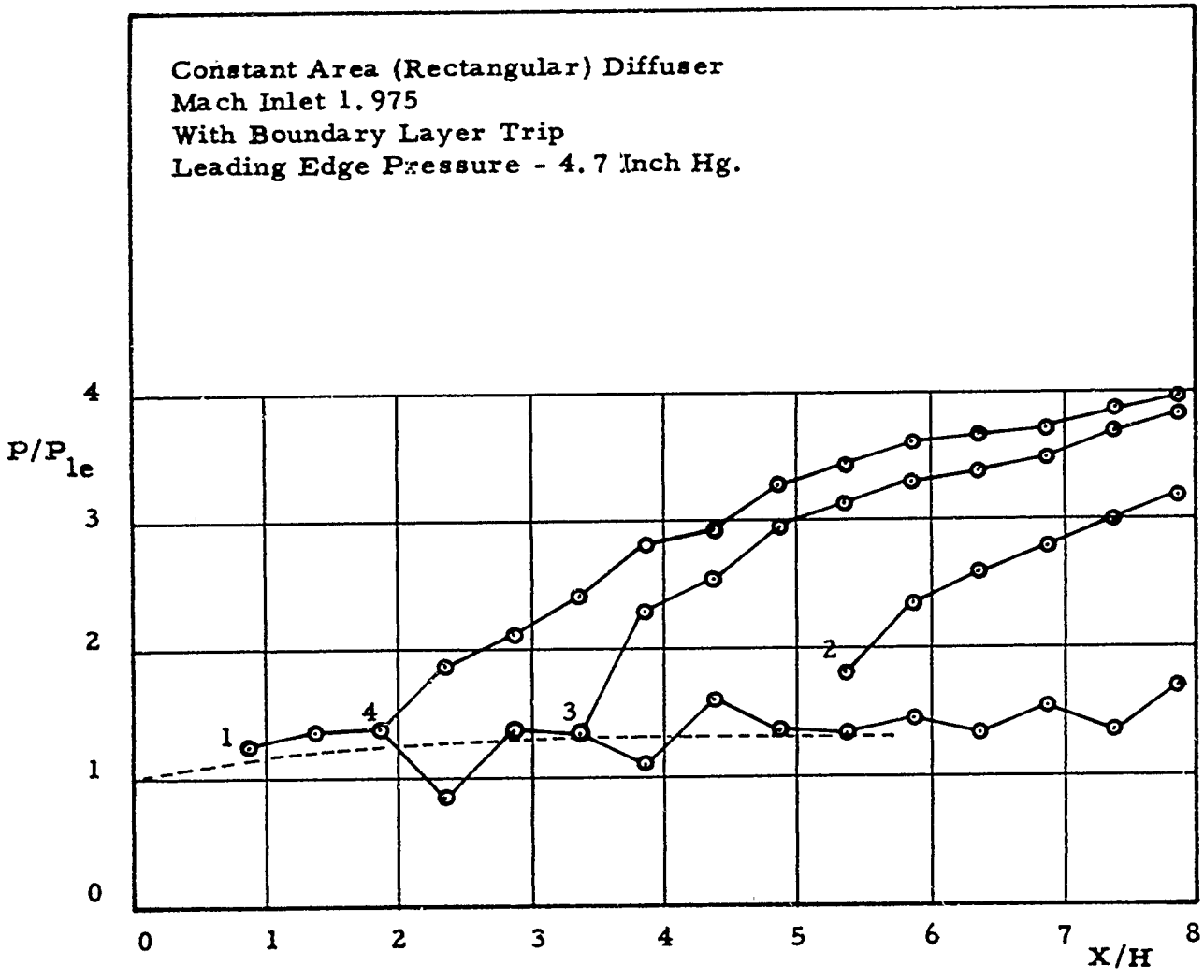

FIGURE 11 STATIC PRESSURE RATIO VERSUS LENGTH TO HEIGHT RATIO

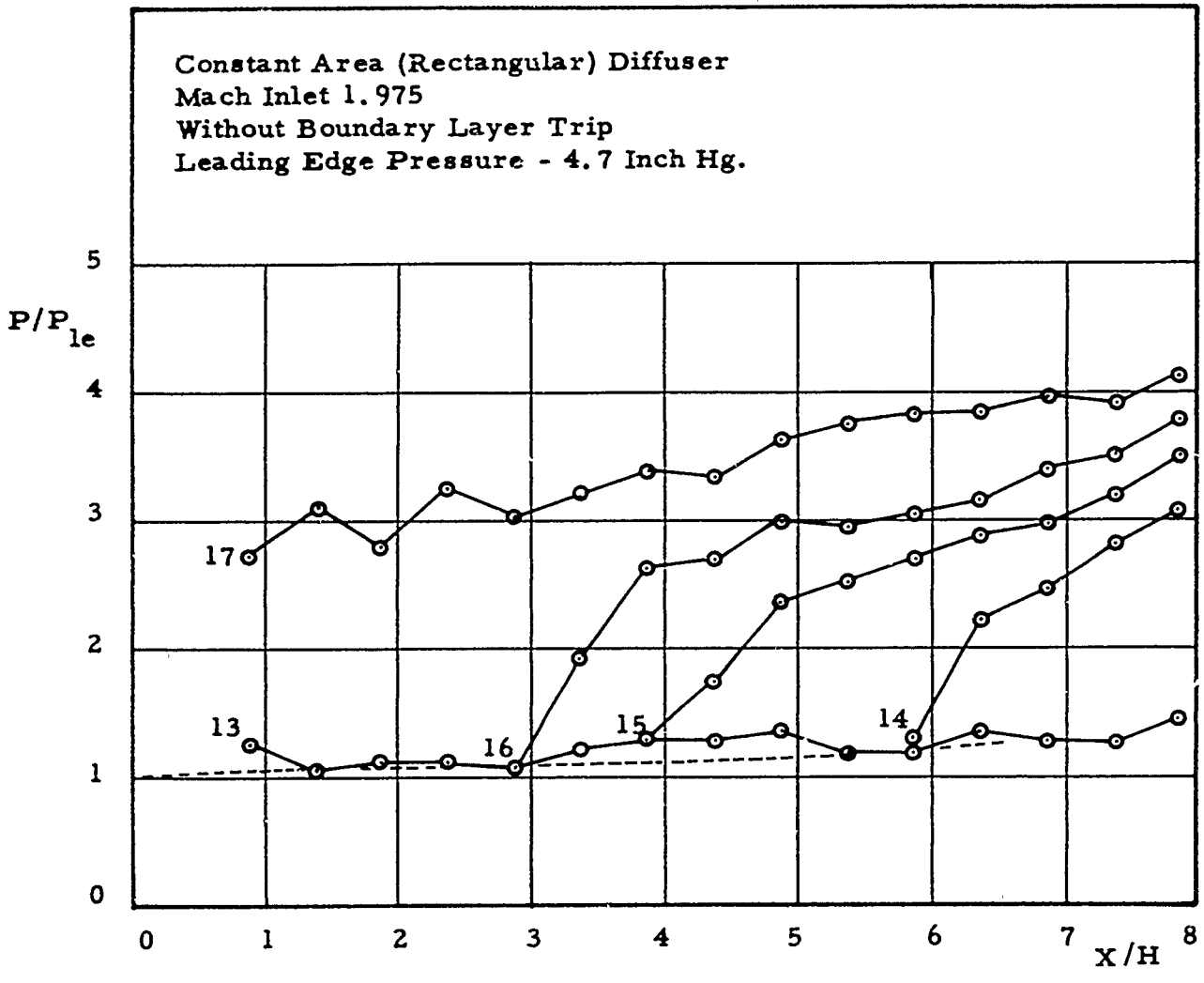

FIGURE 12 STATIC PRESSURE RATIO VERSUS LENGTH TO HEIGHT RATIO

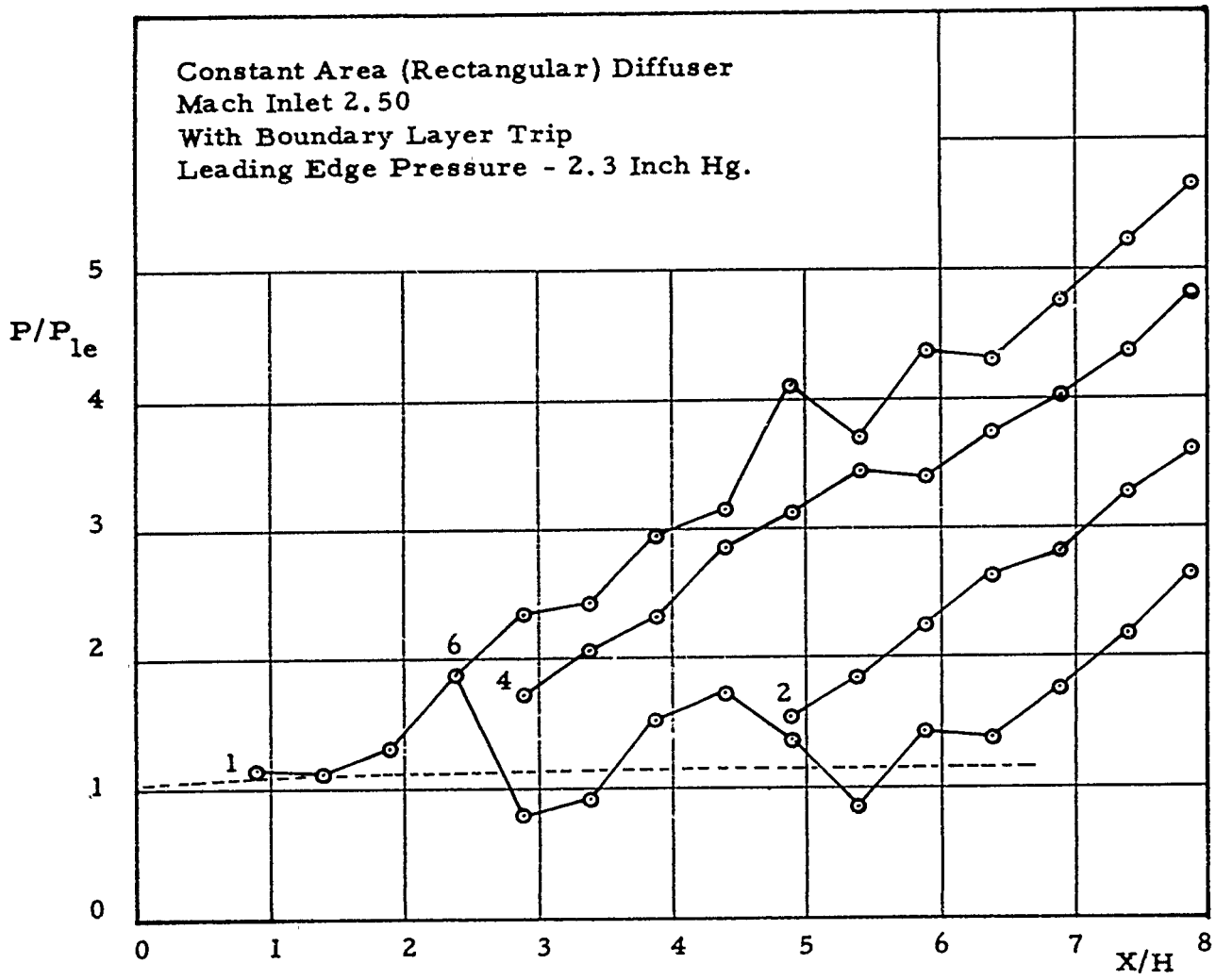

FIGURE 13 STATIC PRESSURE RATIO VERSUS LENGTH TO HEIGHT RATIO

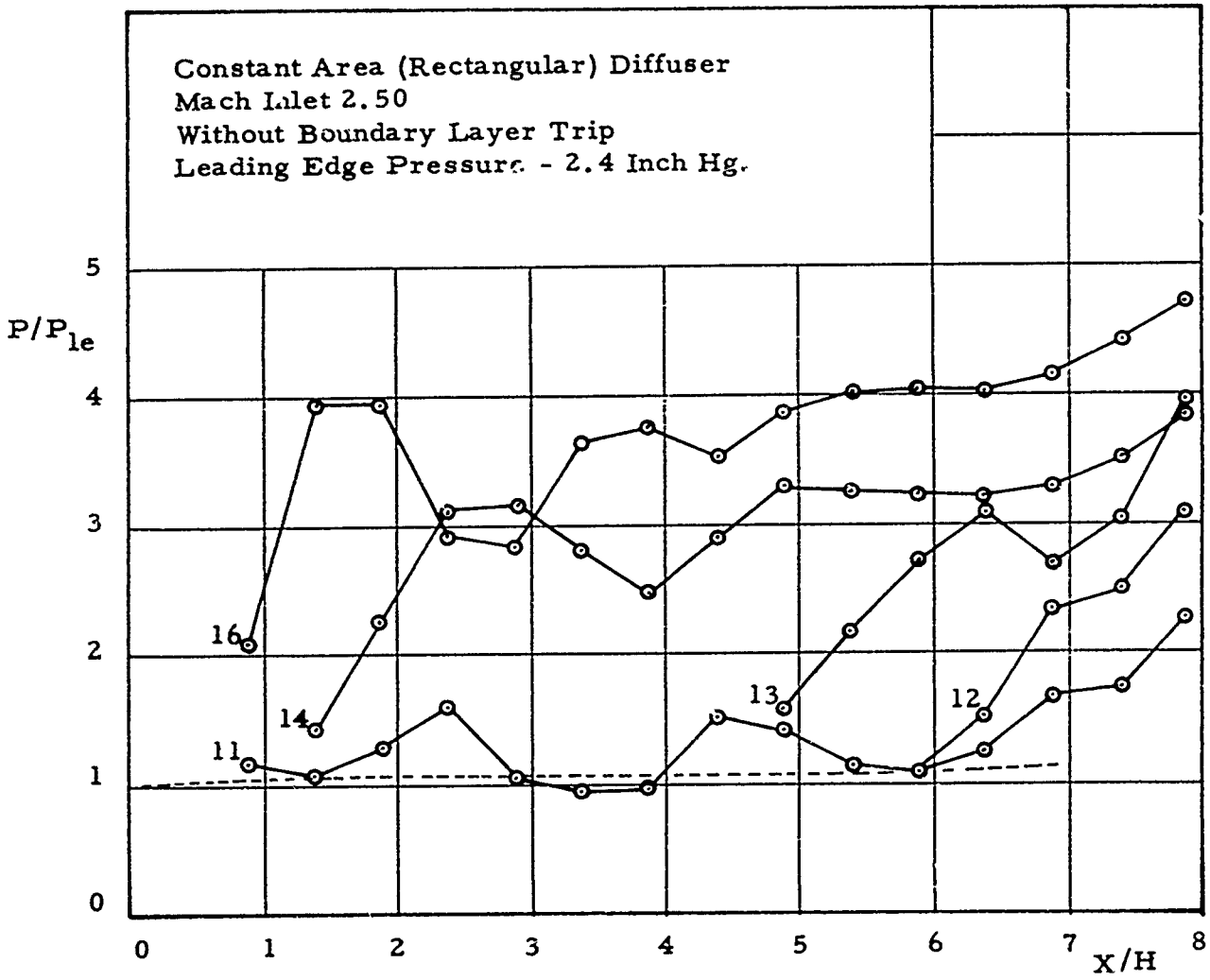

FIGURE 14 STATIC PRESSURE RATIO VERSUS LENGTH TO HEIGHT RATIO

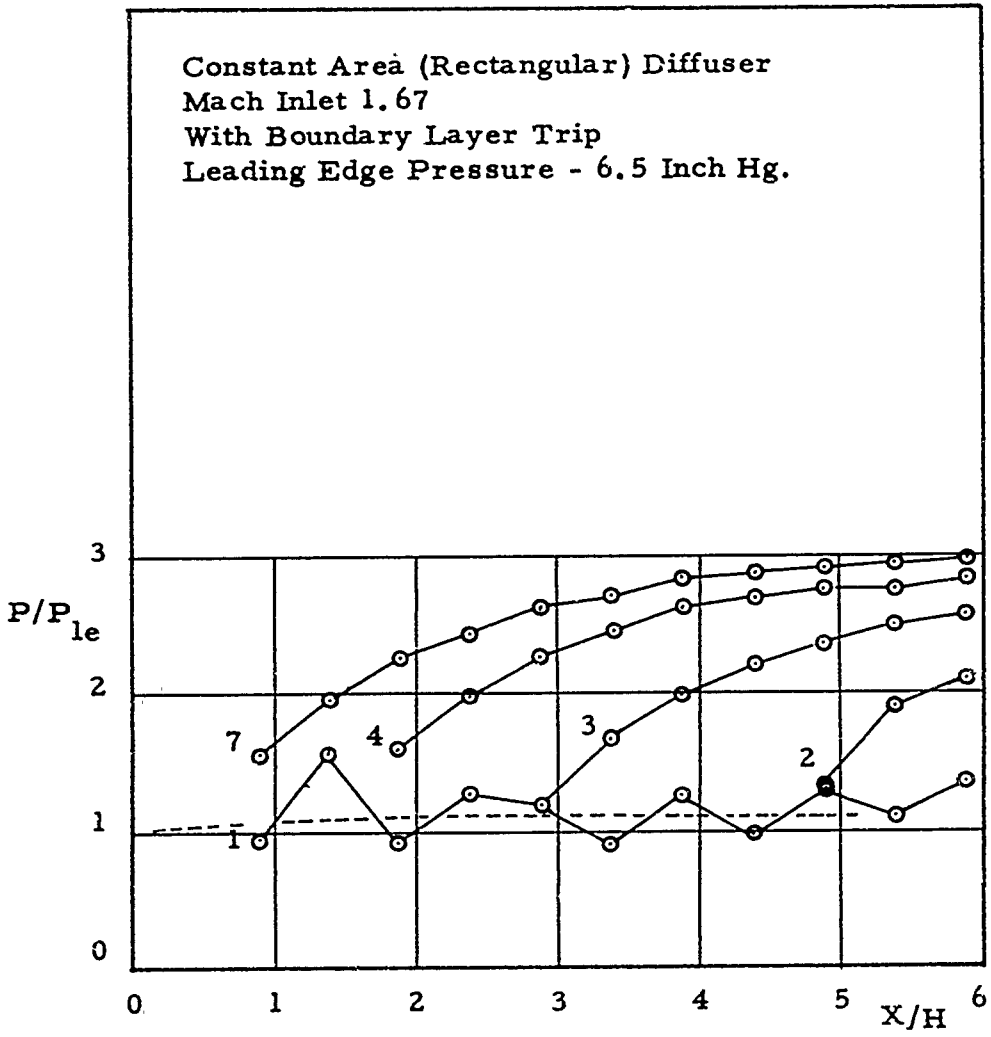

FIGURE 15 STATIC PRESSURE RATIO
VERSUS LENGTH TO HEIGHT RATIO

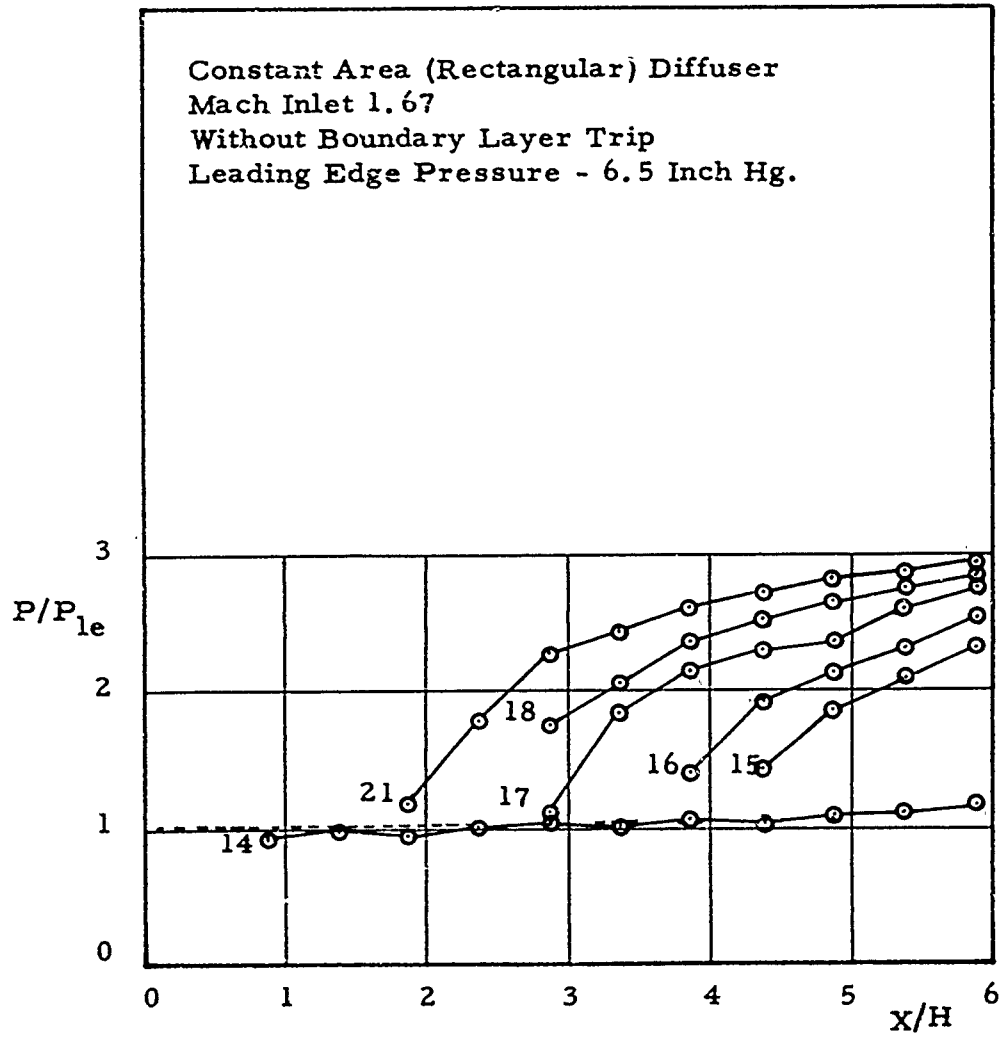

FIGURE 16 STATIC PRESSURE RATIO VERSUS LENGTH TO HEIGHT RATIO

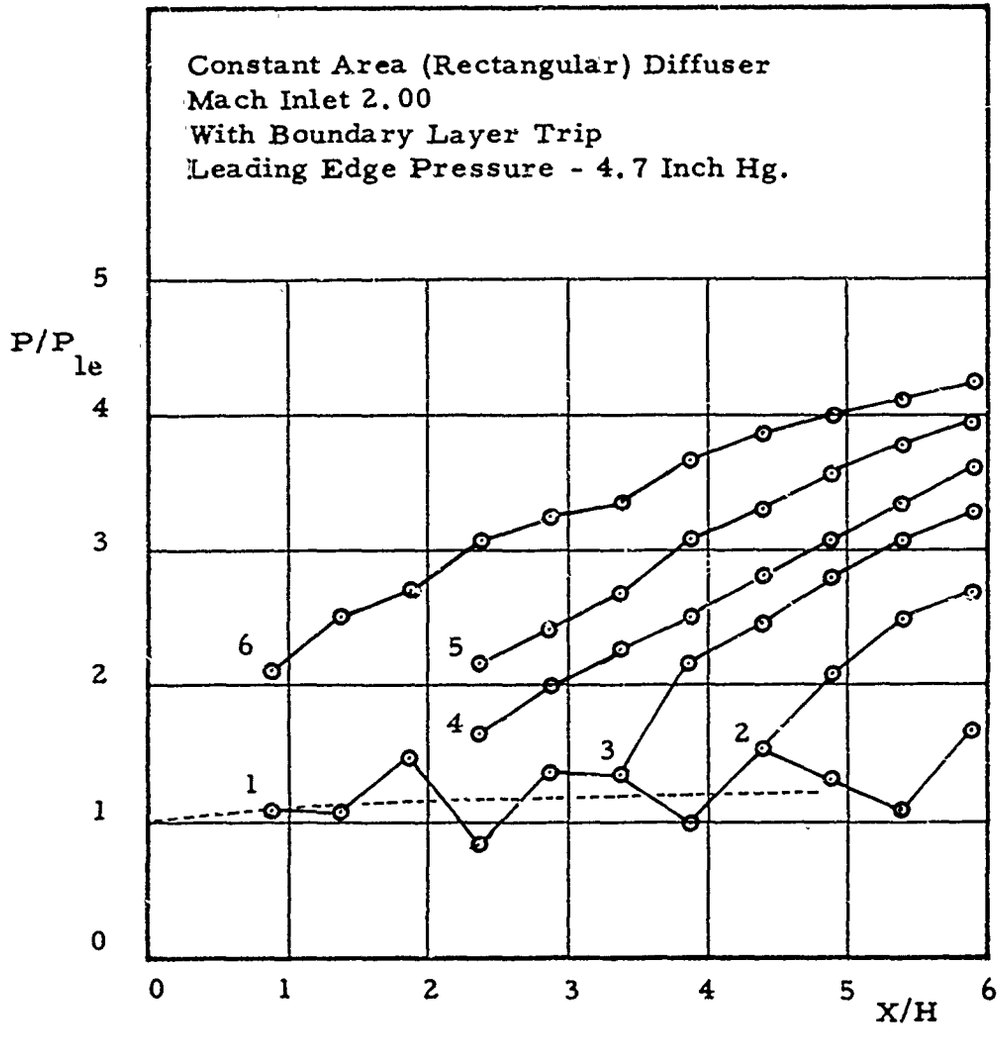

FIGURE 17 STATIC PRESSURE RATIO VERSUS LENGTH TO HEIGHT RATIO

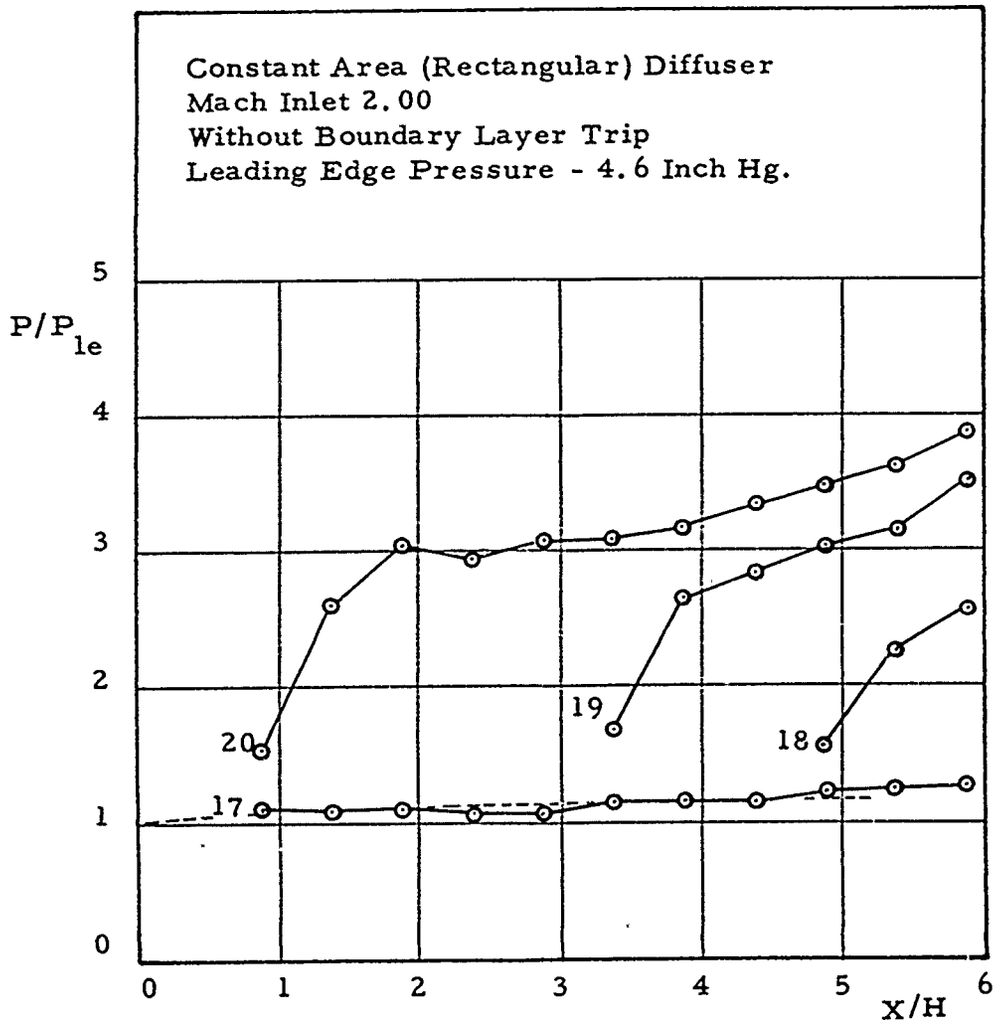

FIGURE 18 STATIC PRESSURE RATIO VERSUS LENGTH TO HEIGHT RATIO

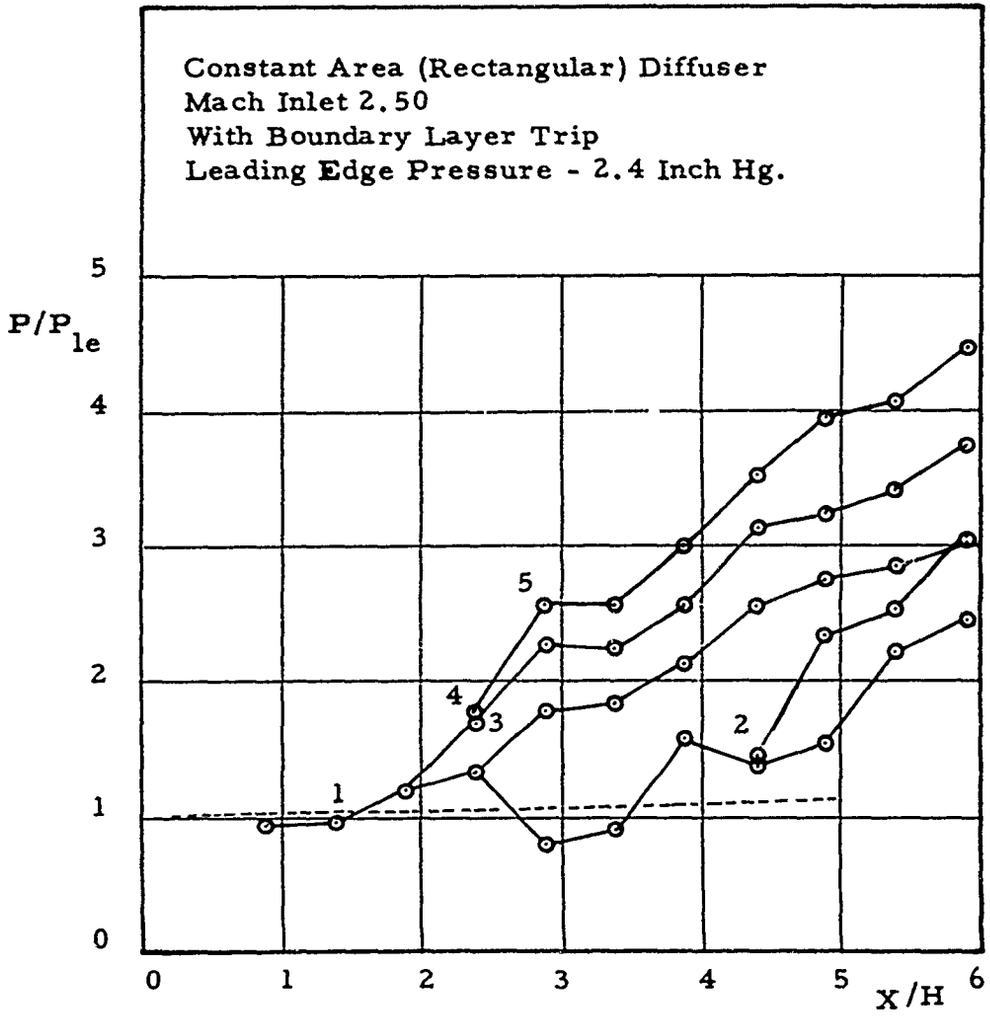

FIGURE 19 STATIC PRESSURE RATIO VERSUS LENGTH TO HEIGHT RATIO

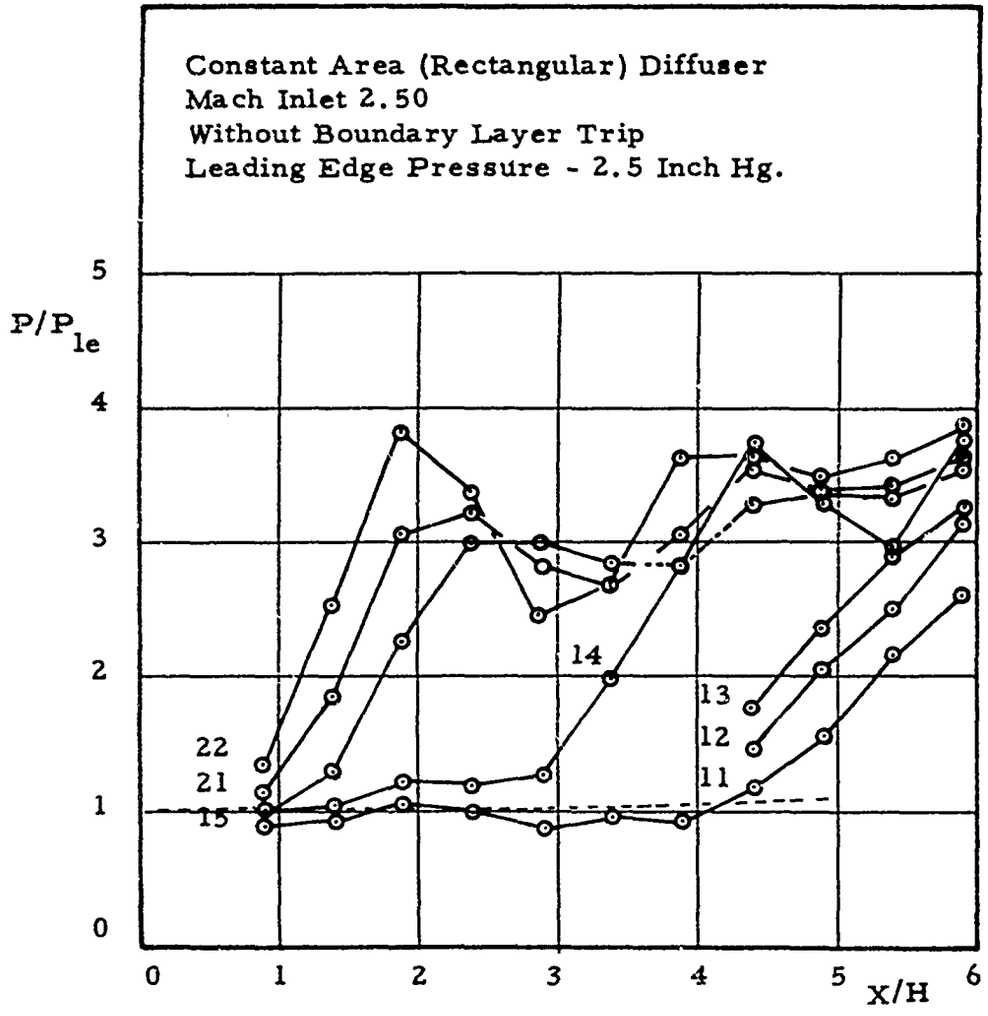

FIGURE 20 STATIC PRESSURE RATIO VERSUS LENGTH TO HEIGHT RATIO

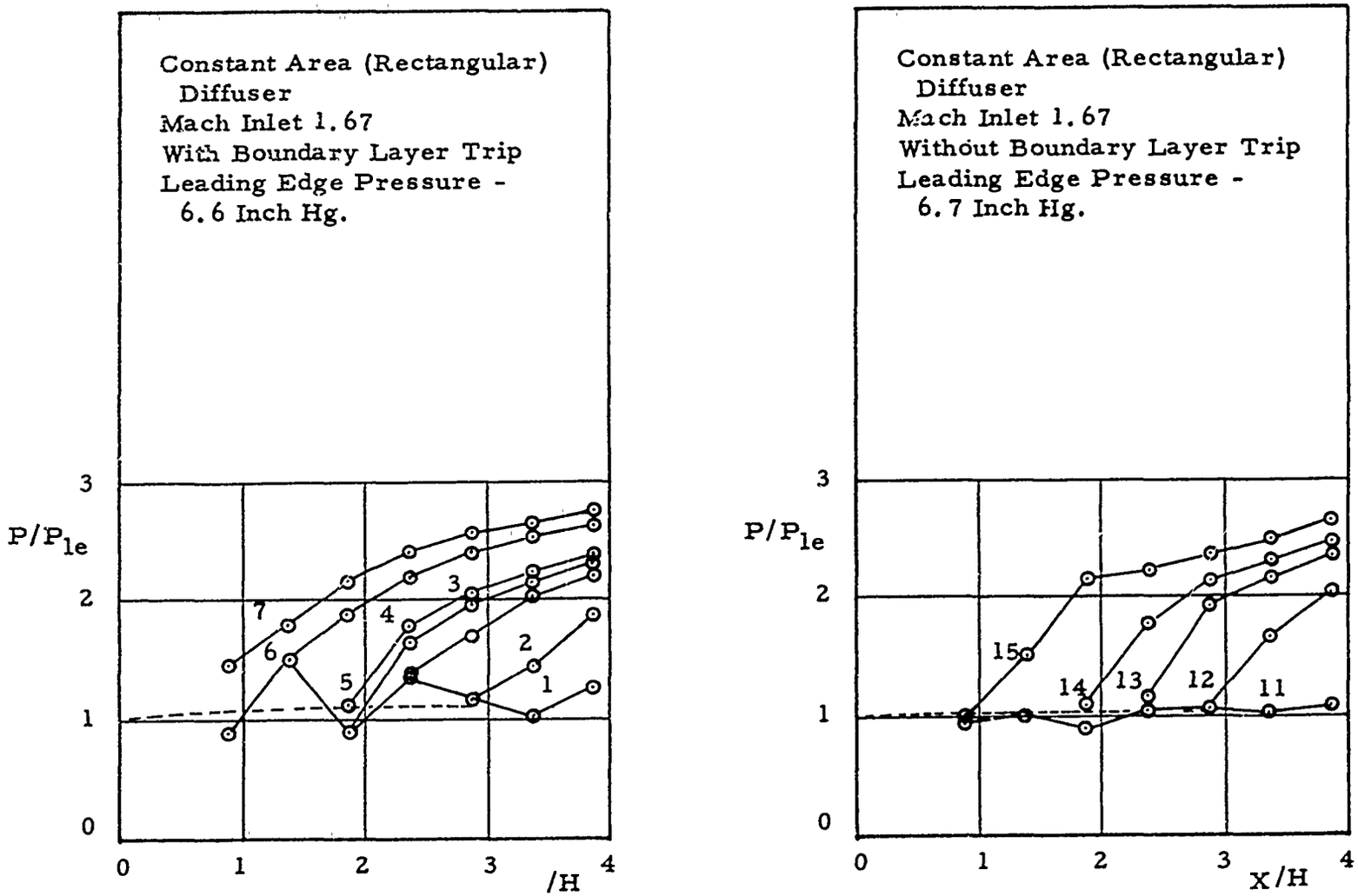

FIGURE 21 STATIC PRESSURE RATIO VERSUS LENGTH TO HEIGHT RATIO

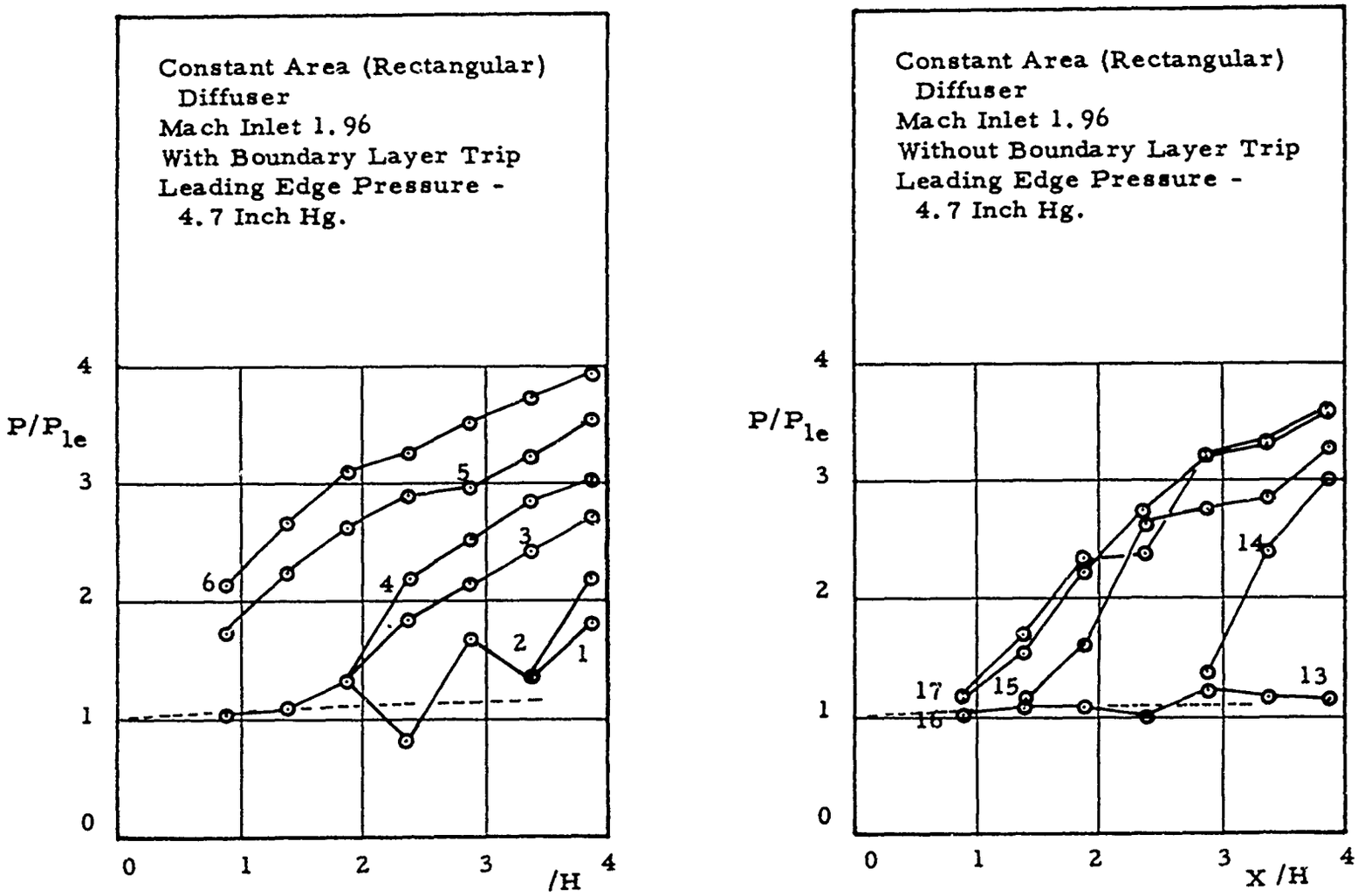

FIGURE 22 STATIC PRESSURE RATIO VERSUS LENGTH TO HEIGHT RATIO

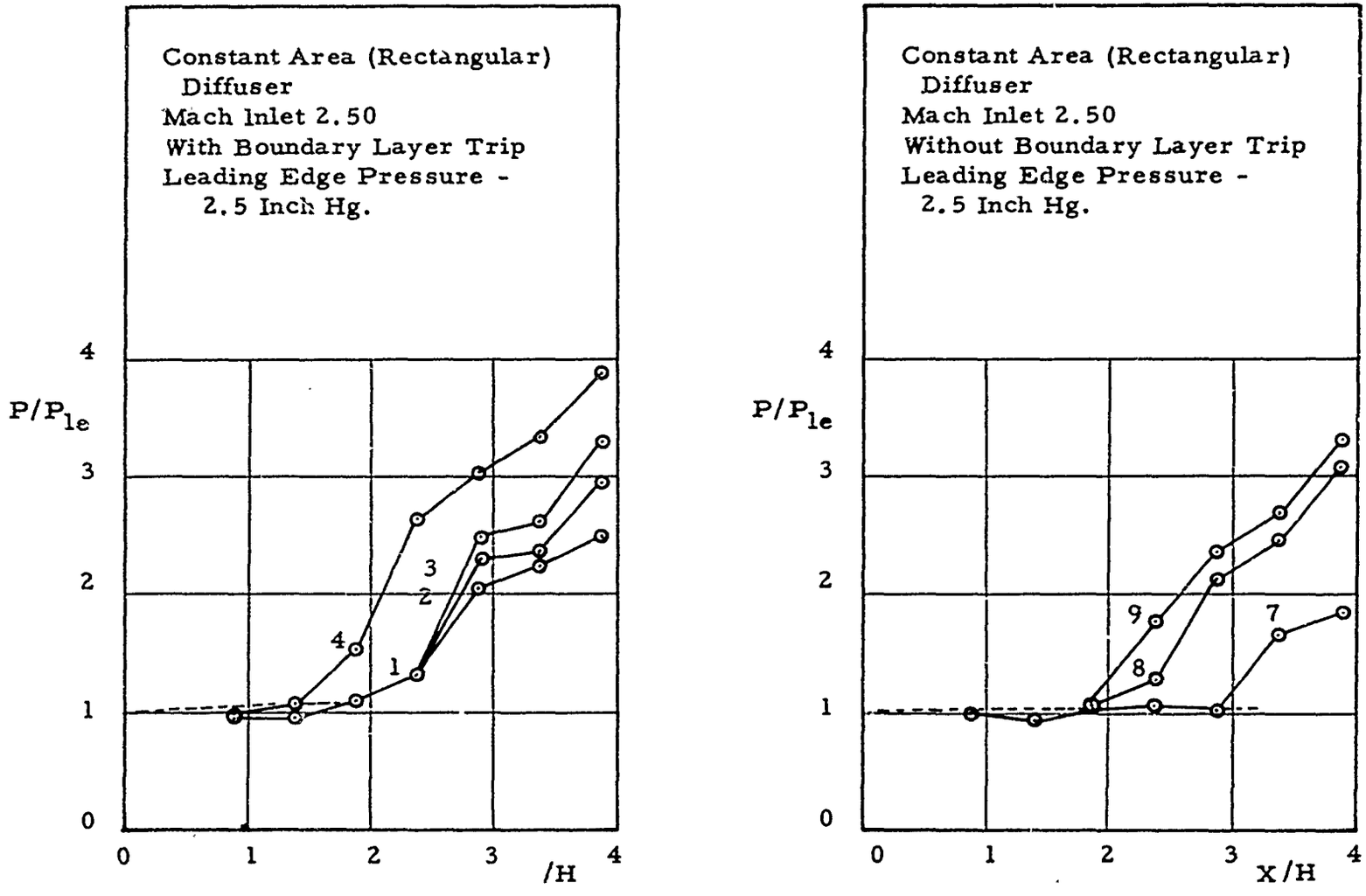

FIGURE 23 STATIC PRESSURE RATIO VERSUS LENGTH TO HEIGHT RATIO

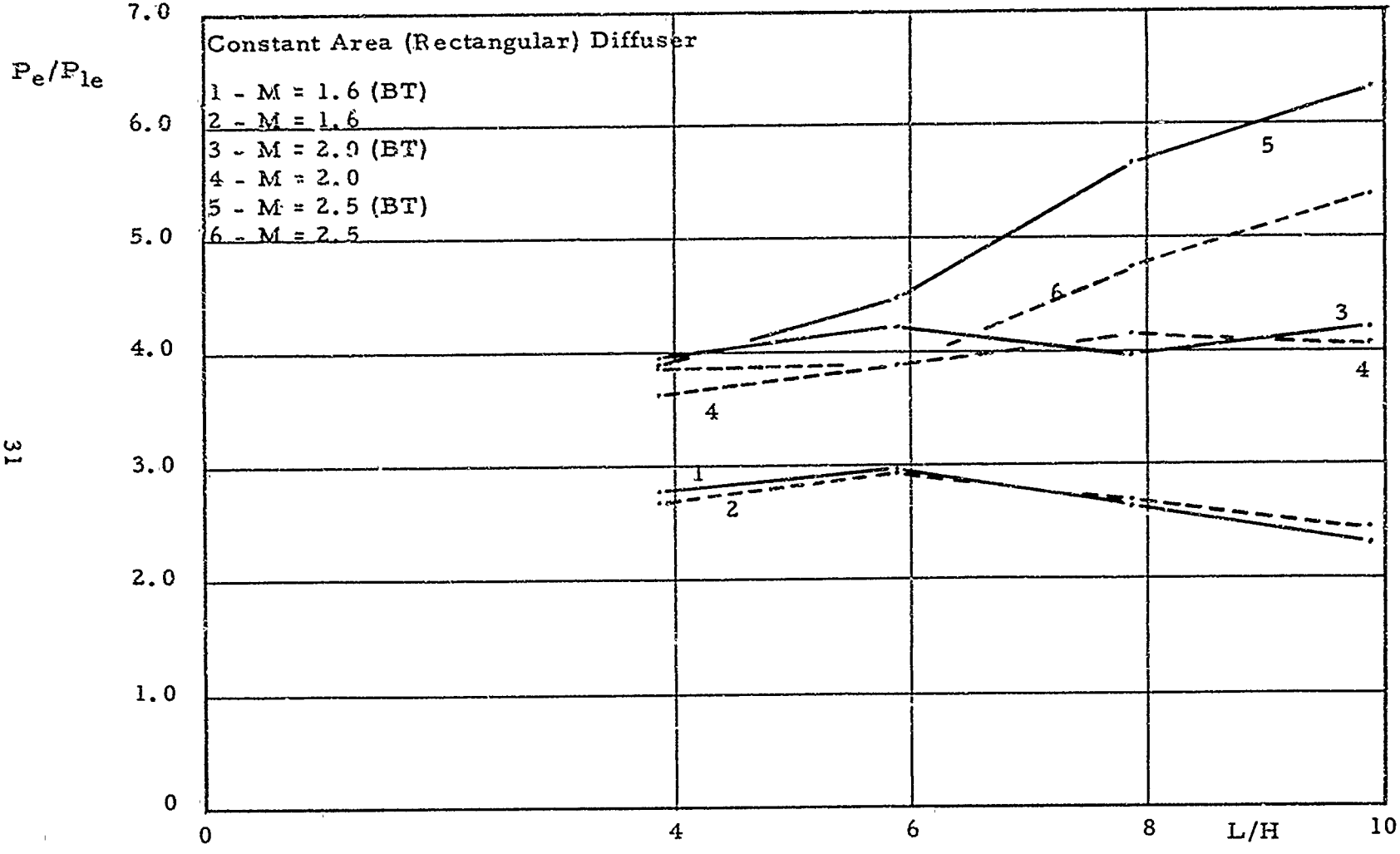

FIGURE 24 THE MAXIMUM STATIC PRESSURE RATIO (EXIT TO INLET) VERSUS THE LENGTH TO HEIGHT RATIO

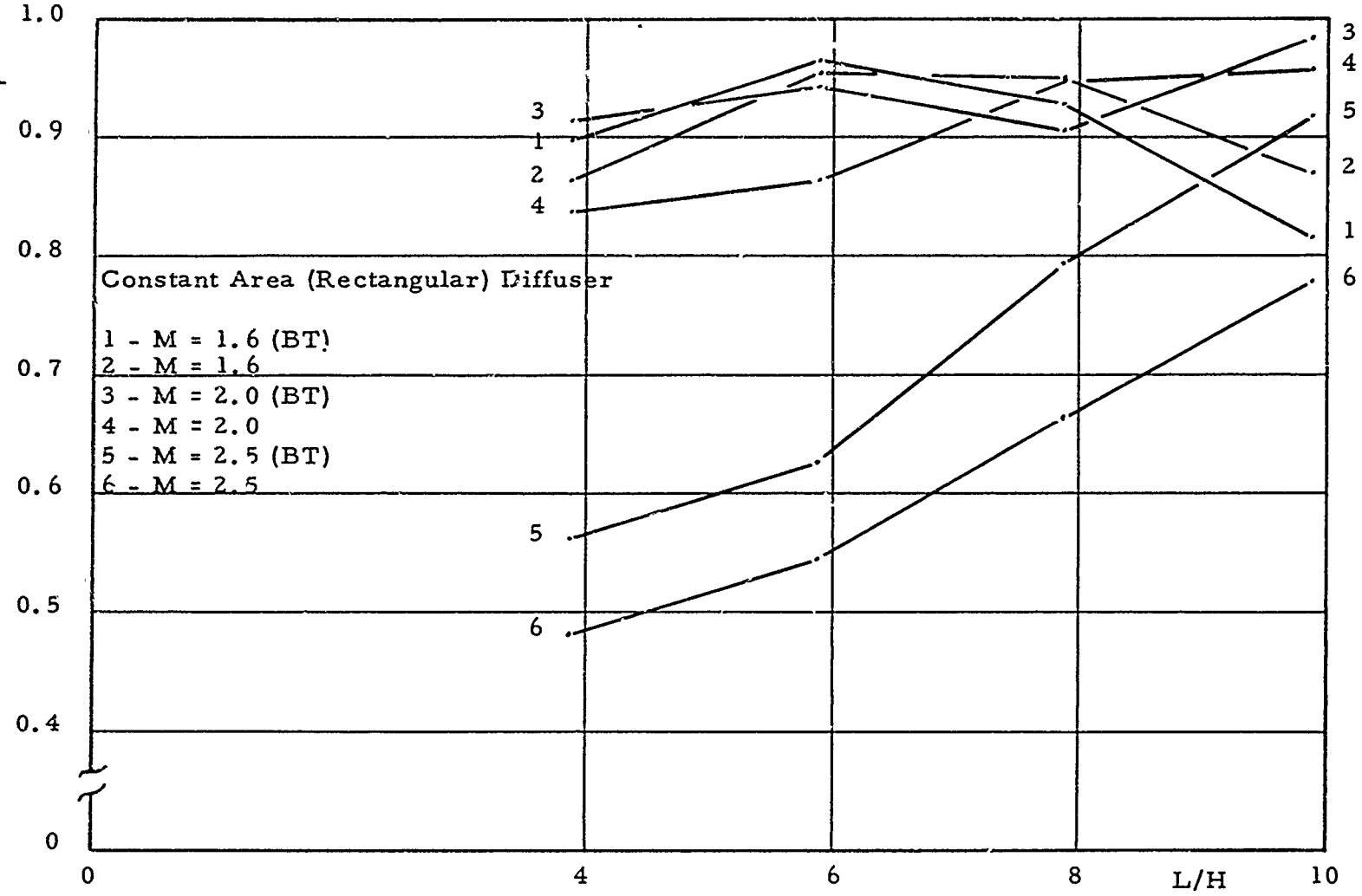

FIGURE 25 THE RATIO OF THE MAXIMUM STATIC PRESSURE RATIO (EXIT TO INLET) TO THE NORMAL SHOCK STATIC PRESSURE RATIO VERSUS THE LENGTH TO HEIGHT RATIO

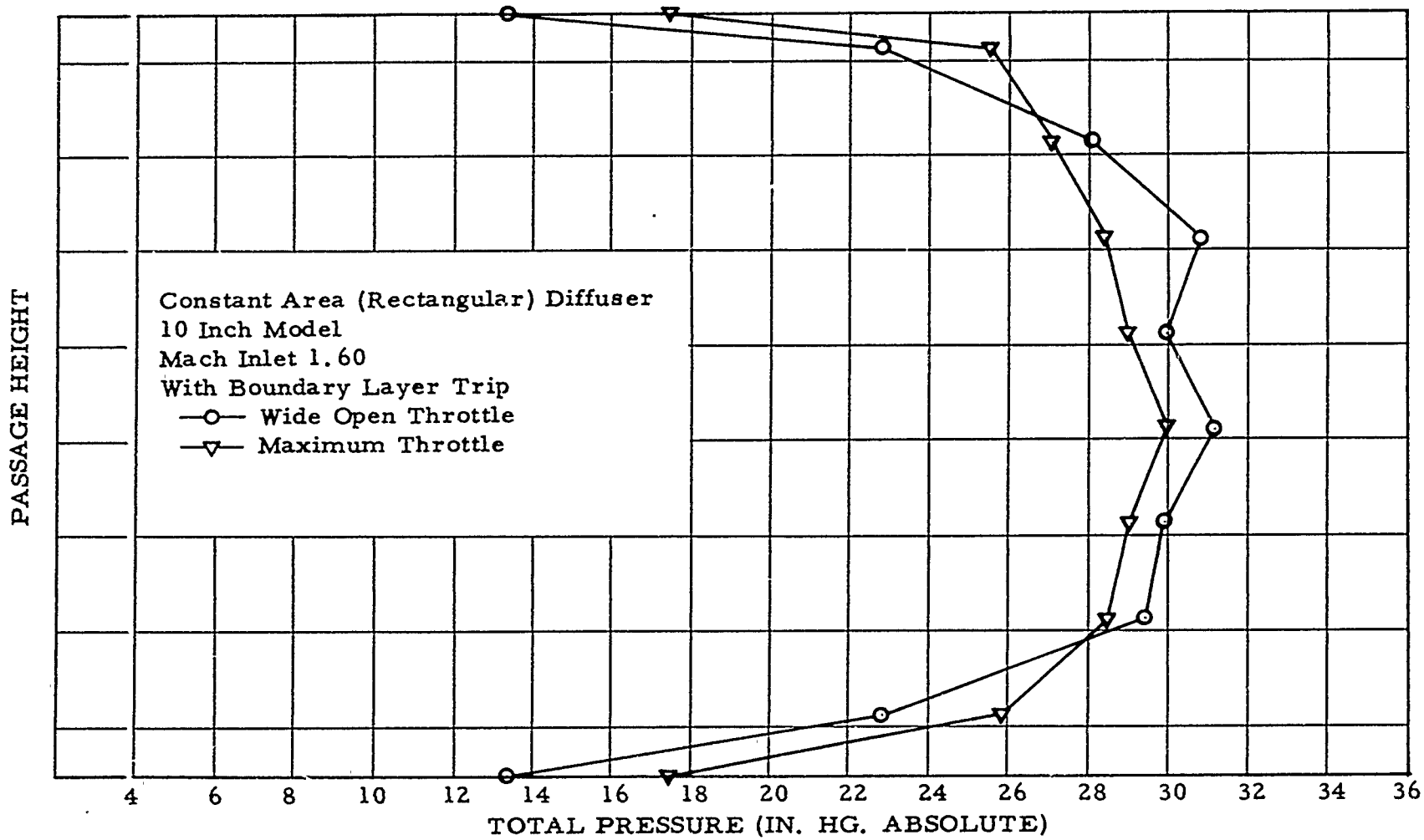

FIGURE 26 TOTAL PRESSURE DISTRIBUTION AT THE PASSAGE EXIT VERTICAL CENTER PLANE

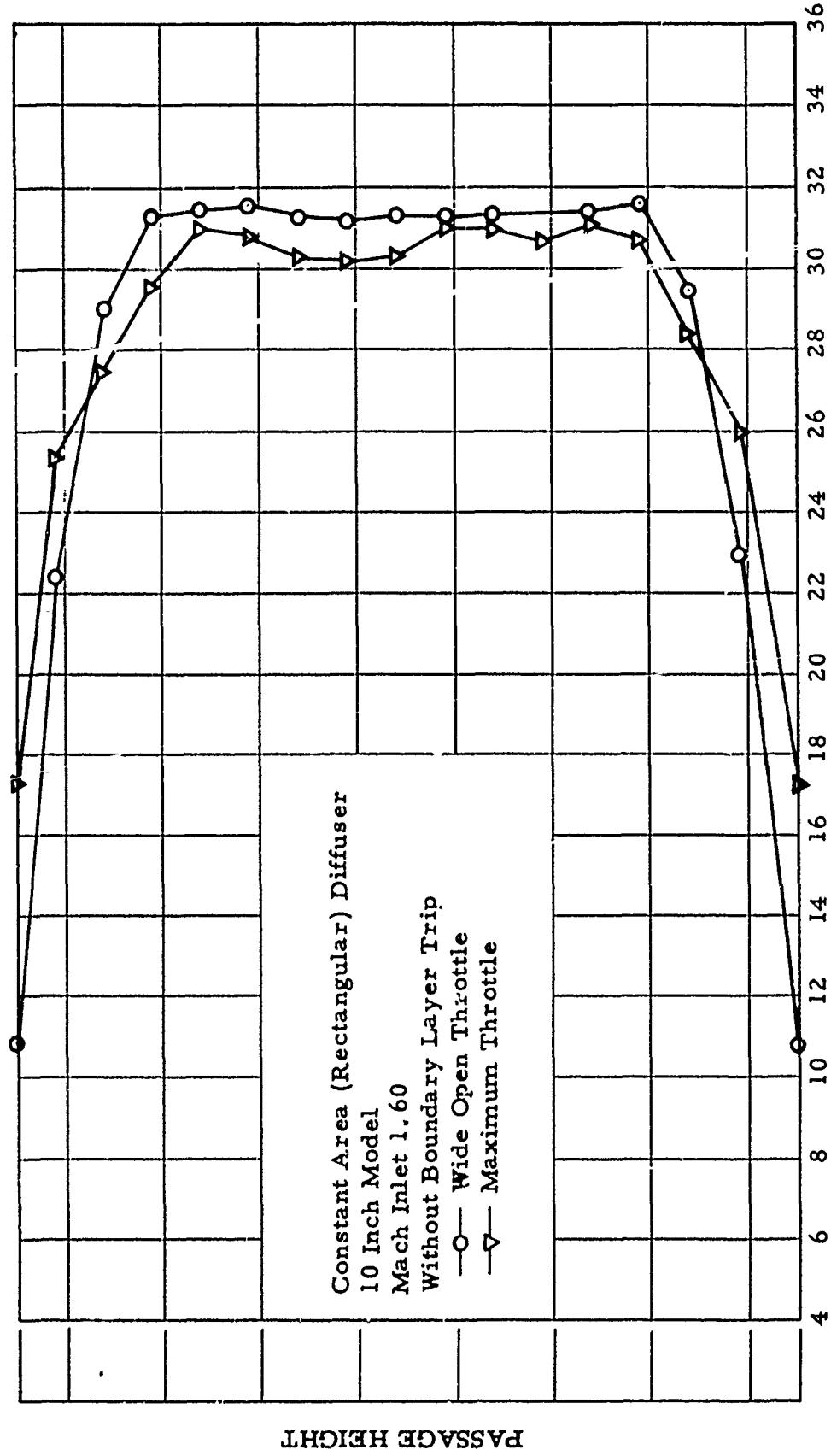

FIGURE 27 TOTAL PRESSURE DISTRIBUTION AT THE PASSAGE EXIT VERTICAL CENTER PLANE

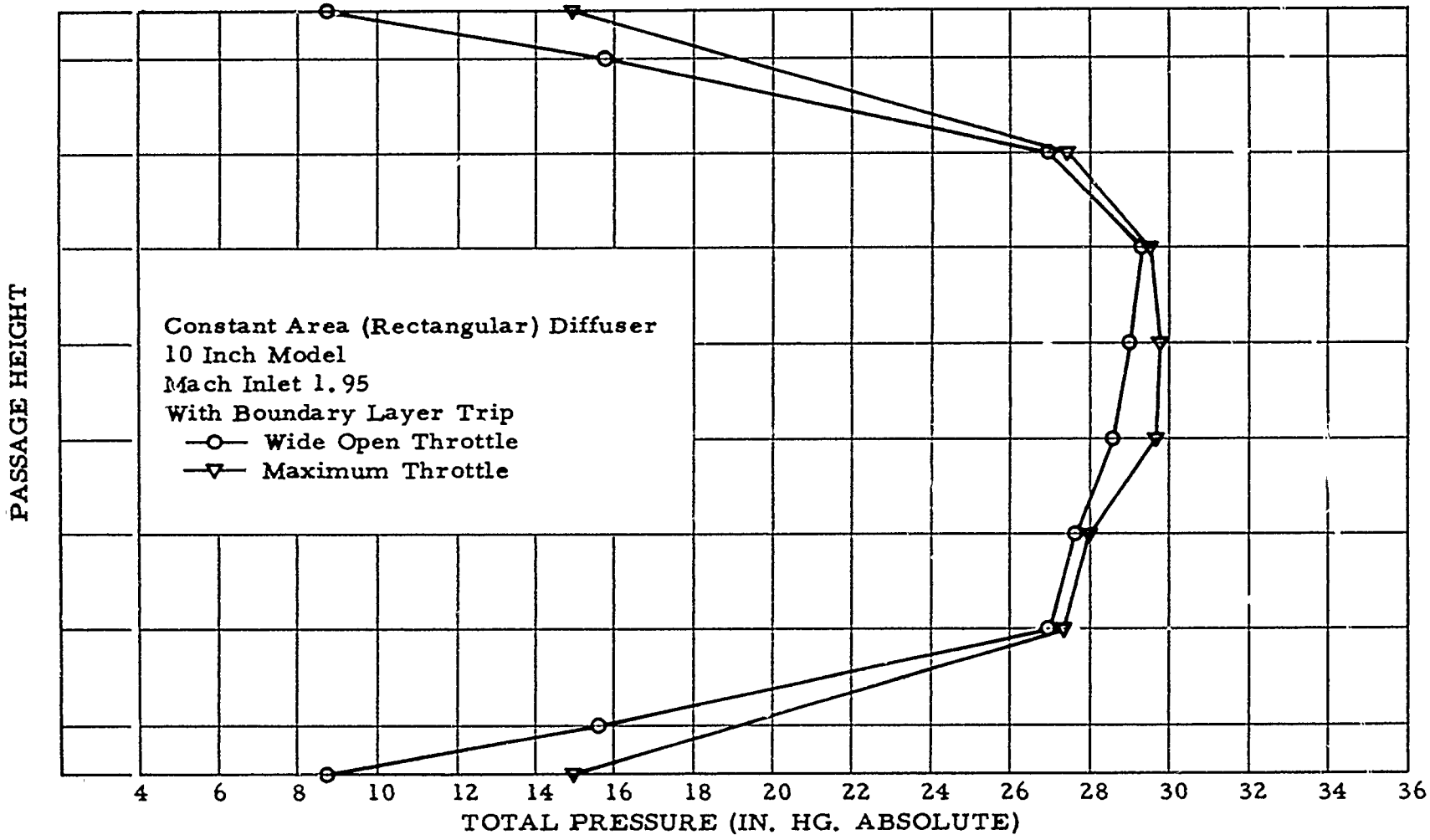

FIGURE 28 TOTAL PRESSURE DISTRIBUTION AT THE PASSAGE EXIT VERTICAL CENTER PLANE

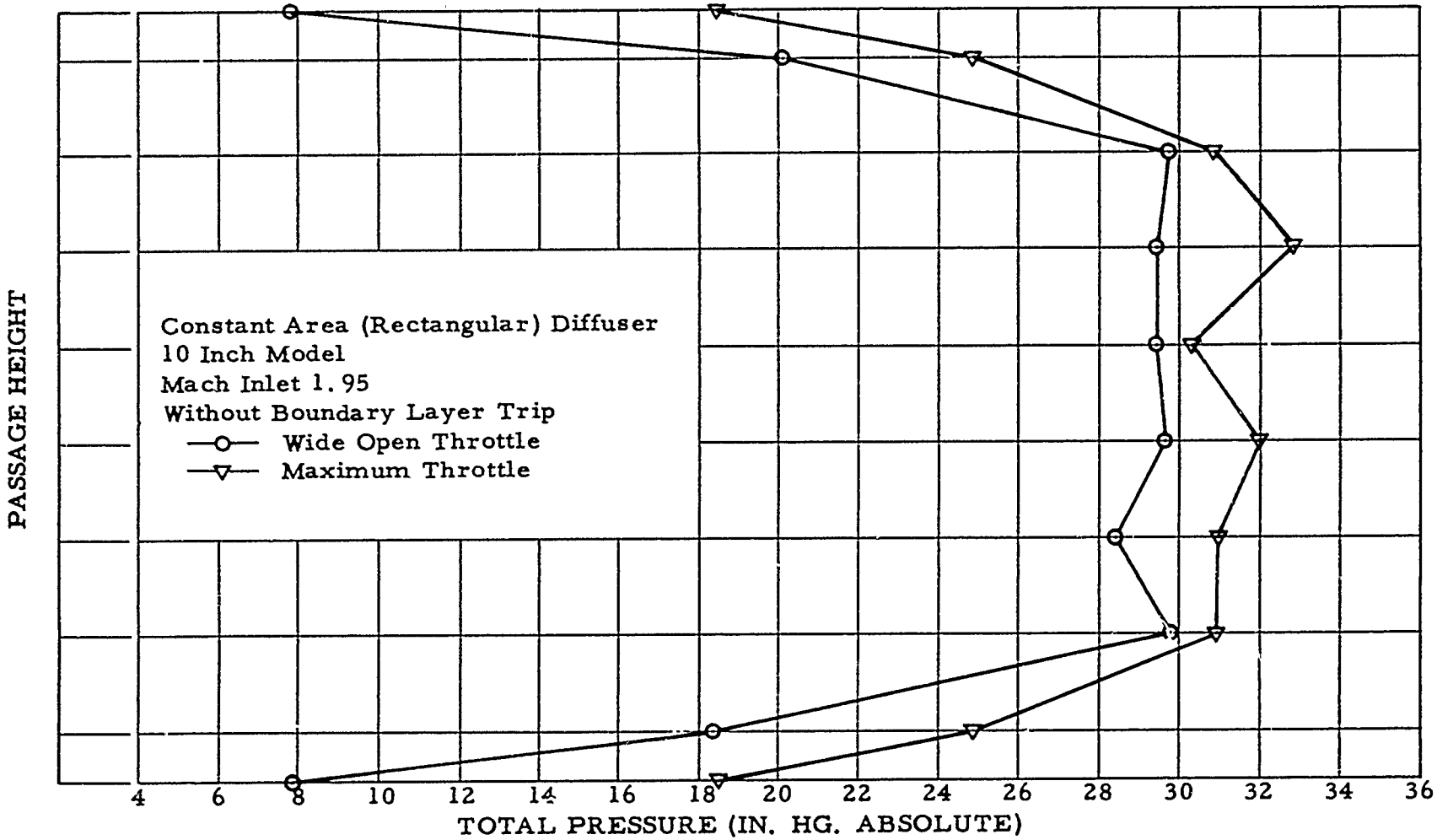

FIGURE 29 TOTAL PRESSURE DISTRIBUTION AT THE PASSAGE EXIT VERTICAL CENTER PLANE

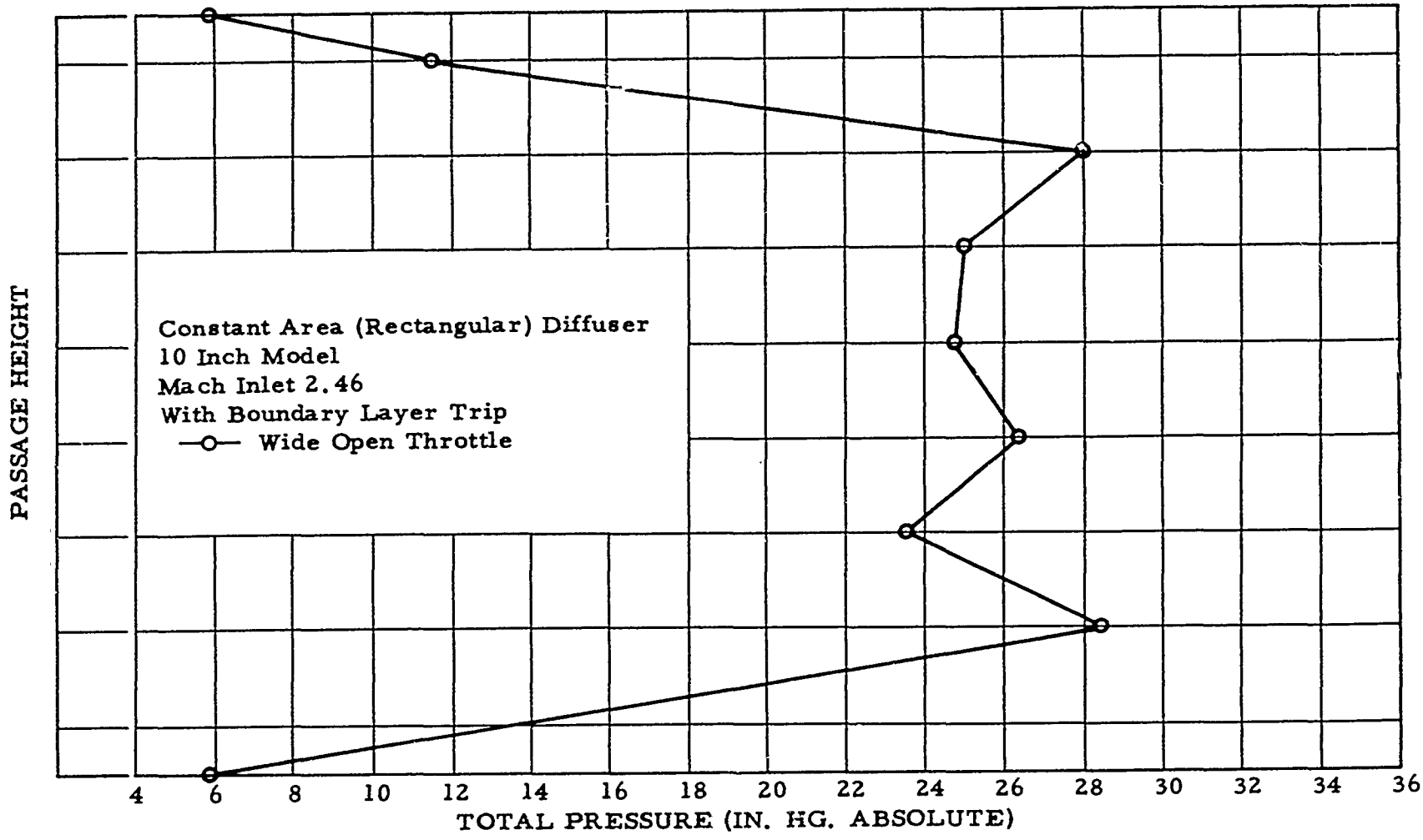

FIGURE 30 TOTAL PRESSURE DISTRIBUTION AT THE PASSAGE EXIT VERTICAL CENTER PLANE

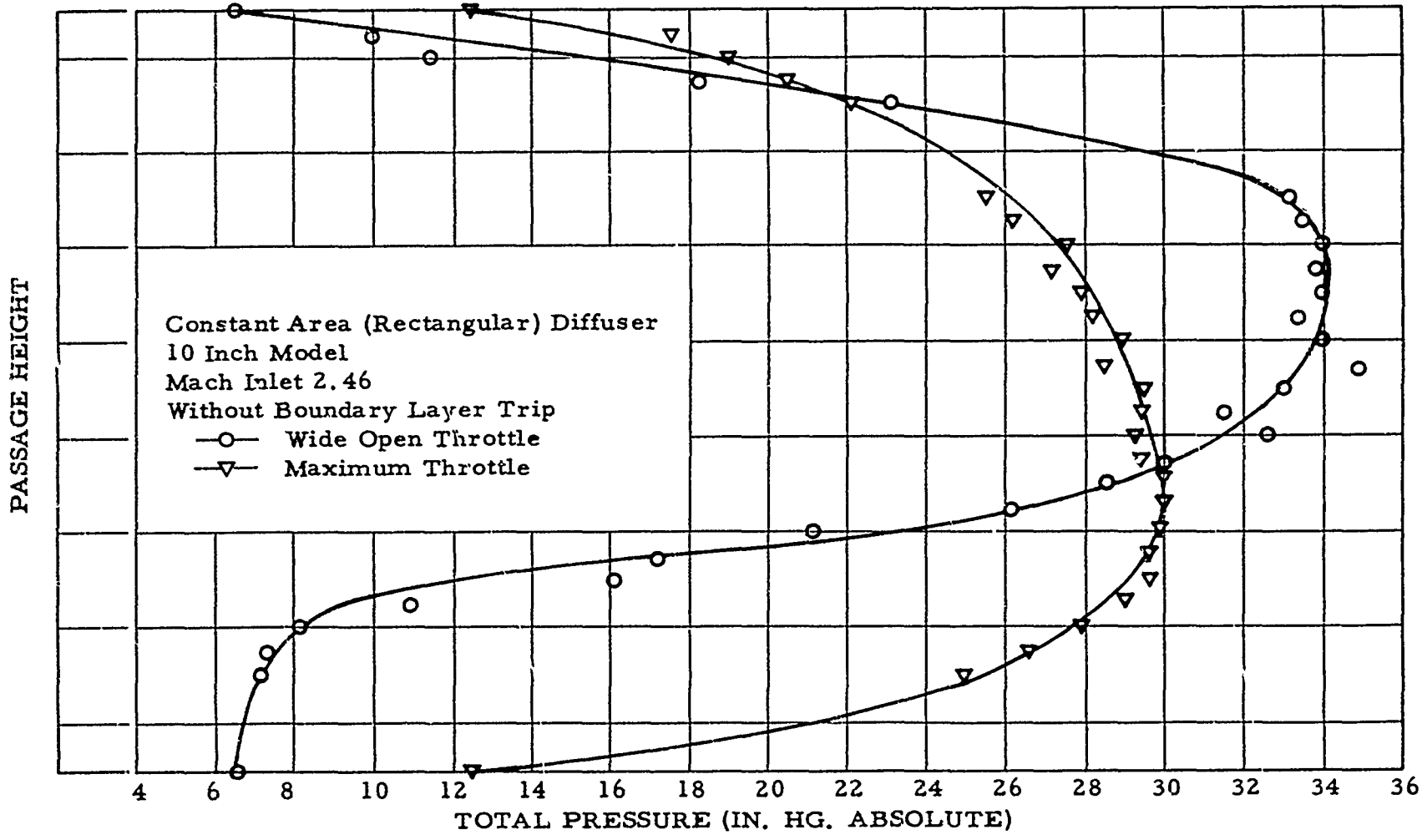

FIGURE 31 TOTAL PRESSURE DISTRIBUTION AT THE PASSAGE EXIT VERTICAL CENTER PLANE

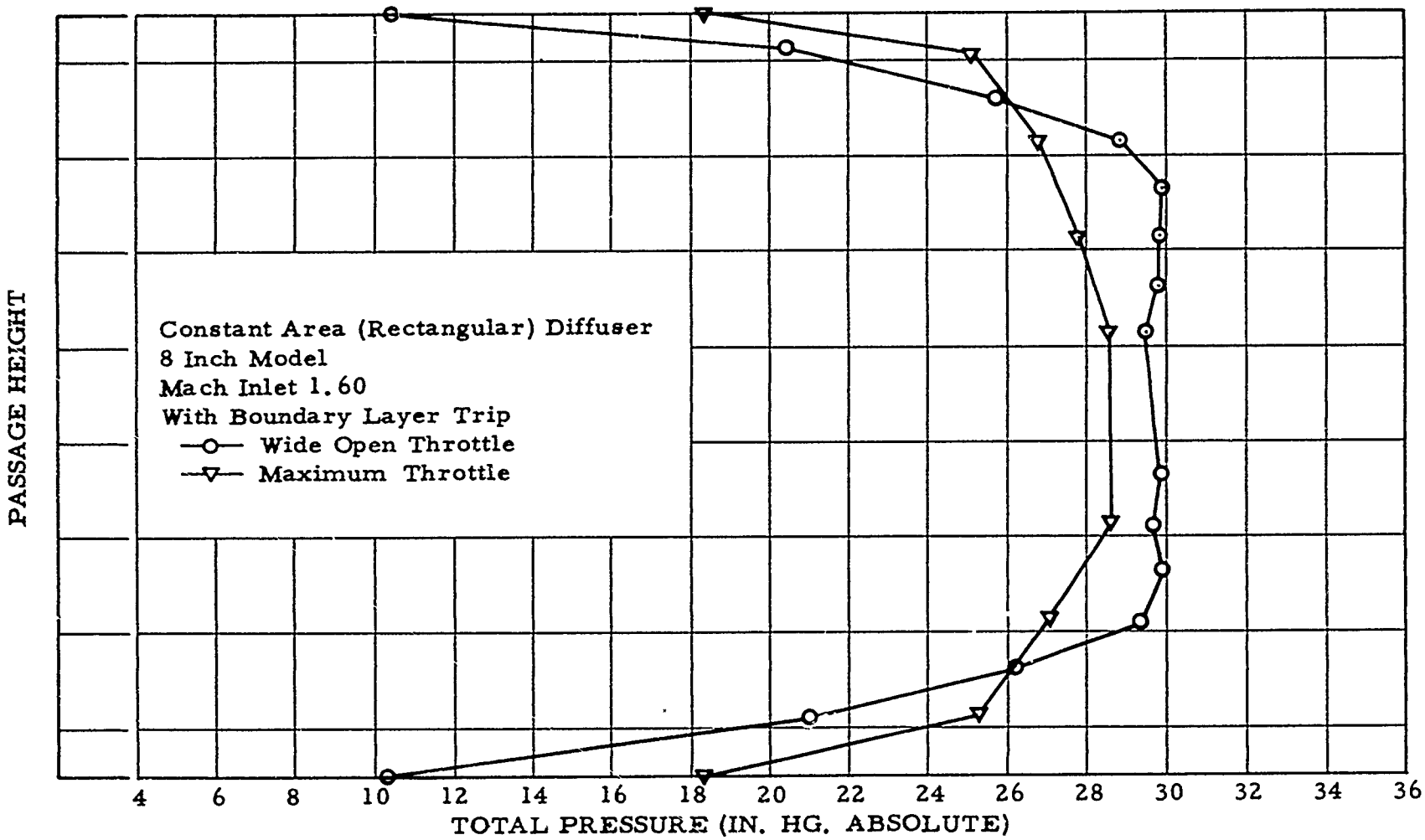

FIGURE 32 TOTAL PRESSURE DISTRIBUTION AT THE PASSAGE EXIT VERTICAL CENTER PLANE

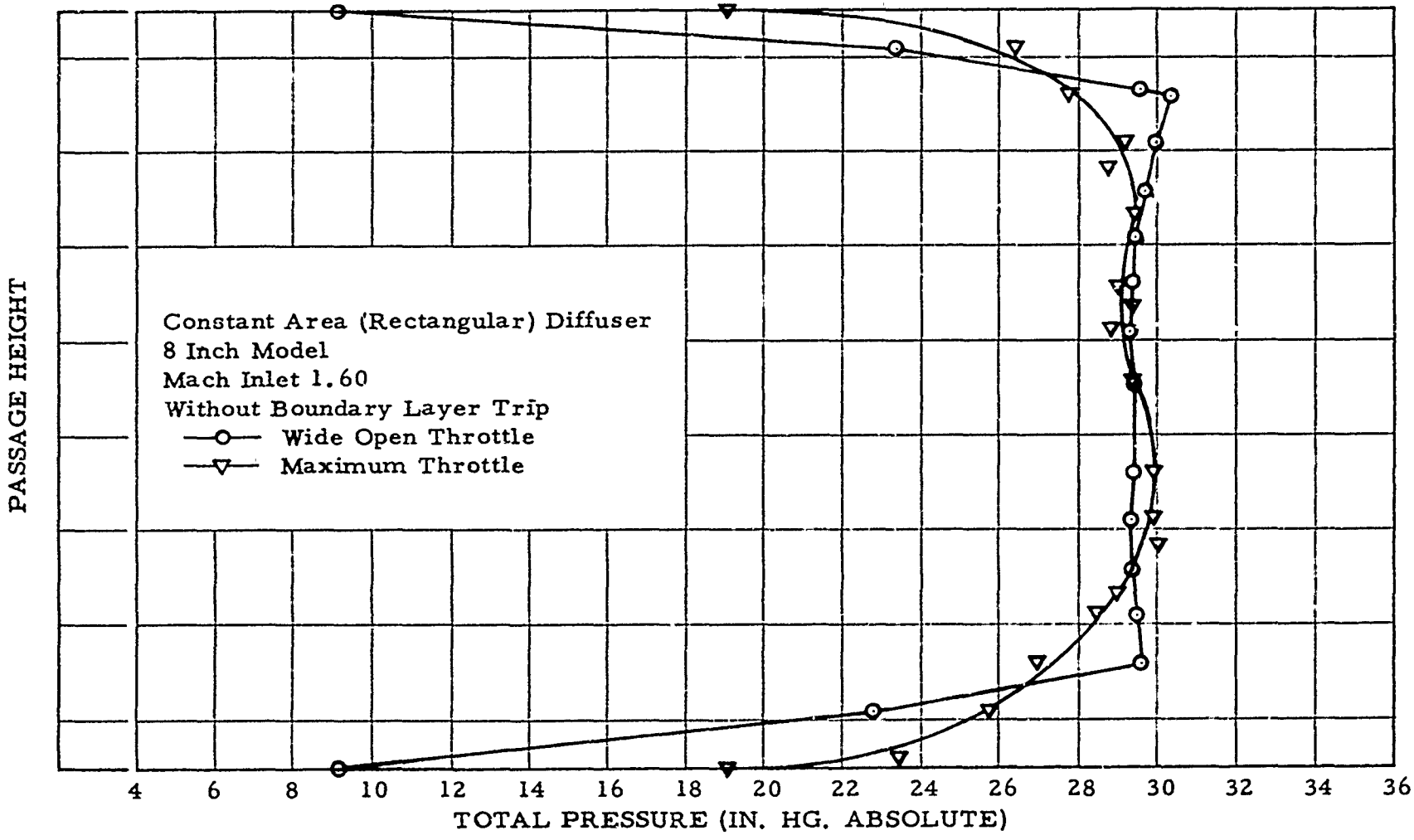

FIGURE 33 TOTAL PRESSURE DISTRIBUTION AT THE PASSAGE EXIT VERTICAL CENTER PLANE

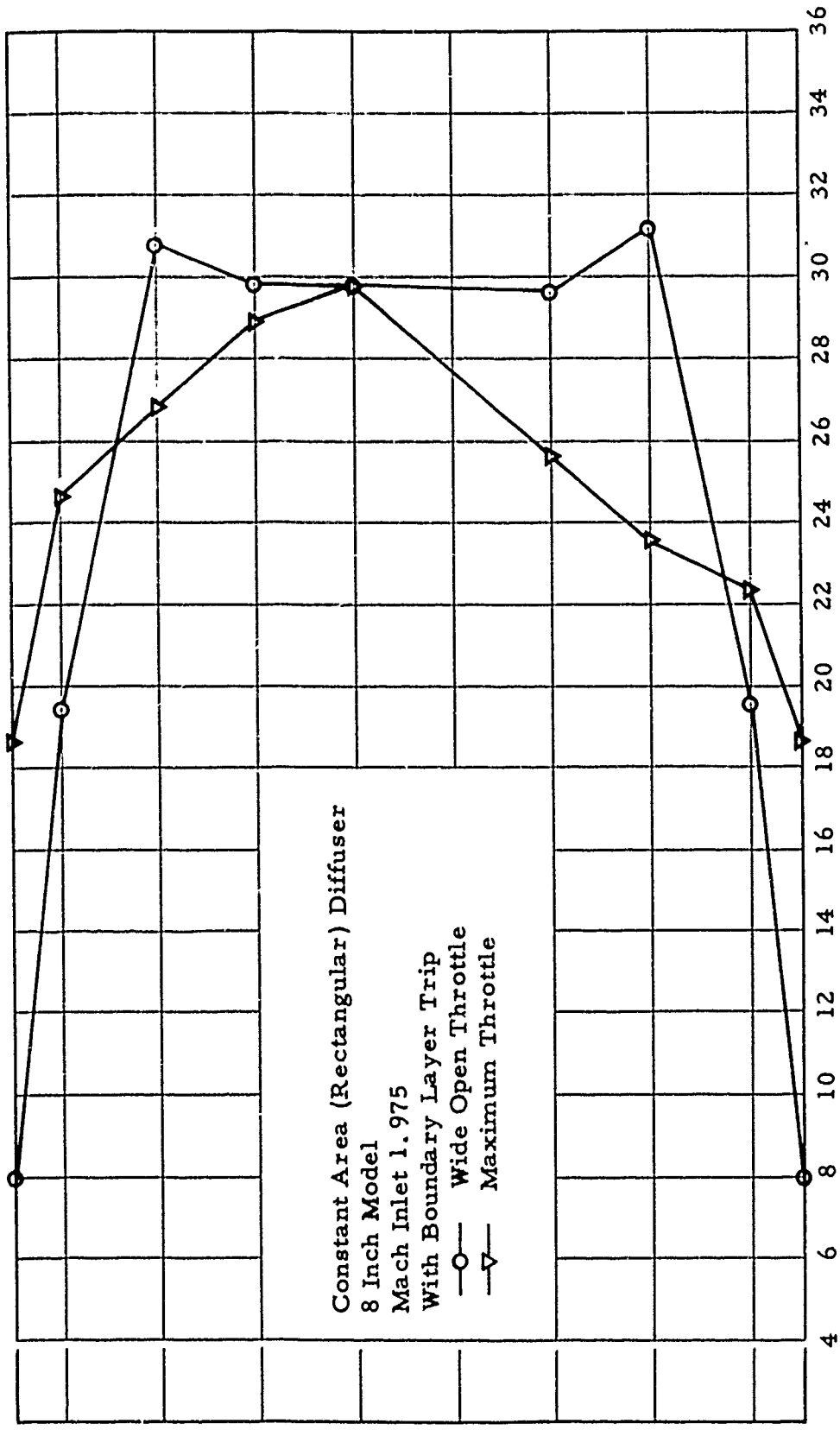

FIGURE 34 TOTAL PRESSURE DISTRIBUTION AT THE PASSAGE EXIT VERTICAL CENTER PLANE

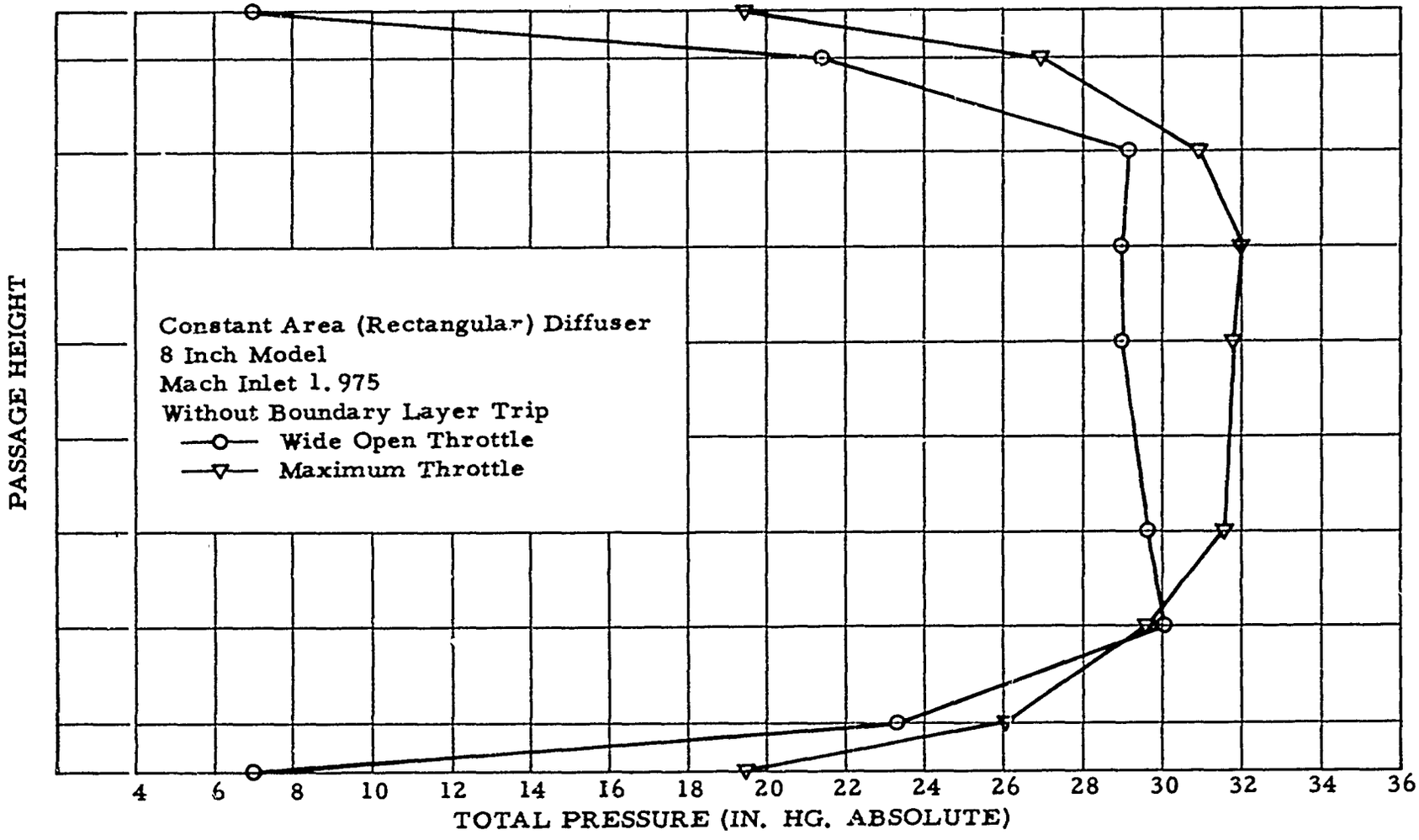

FIGURE 35 TOTAL PRESSURE DISTRIBUTION AT THE PASSAGE EXIT VERTICAL CENTER PLANE

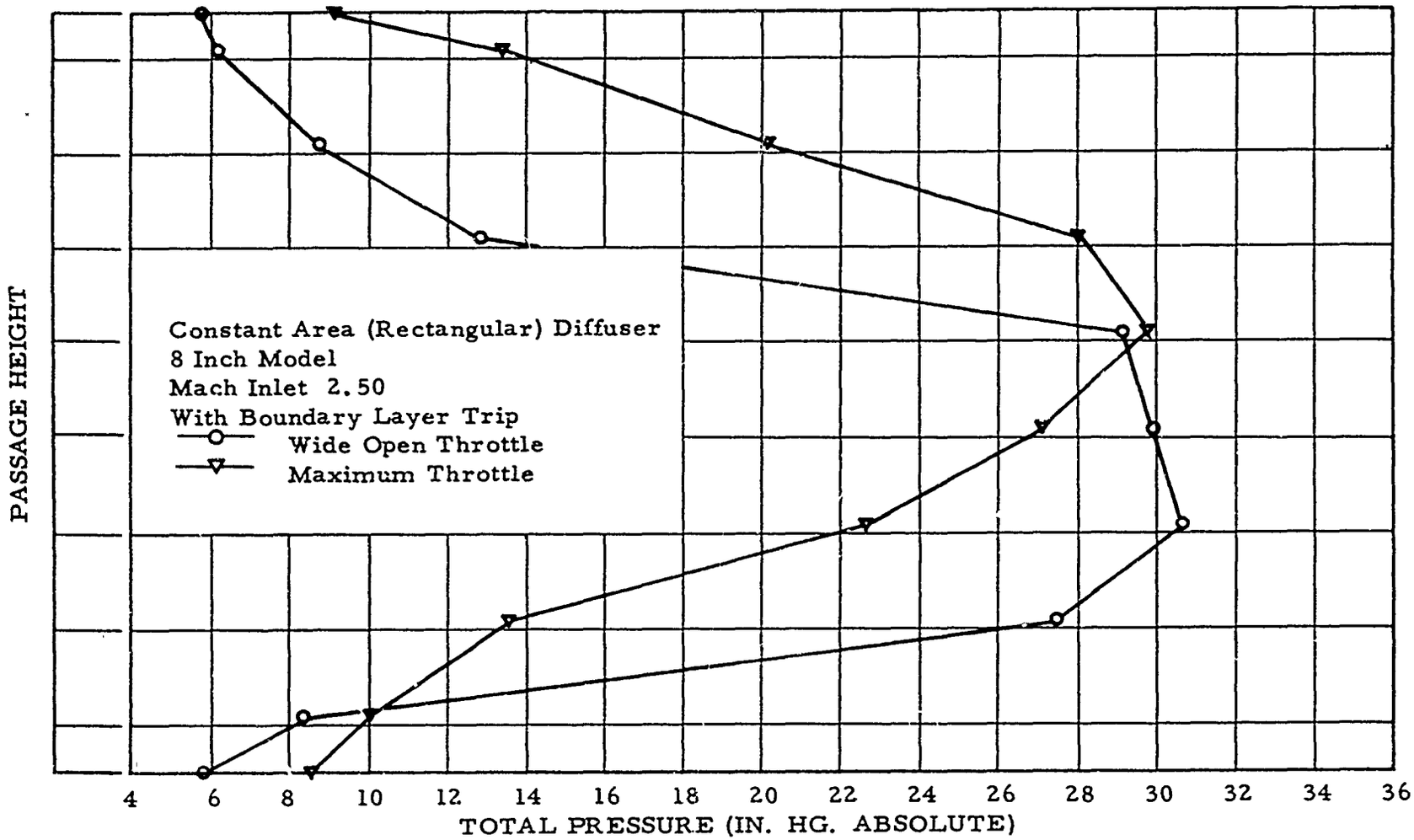

FIGURE 36 TOTAL PRESSURE DISTRIBUTION AT THE PASSAGE EXIT VERTICAL CENTER PLANE

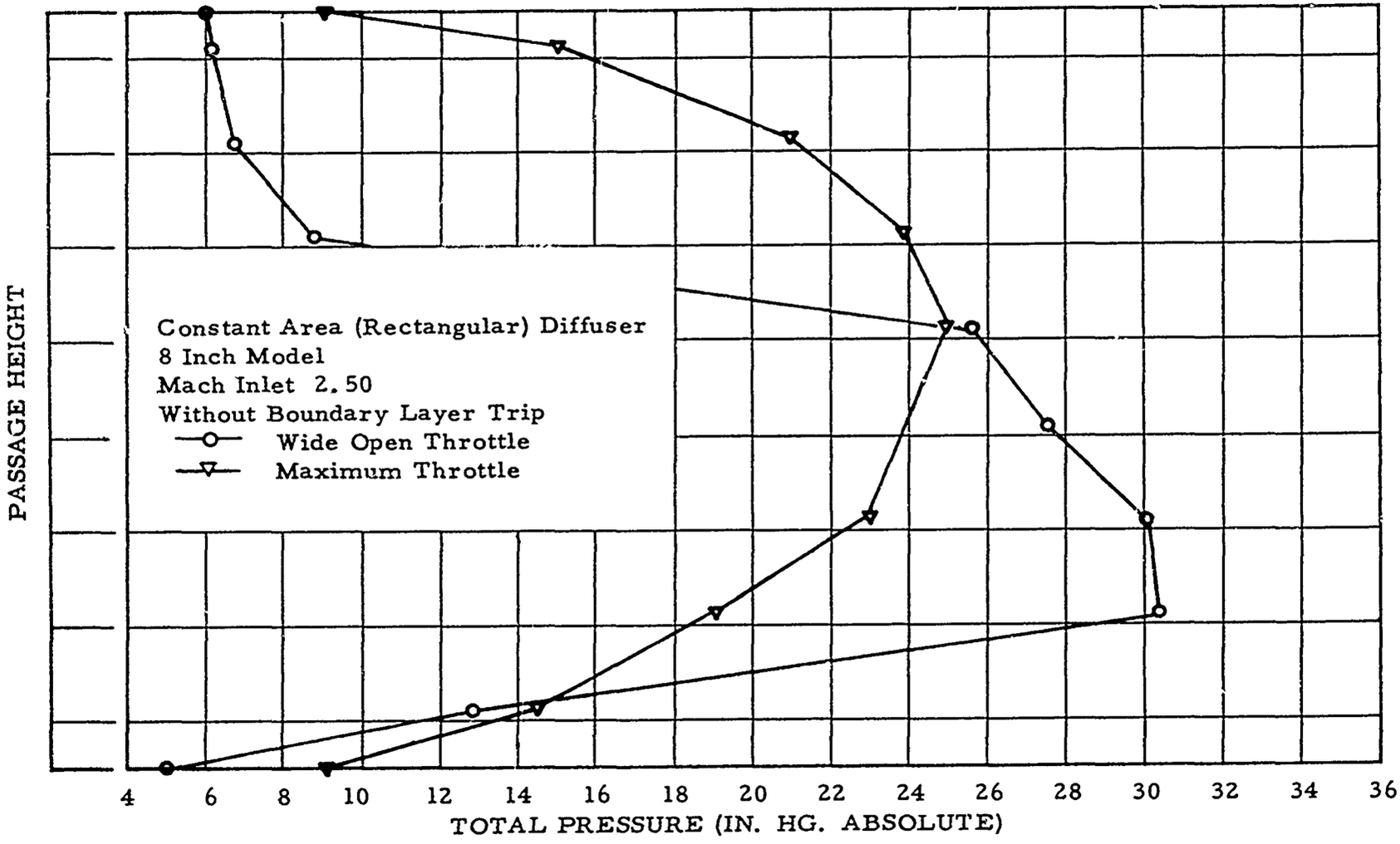

FIGURE 37 TOTAL PRESSURE DISTRIBUTION AT THE PASSAGE EXIT VERTICAL CENTER PLANE

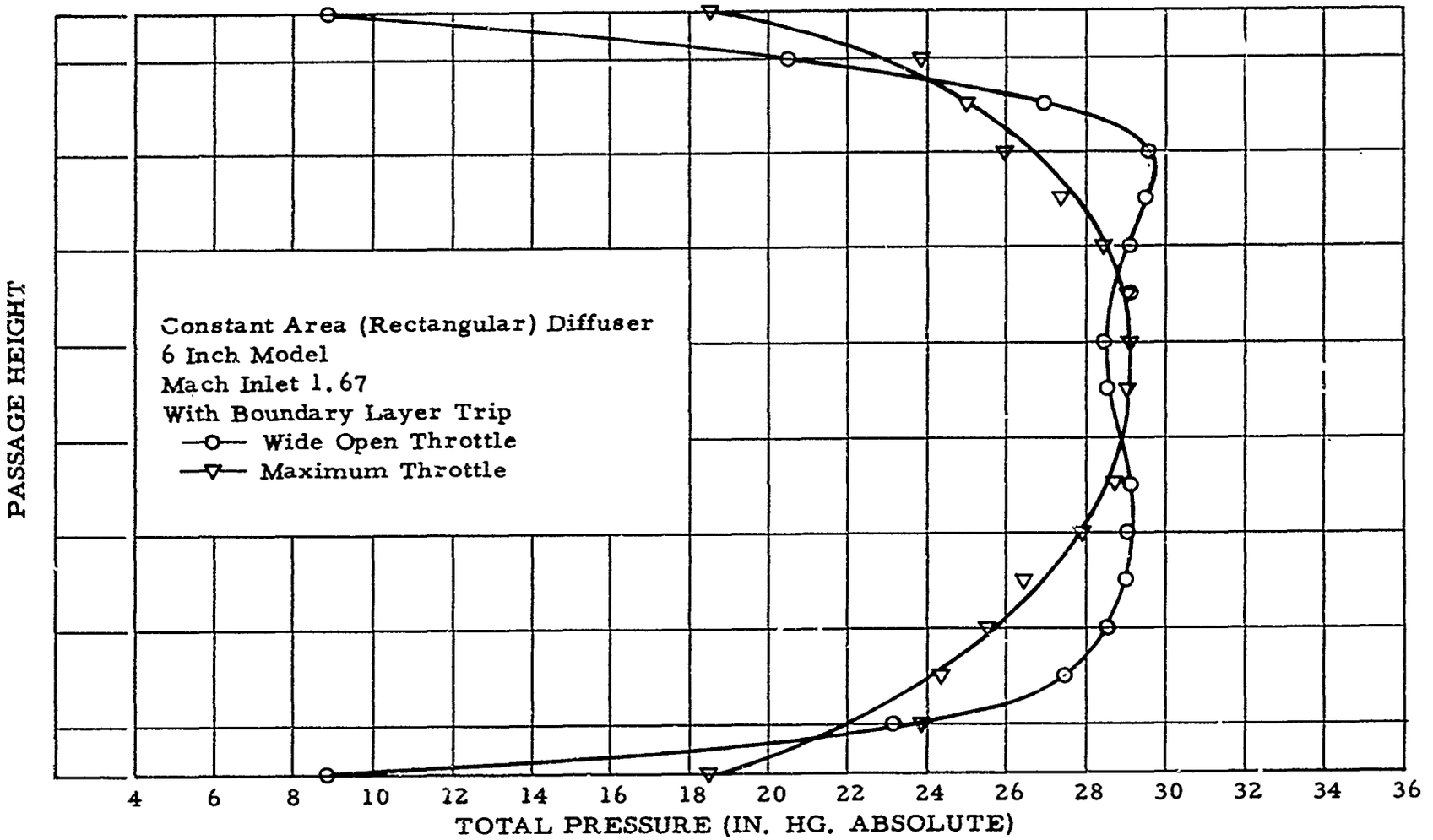

FIGURE 38 TOTAL PRESSURE DISTRIBUTION AT THE PASSAGE EXIT VERTICAL CENTER PLANE

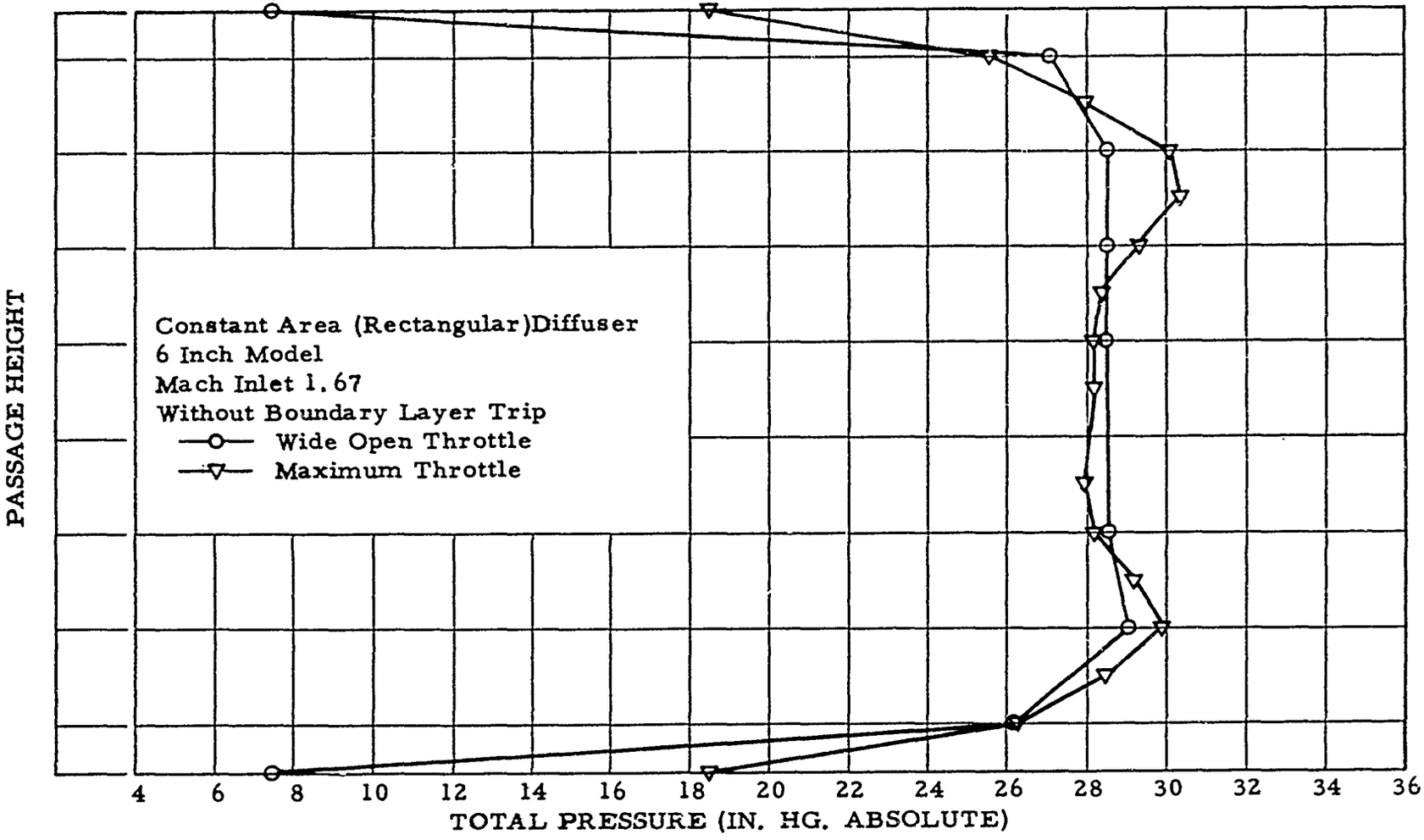

FIGURE 39 TOTAL PRESSURE DISTRIBUTION AT THE PASSAGE EXIT VERTICAL CENTER PLANE

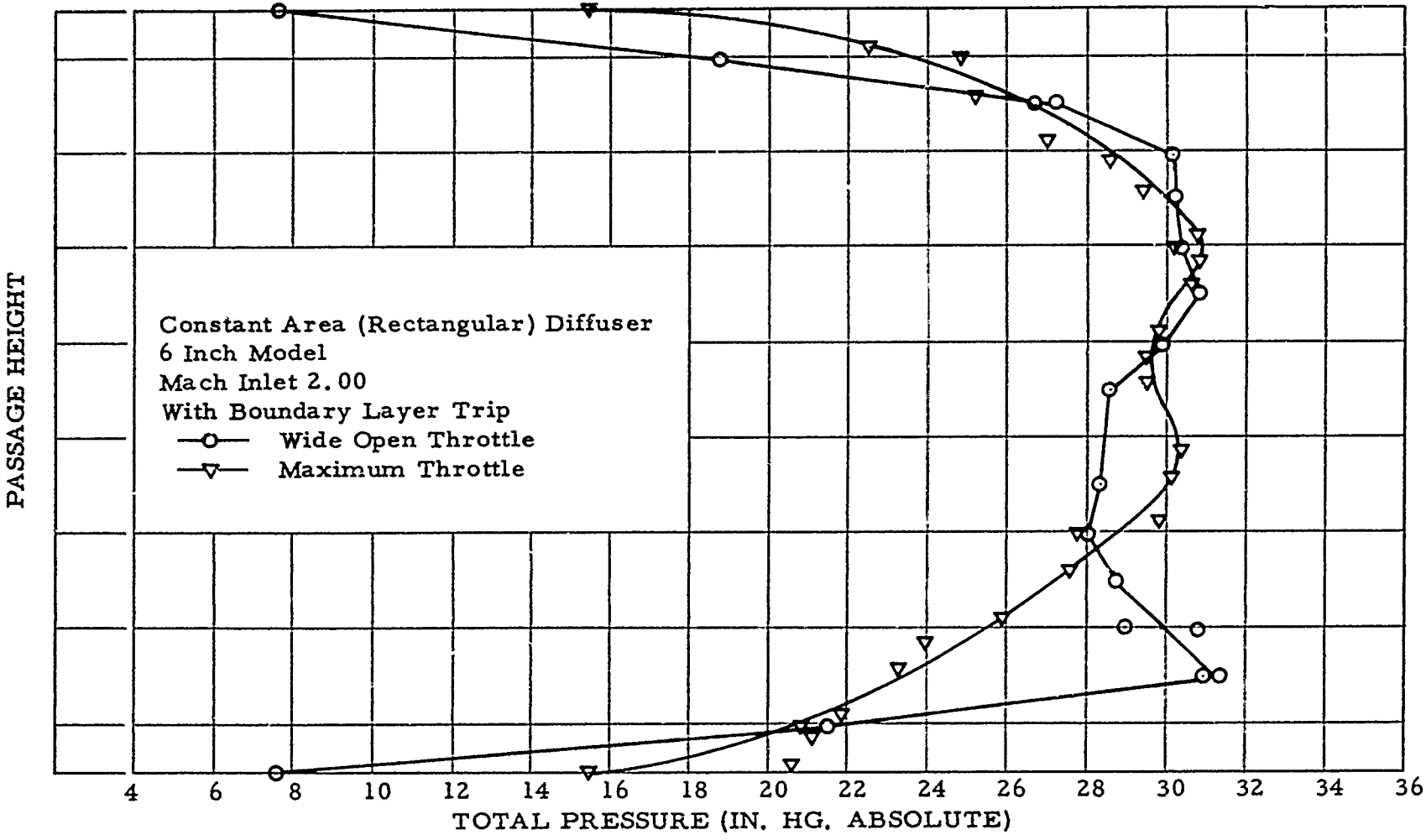

FIGURE 40 TOTAL PRESSURE DISTRIBUTION AT THE PASSAGE EXIT VERTICAL CENTER PLANE

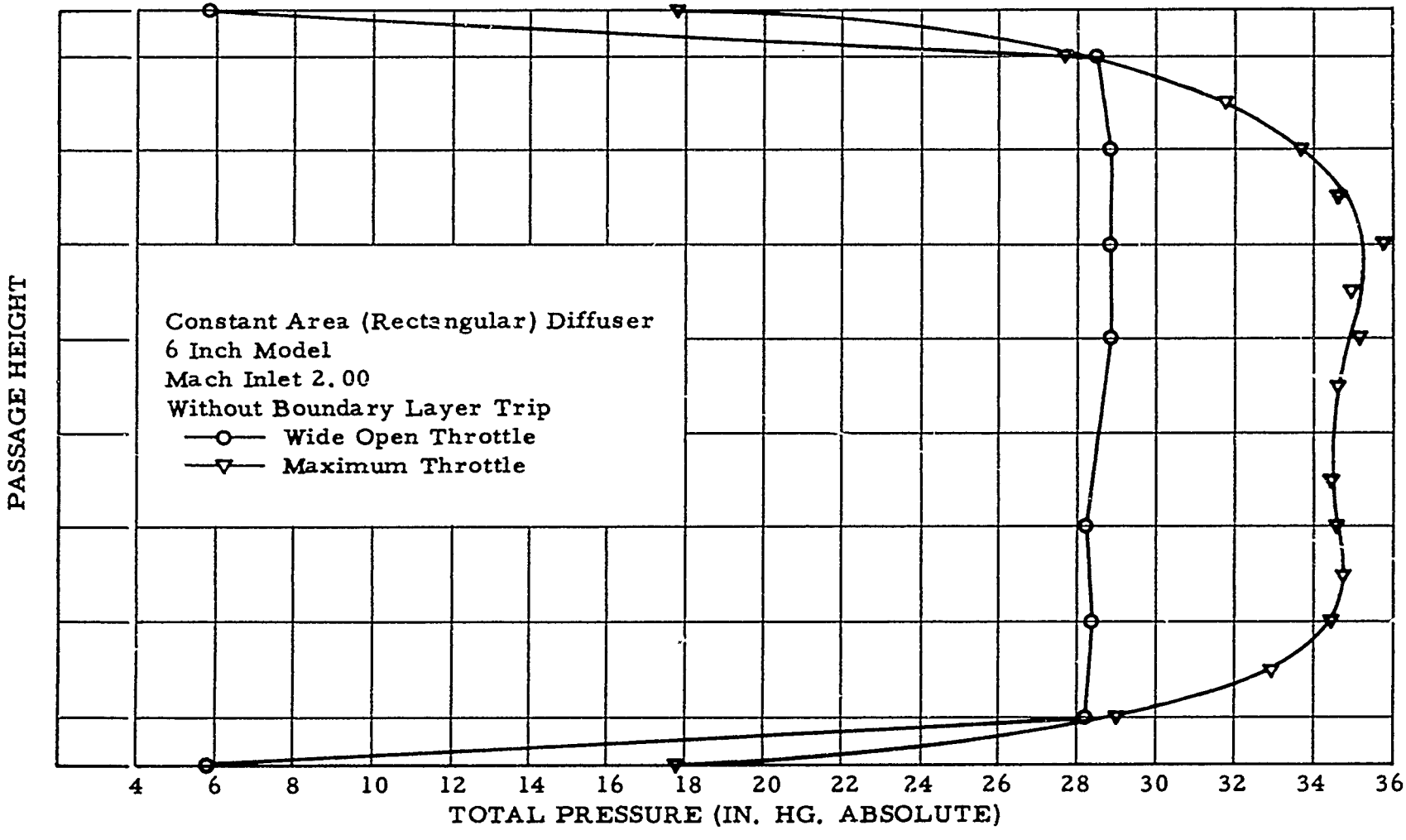

FIGURE 41 TOTAL PRESSURE DISTRIBUTION AT THE PASSAGE EXIT VERTICAL CENTER PLANE

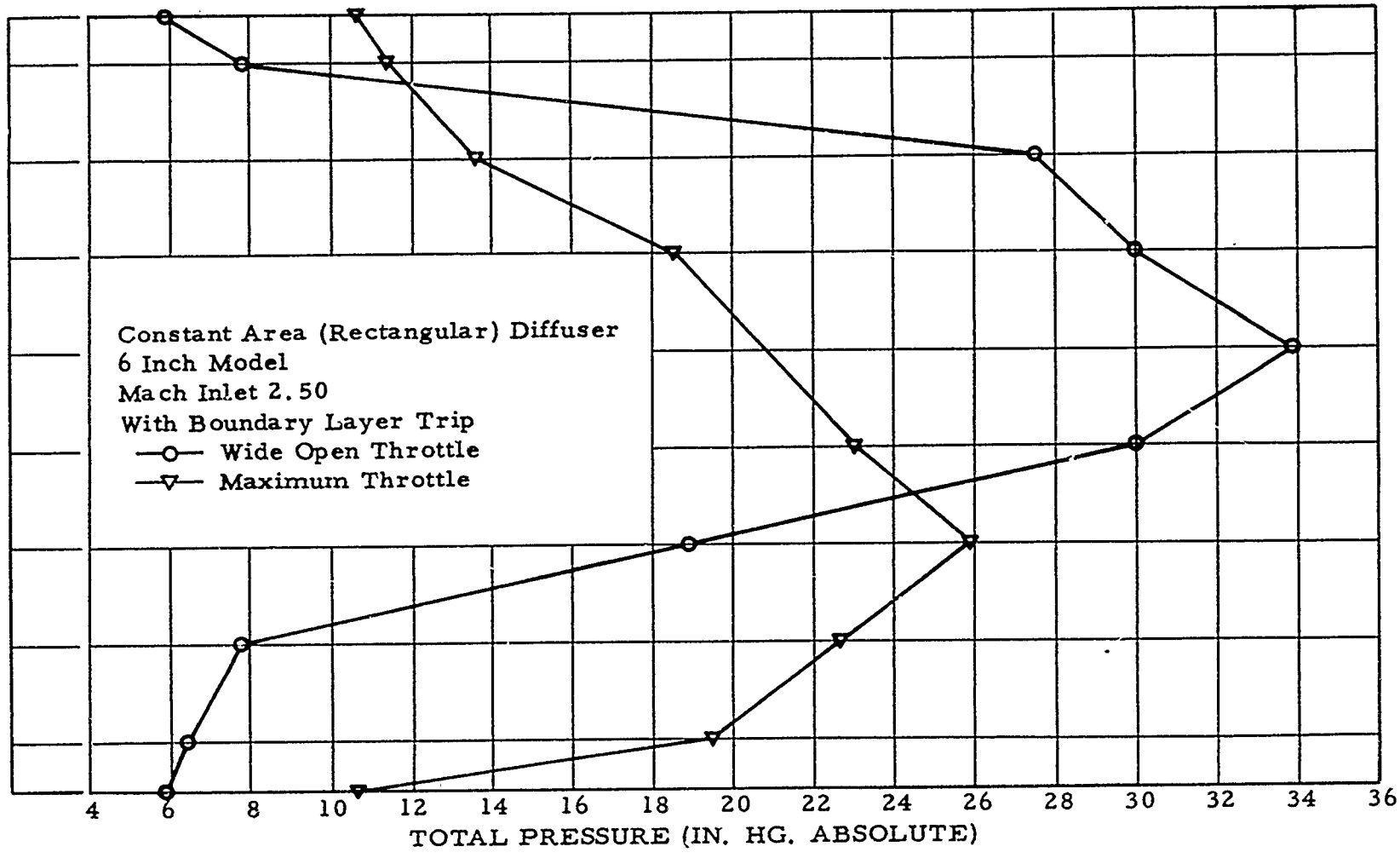

FIGURE 42 TOTAL PRESSURE DISTRIBUTION AT THE PASSAGE EXIT VERTICAL CENTER PLANE

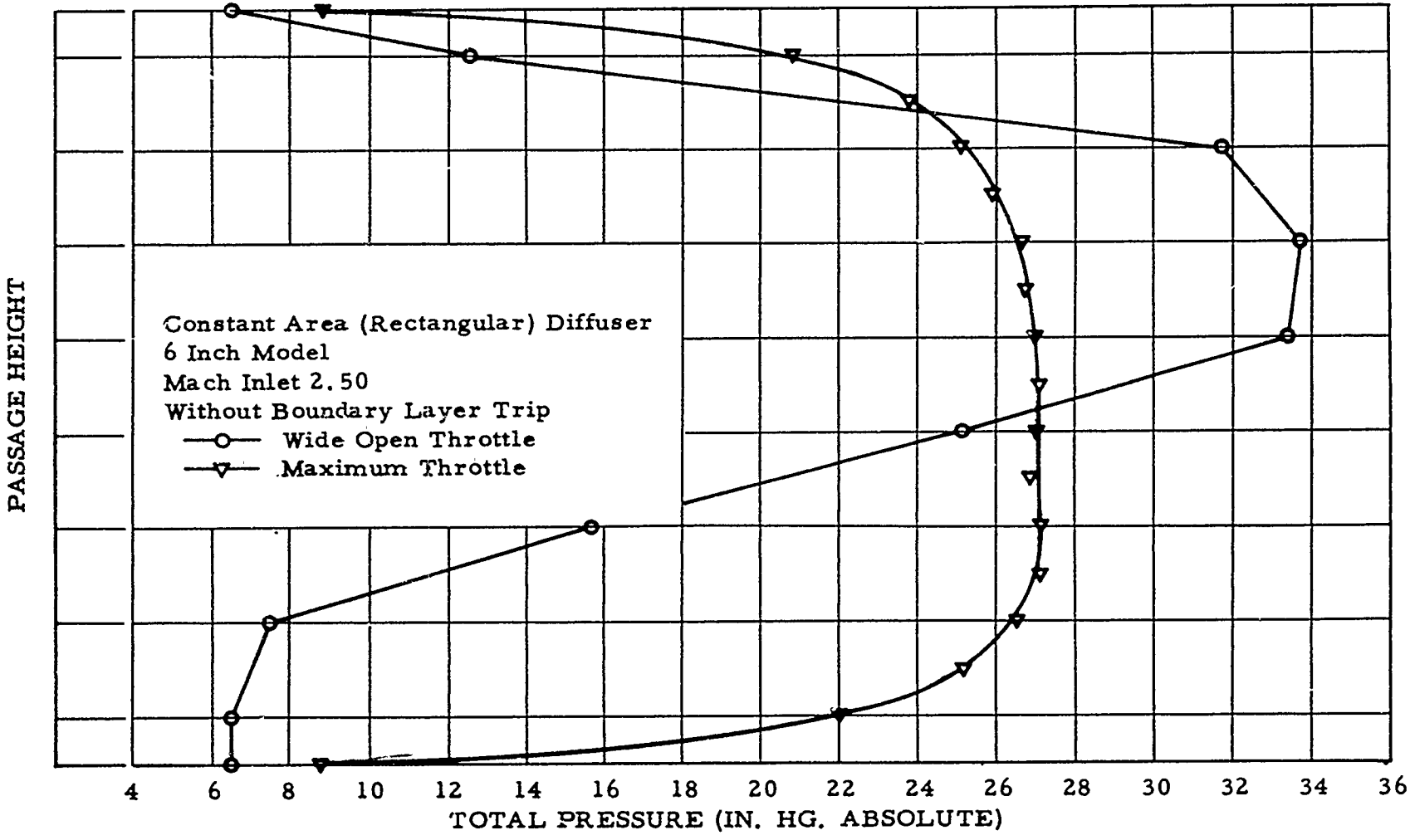

FIGURE 43 TOTAL PRESSURE DISTRIBUTION AT THE PASSAGE EXIT VERTICAL CENTER PLANE

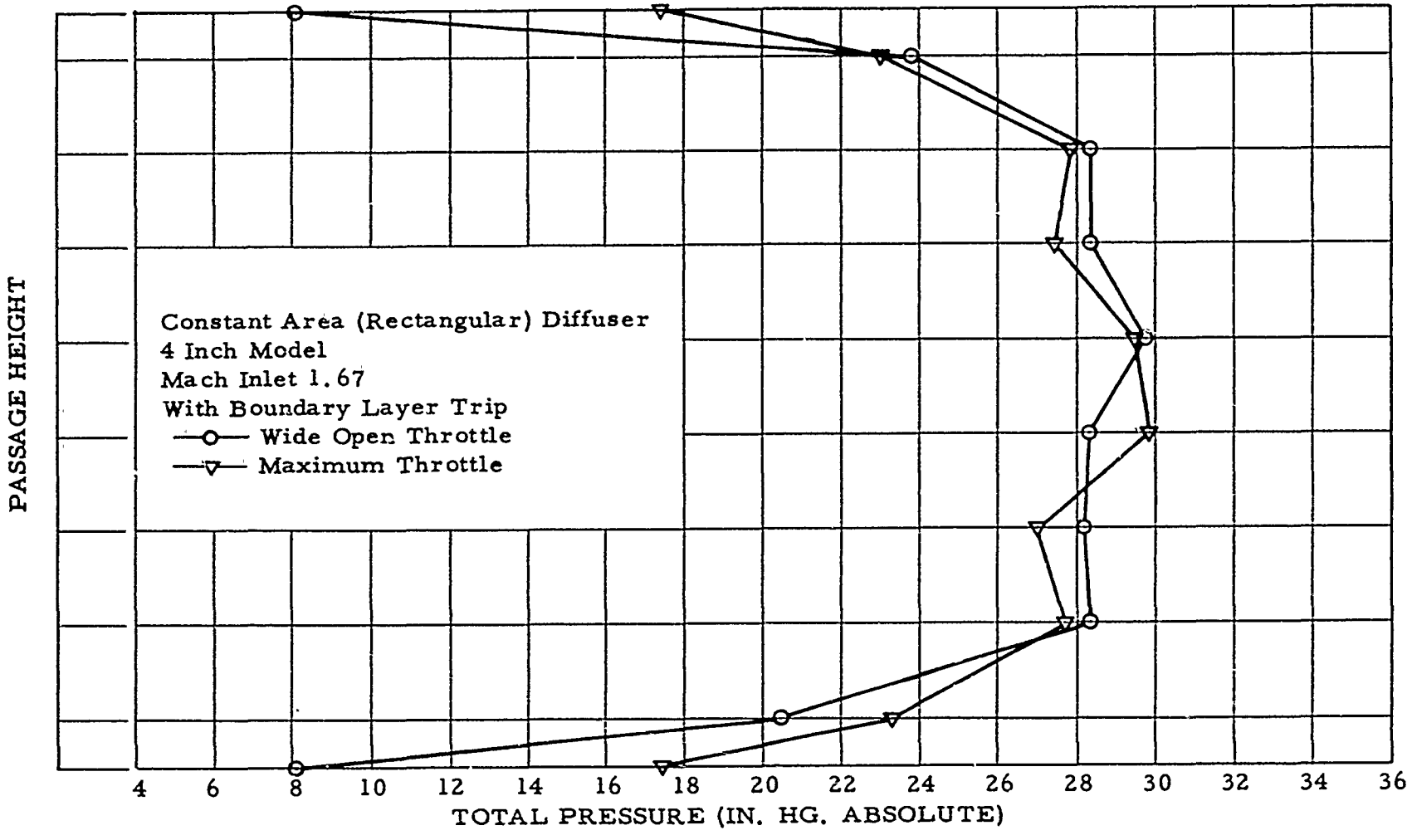

FIGURE 44 TOTAL PRESSURE DISTRIBUTION AT THE PASSAGE EXIT VERTICAL CENTER PLANE

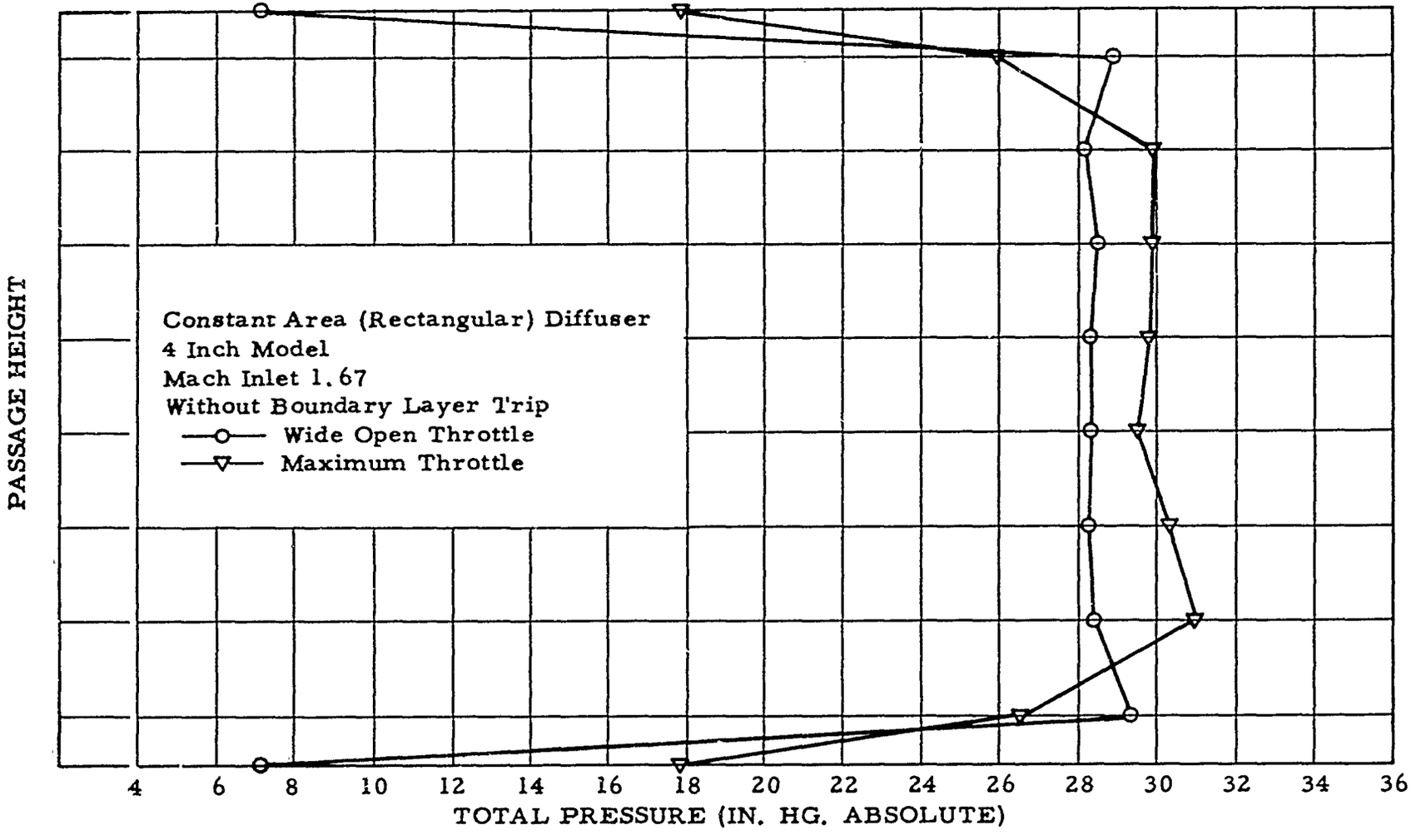

FIGURE 45 TOTAL PRESSURE DISTRIBUTION AT THE PASSAGE EXIT VERTICAL CENTER PLANE

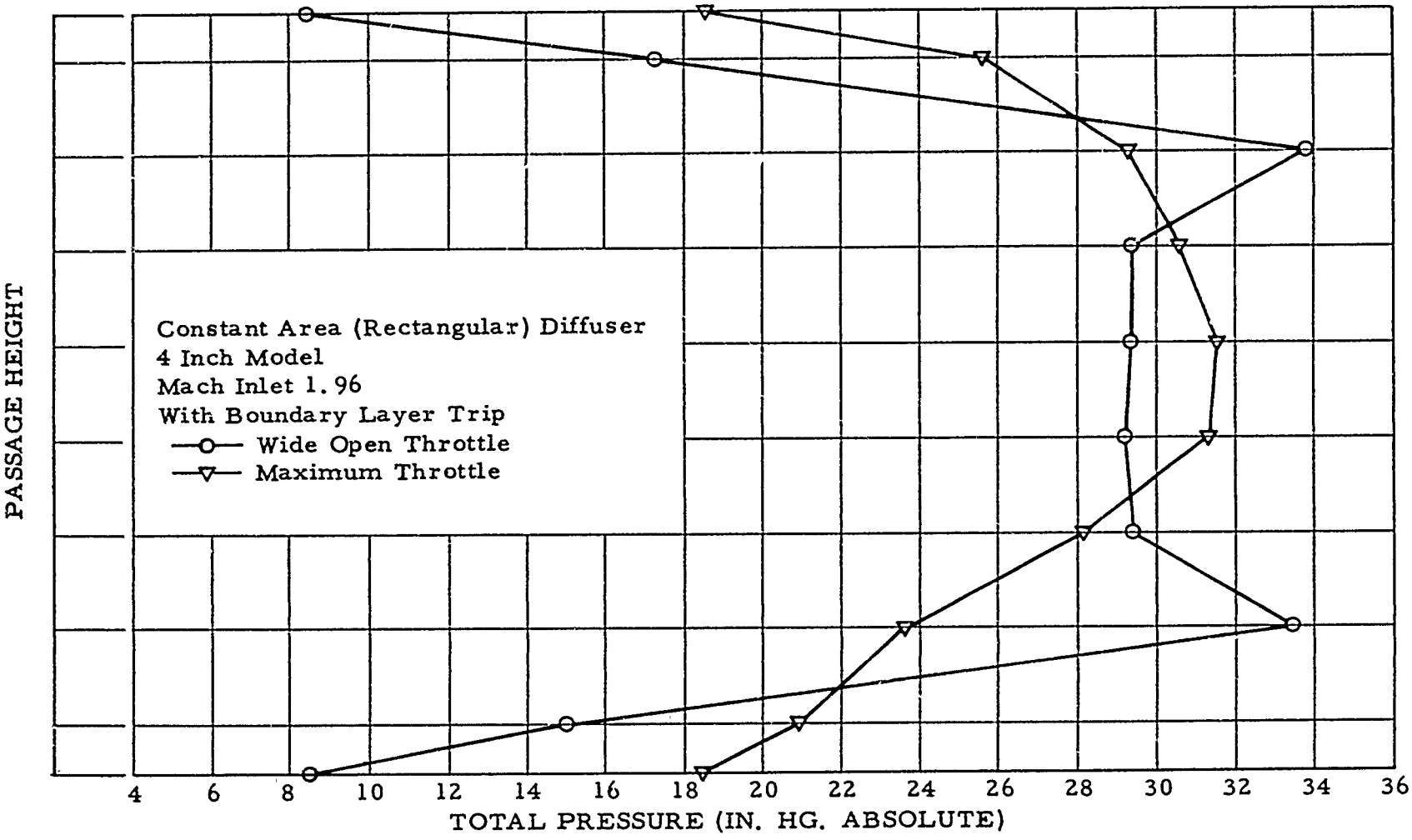

FIGURE 46 TOTAL PRESSURE DISTRIBUTION AT THE PASSAGE EXIT VERTICAL CENTER PLANE

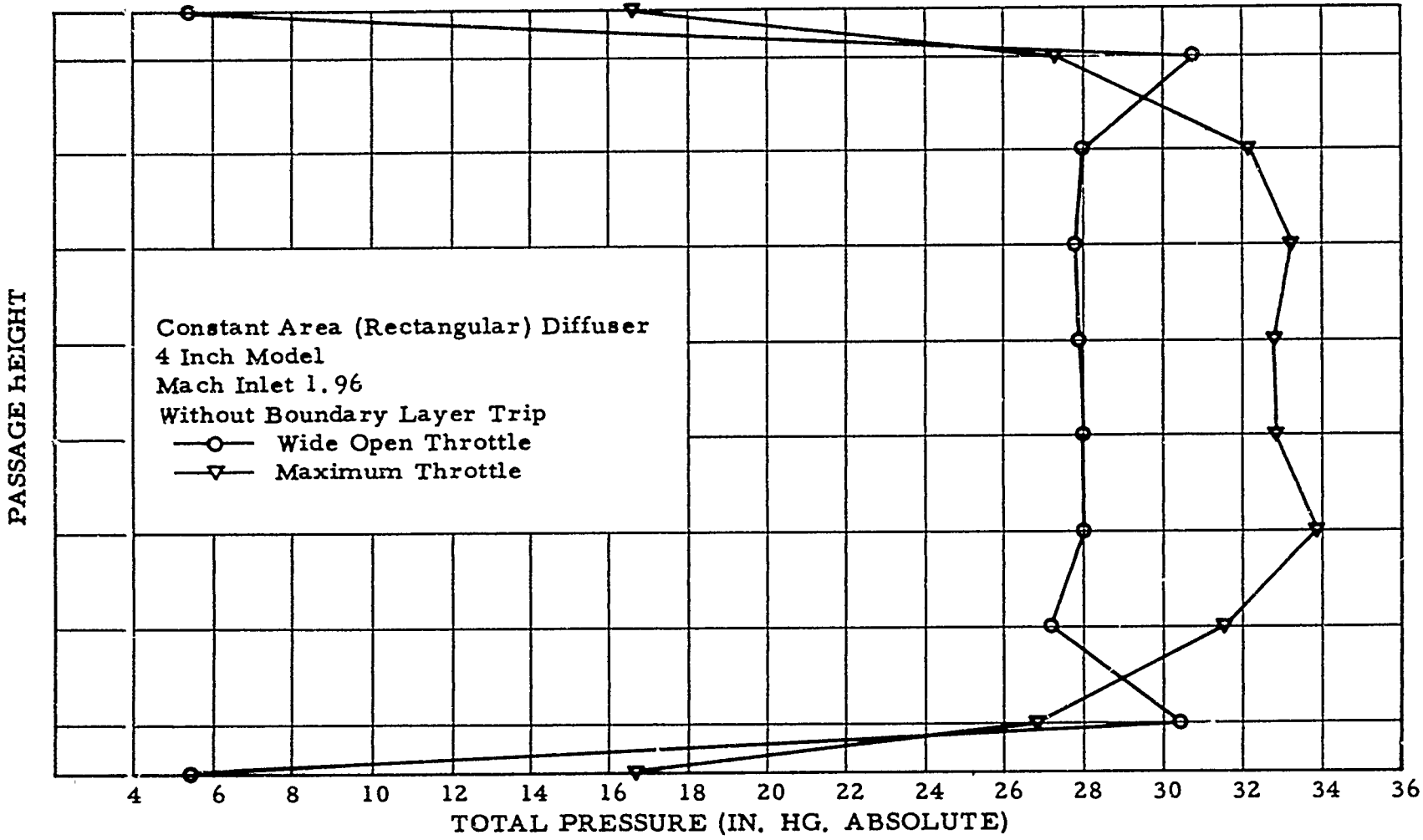

FIGURE 47 TOTAL PRESSURE DISTRIBUTION AT THE PASSAGE EXIT VERTICAL CENTER PLANE

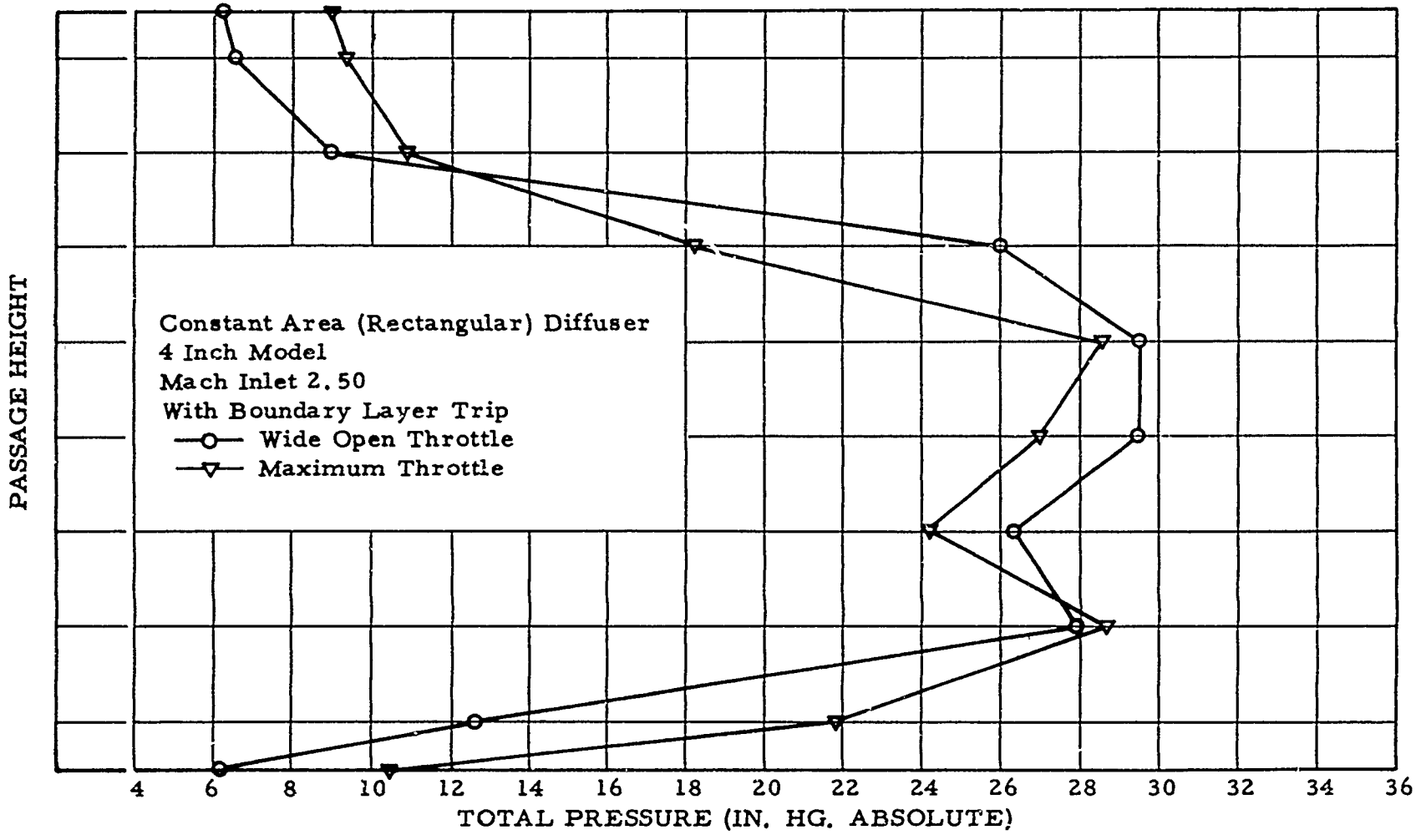

FIGURE 48 TOTAL PRESSURE DISTRIBUTION AT THE PASSAGE EXIT VERTICAL CENTER PLANE

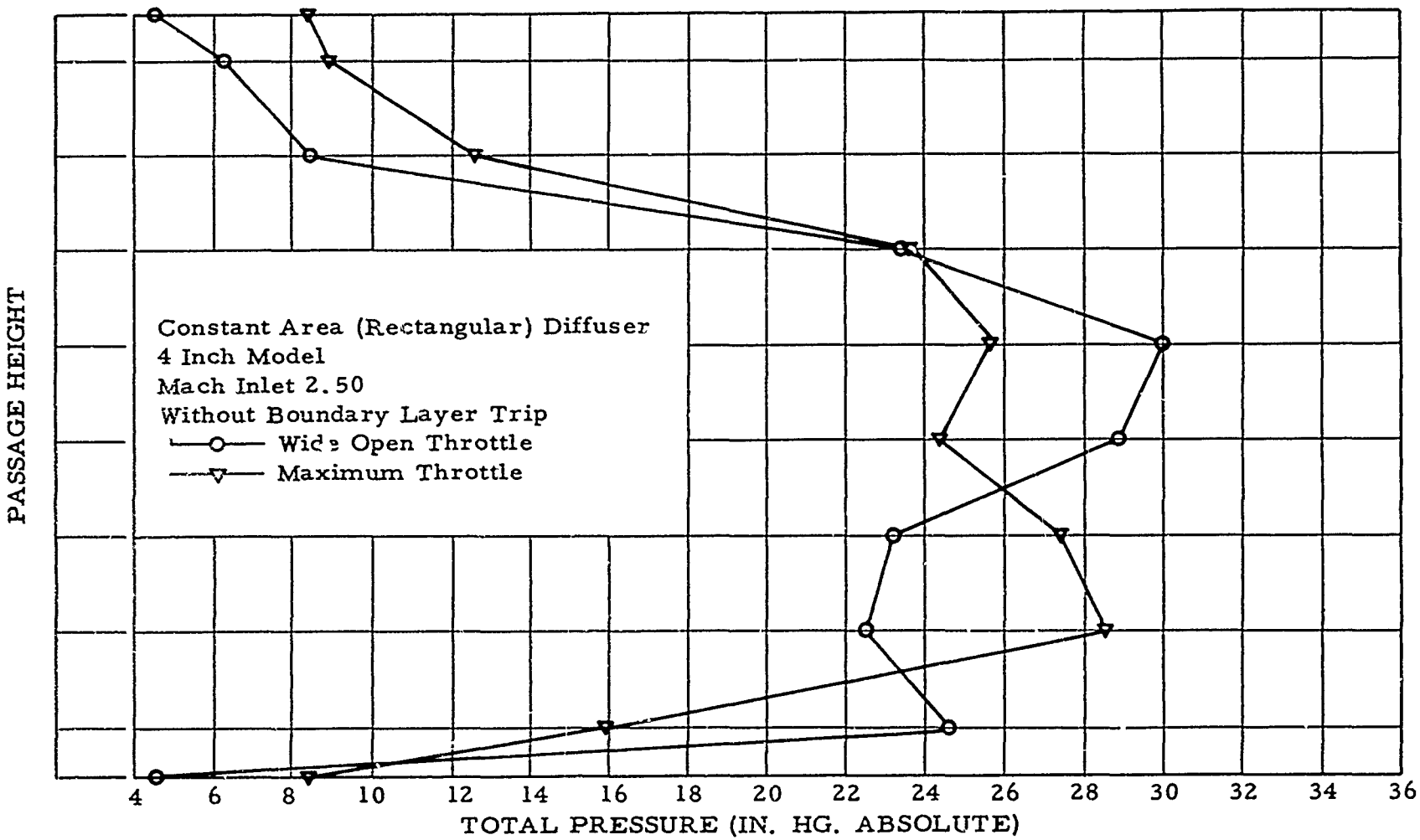

FIGURE 49 TOTAL PRESSURE DISTRIBUTION AT THE PASSAGE EXIT VERTICAL CENTER PLANE

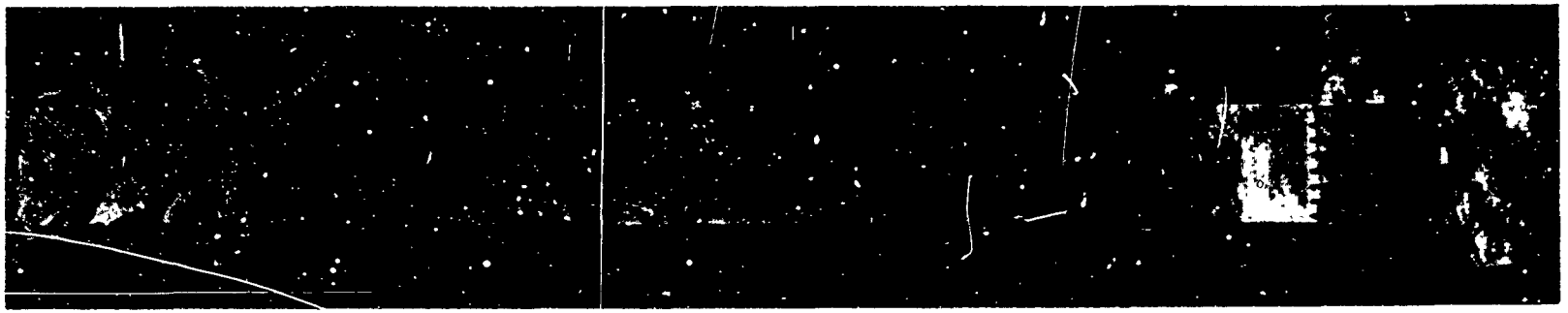

FIGURE 50 SCHLIEREN PHOTOGRAPH, 10 INCH MODEL, MACH = 1.60, (BT), RUN 5

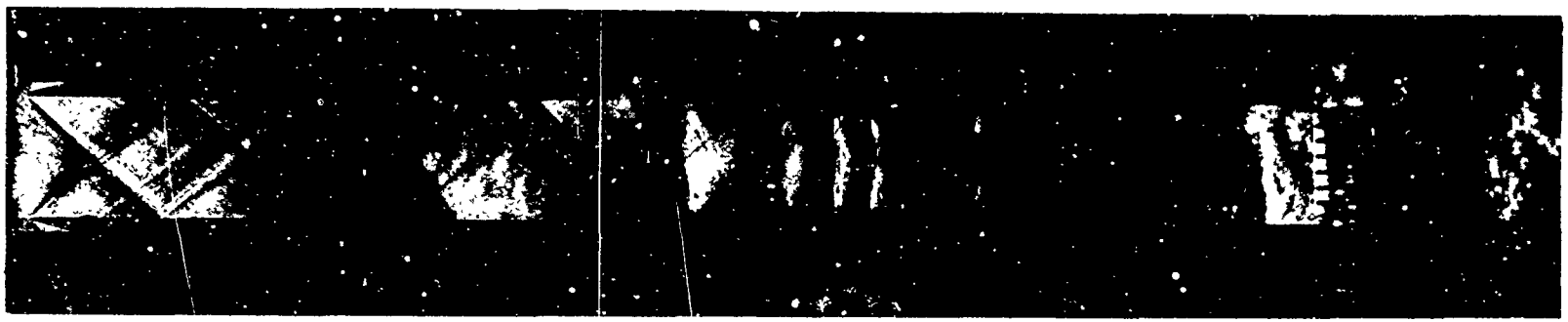

FIGURE 51 SCHLIEREN PHOTOGRAPH, 10 INCH MODEL, MACH = 1.60, RUN 15

FIGURE 52 SCHLIEREN PHOTOGRAPH 10 INCH MODEL, MACH = 1.95, (BT), RUN 6

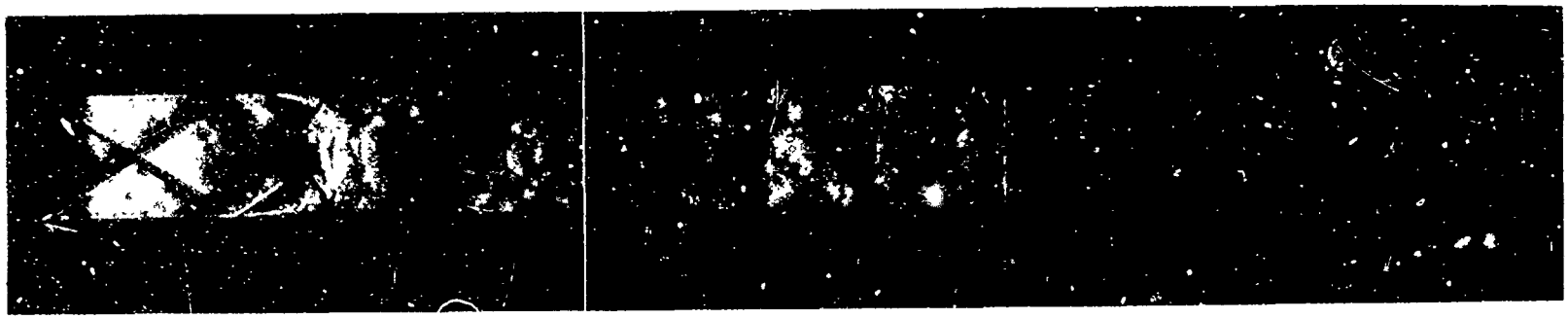

FIGURE 53 SCHLIEREN PHOTOGRAPH 10 INCH MODEL, MACH = 1.95, RUN 6

FIGURE 54 SCHLIEREN PHOTOGRAPH 10 INCH MODEL, MACH = 2.46, (BT), RUN 6

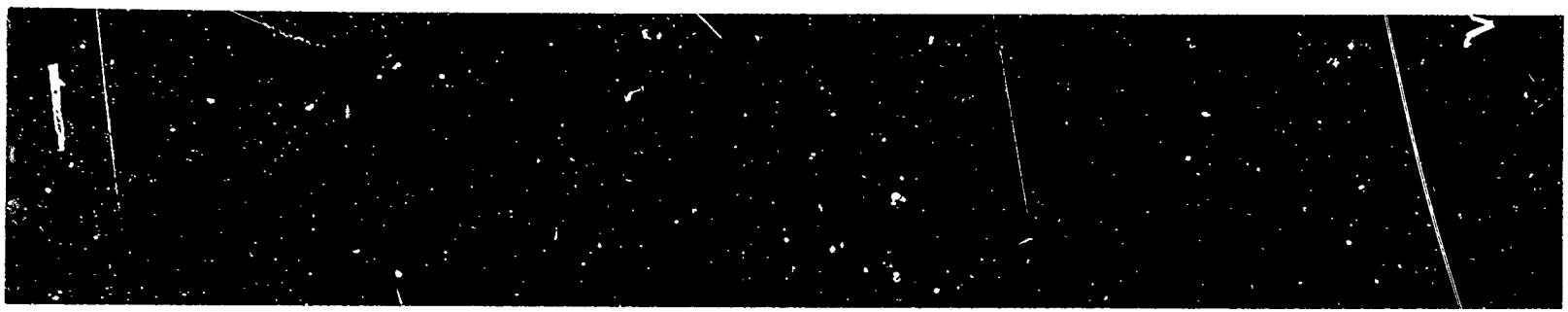

FIGURE 55 SCHLIEREN PHOTOGRAPH 10 INCH MODEL, MACH = 2.46, RUN 6

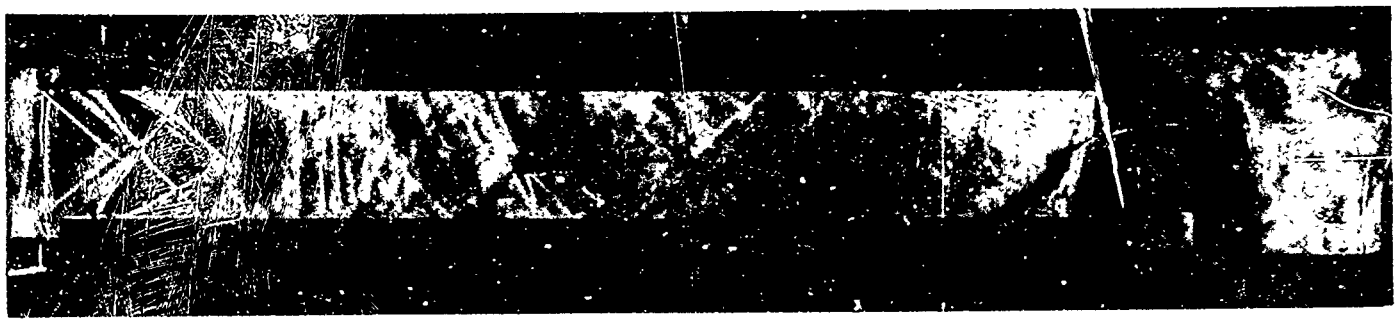

FIGURE 56 SCHLIEREN PHOTOGRAPH 8 INCH MODEL, MACH = 1.60, (BT), RUN 4

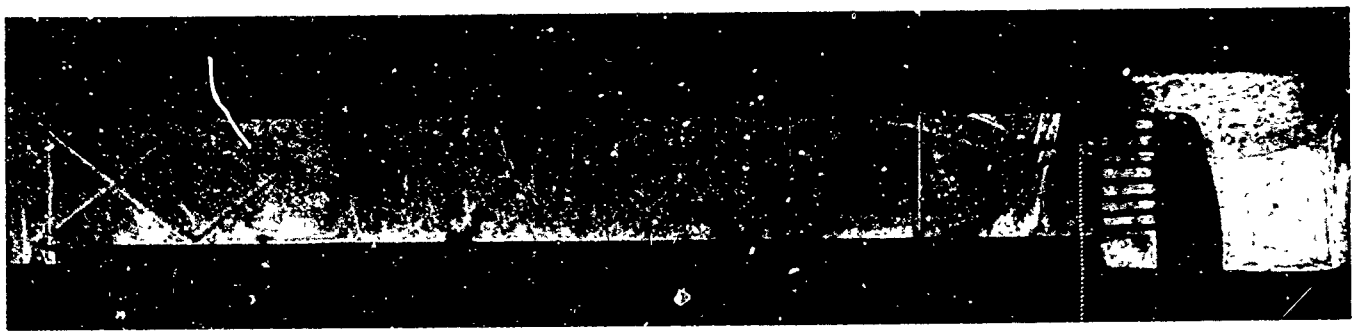

FIGURE 57 SCHLIEREN PHOTOGRAPH 8 INCH MODEL, MACH = 1.60, RUN 19

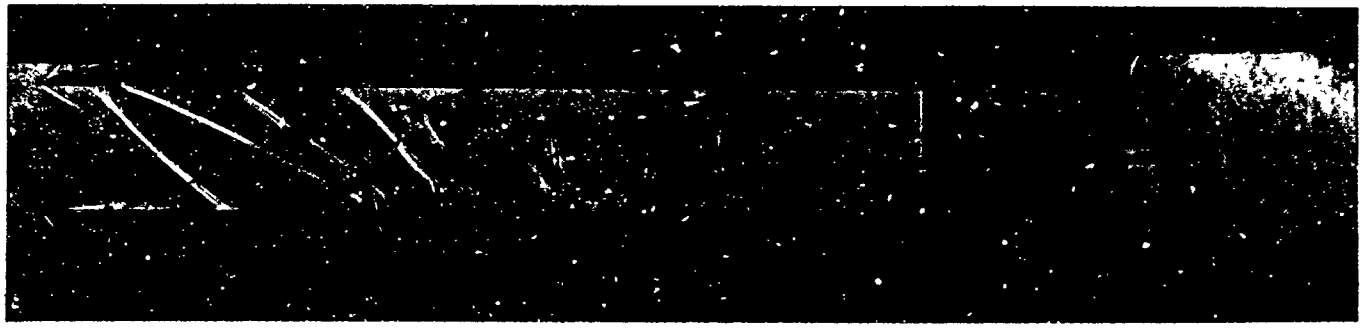

FIGURE 58 SCHLIEREN PHOTOGRAPH 8 INCH MODEL, MACH = 1.975, (BT), RUN 4

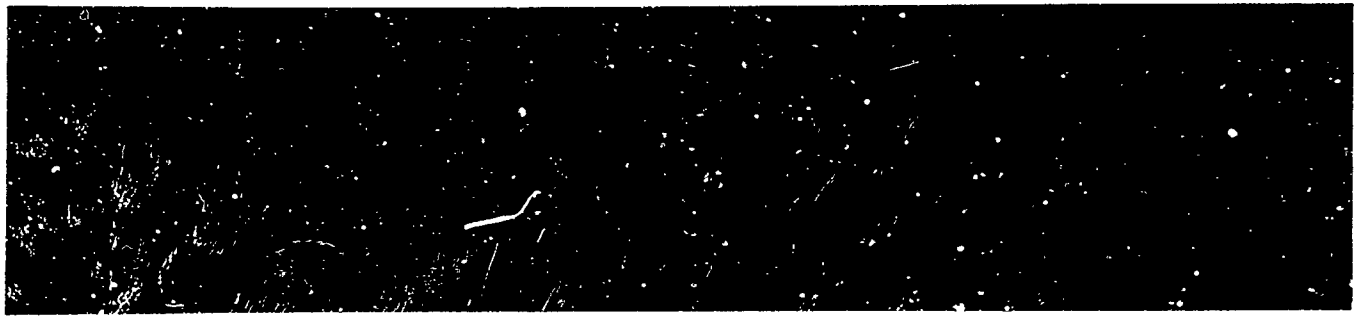

FIGURE 59 SCHLIEREN PHOTOGRAPH 8 INCH MODEL, MACH = 1.975, RUN 17

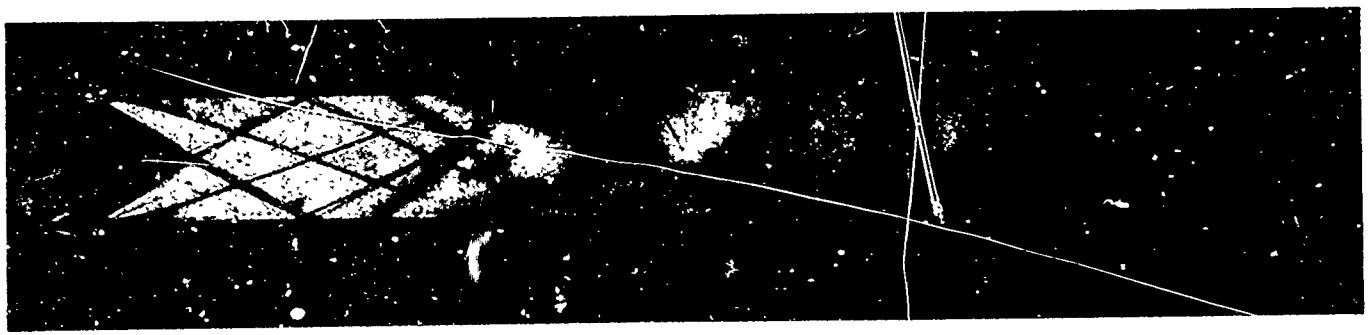

FIGURE 60 SCHLIEREN PHOTOGRAPH 8 INCH MODEL, MACH = 2.50, (BT), RUN 6

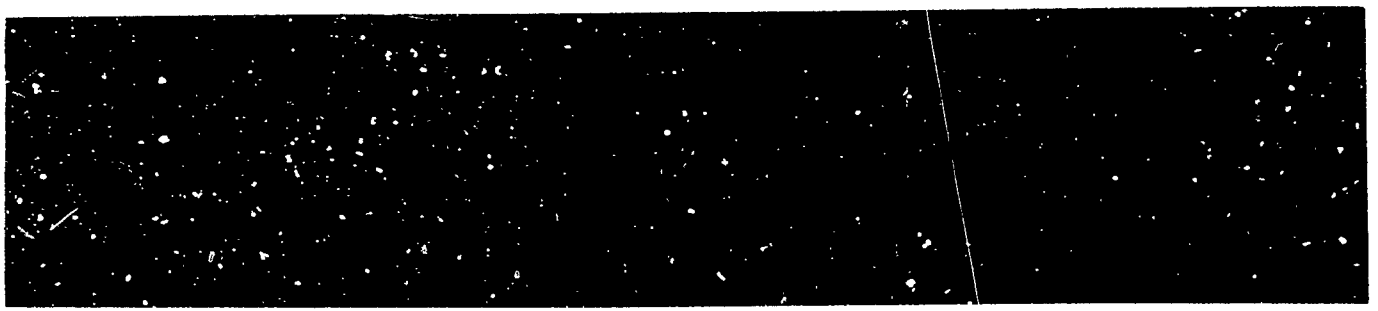

FIGURE 61 SCHLIEREN PHOTOGRAPH 8 INCH MODEL, MACH = 2.50, RUN 16

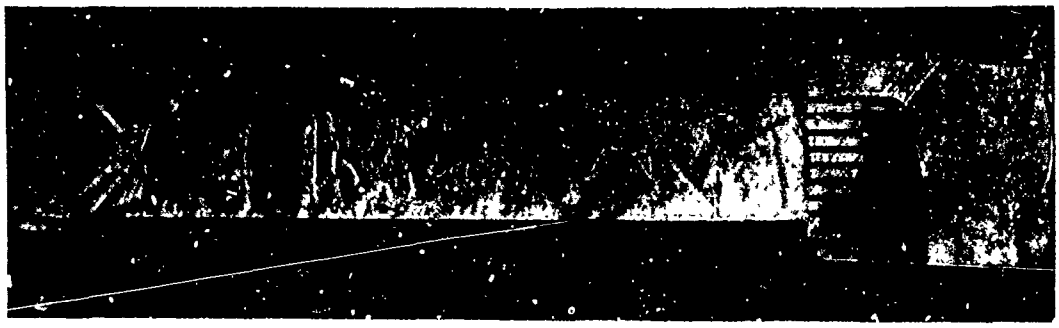

FIGURE 62 SCHLIEREN PHOTOGRAPH 6 INCH MODEL, MACH = 1.67, (BT), RUN 7

FIGURE 63 SCHLIEREN PHOTOGRAPH 6 INCH MODEL, MACH = 1.67, RUN 21

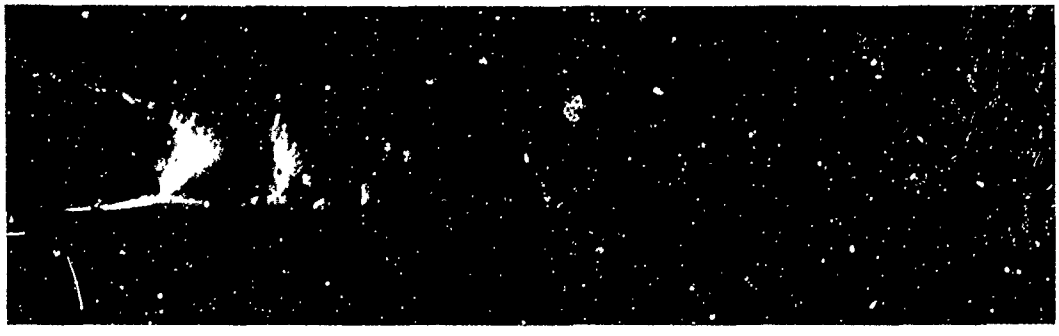

FIGURE 64 SCHLIEREN PHOTOGRAPH 6 INCH MODEL, MACH = 2.00, (BT), RUN 6

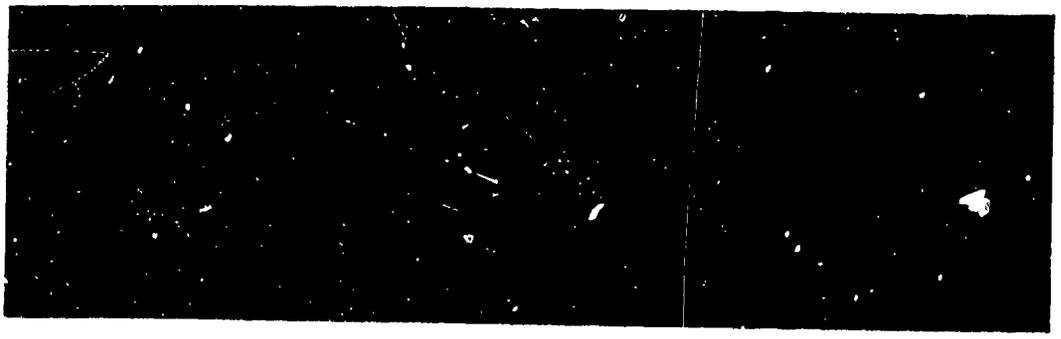

FIGURE 65 SCHLIEREN PHOTOGRAPH 6 INCH MODEL, MACH = 2.00, RUN 20

FIGURE 66 SCHLIEREN PHOTOGRAPH 6 INCH MODEL, MACH = 2.50, (BT), RUN 5

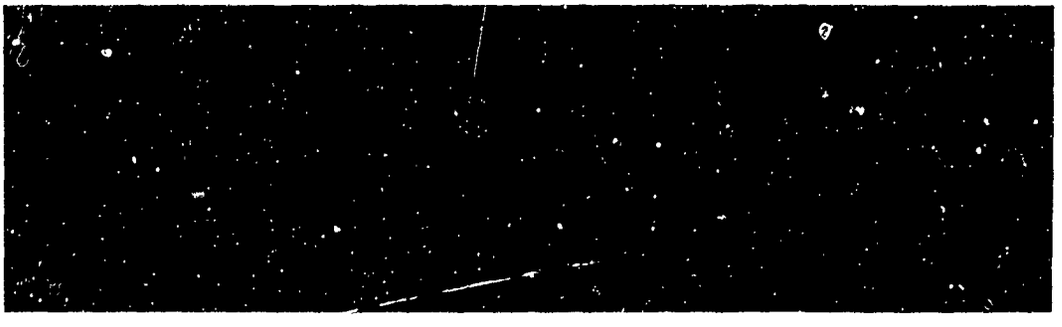

FIGURE 67 SCHLIEREN PHOTOGRAPH 6 INCH MODEL, MACH = 2.50, RUN 22

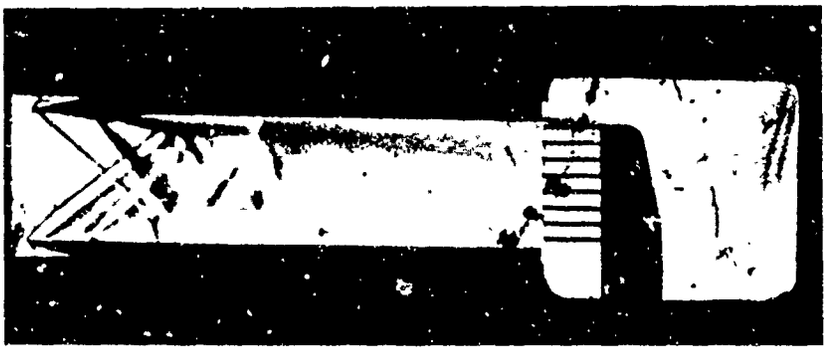

FIGURE 68 SCHLIEREN PHOTOGRAPH 4 INCH MODEL, MACH = 1.67, (BT), RUN 7

FIGURE 69 SCHLIEREN PHOTOGRAPH 4 INCH MODEL, MACH = 1.67, RUN 15

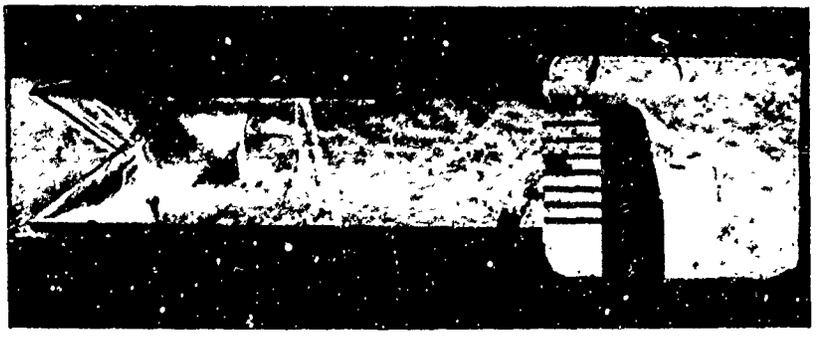

FIGURE 70 SCHLIEREN PHOTOGRAPH 4 INCH MODEL, MACH = 1.96, (BT), RUN 8

FIGURE 71 SCHLIEREN PHOTOGRAPH 4 INCH MODEL, MACH = 1.96, RUN 19

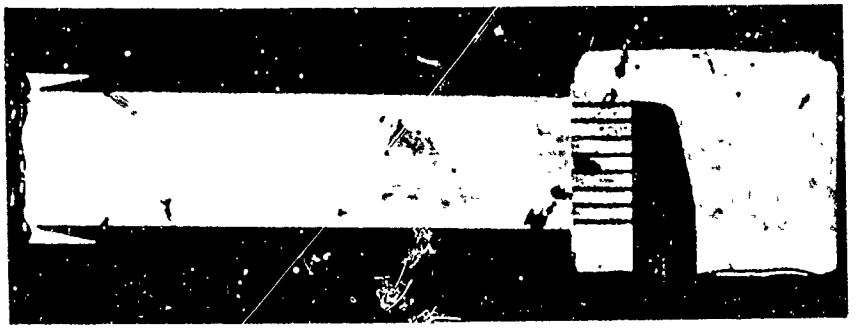

FIGURE 72 SCHLIEREN PHOTOGRAPH 4 INCH MODEL, MACH = 2.50, (BT), RUN 4

FIGURE 73 SCHLIEREN PHOTOGRAPH 4 INCH MODEL, MACH = 2.50, RUN 9